BOEING
ENGINEERING &
CONSTRUCTION
THE BOEING ENERGY
AND ENVIRONMENT DIVISION

SAND 81-8175

Final Report

Second Generation Heliostat Development

for SOLAR CENTRAL RECEIVERS

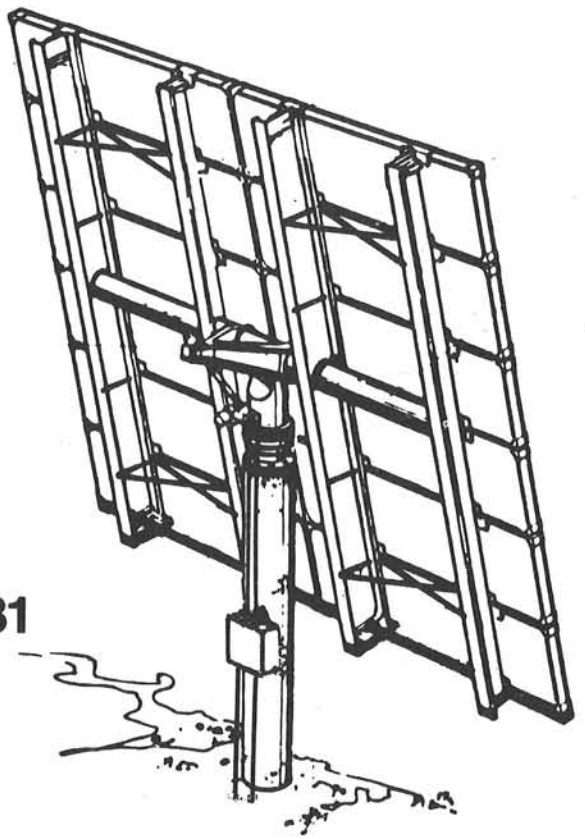

March 31, 1981

Detail Design Report
Volume I - Appendices I

SAND 81-8175

FINAL REPORT
SECOND GENERATION HELIOSTAT DEVELOPMENT
FOR SOLAR CENTRAL RECEIVERS

VOLUME I
DETAIL DESIGN REPORT

(APPENDIX I)

MARCH 31, 1981

BOEING ENGINEERING & CONSTRUCTION
(A Division of The Boeing Company)
P.O. Box 3707
SEATTLE, WASHINGTON 98124

PREPARED FOR
SANDIA NATIONAL LABORATORIES
LIVERMORE, CALIFORNIA
UNDER CONTRACT 83-2729C

APPENDICES I

TABLE OF CONTENTS

APPENDIX A

REQUIREMENTS

APPENDIX A
REQUIREMENTS

1.0 COLLECTOR SUBSYSTEM DESIGN

Design of the collector subsystem was based on functional, performance, design, and construction requirements derived from Sandia's general specification, A10772. These requirements were allocated to each of the major elements which were to be detail-designed: pedestal, gimbal-drive, reflector, and controls. These designs are described in detail in this volume. The remaining subsystem elements (support resources), and necessary production tooling were subjected to a preliminary design effort; they will be described in Volume II of this report.

1.1 FUNCTIONAL REQUIREMENTS AND UTILIZATION

1.1.1 Purpose and Primary Functions

The primary purpose of the collector subsystem is to intercept insolation and concentrate it on an elevated receiver in a safe and efficient manner. To accomplish this purpose, the subsystem must reliably and repetitively perform several functions; these are shown in Figure 1-1.

1.1.2 Operation and Expected Usage Rate

The BEC collector subsystem can be used for either a solar-electric power plant, or an industrial process heat plant. Both uses require a reliable supply of concentrated insolation to fuel their thermal energy conversion/application process. To ensure consistency in the collector subsystem design approach taken by several contractors, Sandia specified that it would be based on a 50 MW electric plant. Thus, the functional requirements for the detail design of the subsystem elements are based on this application. A typical operational sequence for such a use is shown in Figure 1-2. Using previous BEC work (Reference 2-3) on advanced central receiver systems, the typical operation profiles for a 50 MW electric cycling plant were determined, they are shown in Figure 1-3. The predicted yearly usage hours were then determined, and are summarized in Table 1-1.

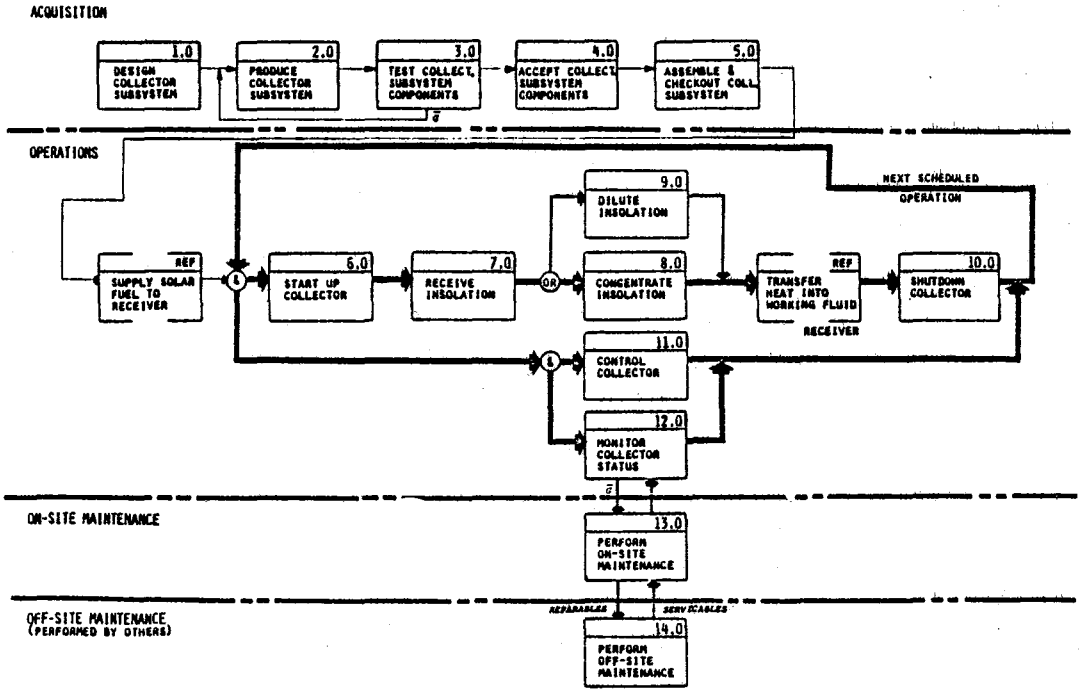

Figure 1-1 Collector Subsystem Top Functional Flow

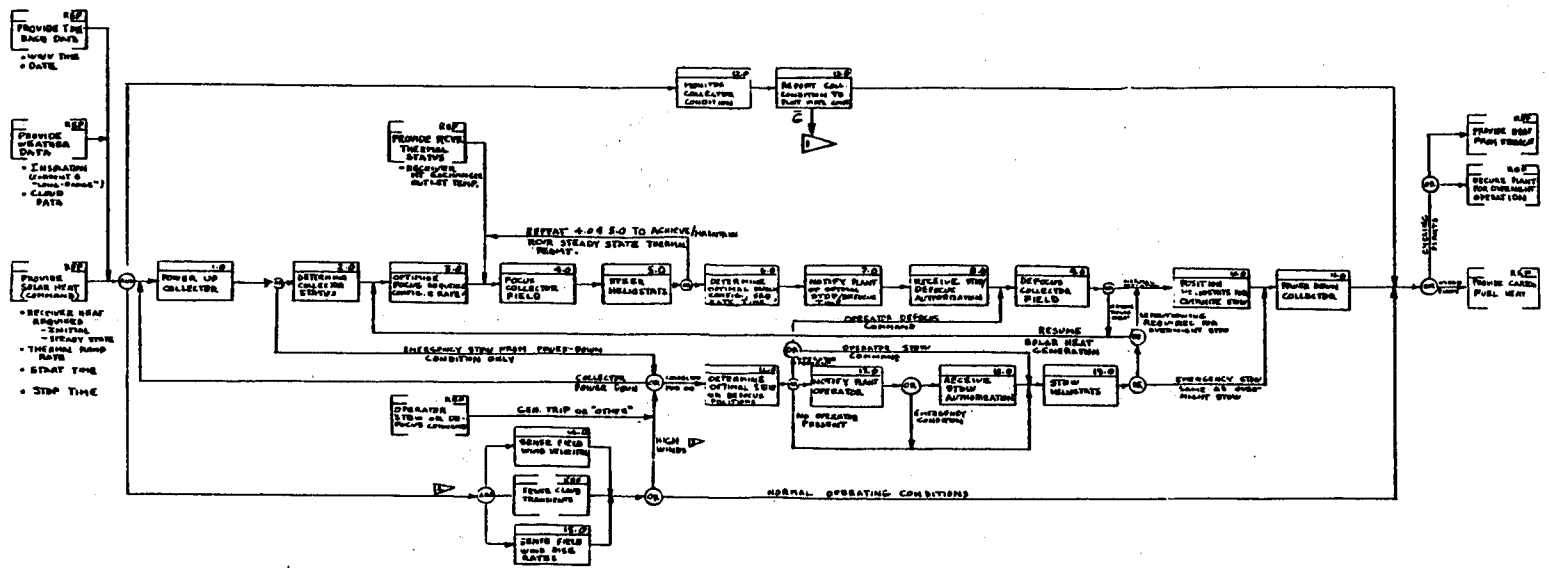

Notes:
1. Sequence shown is for electric cycling plant or industrial process heat.
2. "REF" functions shown for clarification purposes; not part of collector subsystem.

1 For No-Go's, see detail function diagrams for system functions 11.0, 12.0 and 13.0 of subsystem top functional flow diagram.

2 Functions 12.0, 13.0, 14.0, and 15.0 are performed continuously (24 hrs/day); collector condition and heliostat orientation may be reported as a composite.

3 Requires software algorithms; functions 14.0 and 15.0 may require central (array) controller or plant central control system support.

Figure 1-2. Collector Subsystem Typical Operational Sequence

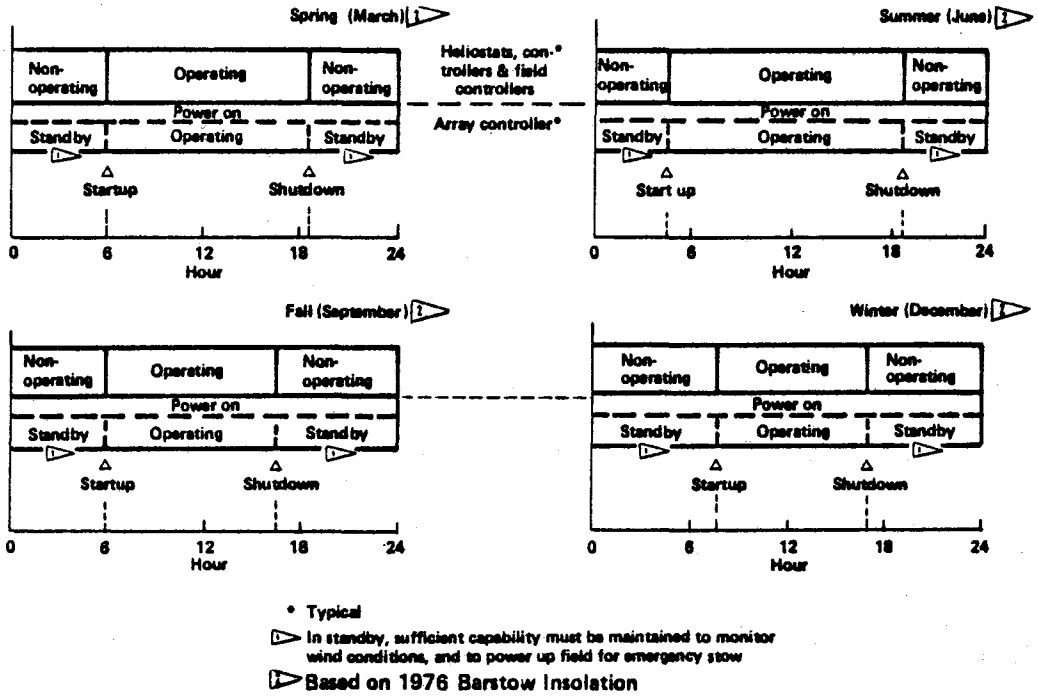

Figure 1-3 *Typical Collector Subsystem Operational Profiles, Electric Plant Utilization*

Table 1-1 *Expected Yearly Usage Hours for Collector Subsystem, Electric Plant Utilization*

Helios element	Average (expected-value) hours per year	
	Operating	Non-operating
Pedestal	8760	–
Gimbal-drive	3985	4775
Reflector	3985	4775
Controls		
Heliostat controller	3985	4775
Field controller	3985	4775
Array controller	8760	–
Data distribution	3985	4775
Power distribution	3985	4775
Wind sensor	8760	–
Time-date receiver	8760	–
Maintenance		
MSE	3875	4885

1.2 PERFORMANCE REQUIREMENTS AND DESIGN POINT

1.2.1 Performance Requirements

To accomplish the functions described in Figures 1-1 and 1-3, primary performance charateristics for the system and certain elements were established; these are listed in Table 1-2. In addition, secondary performance characteristics were also prescribed for the system and certain elements; they are listed in Table 1-3.

1.2.2 Design Point

The design of a solar collector is sensitive to the choice of design point (geographic location, day of the year, elevation, etc.). Sandia prescribed that the collector subsystem could be deployed in California, Nevada, Utah, Colorado, Arizona, New Mexico, Texas and Oklahoma. Further, they determined that the collector field would be designed according to the criteria summarized in Table 1-4.

1.3 DESIGN AND CONSTRUCTION REQUIREMENTS

1.3.1 General Design Requirements

The collector subsystem is intended for use by public and private electric utilities, and by commercial firms which use high-quality heat for industrial processes. Thus, prime considerations in designing the collector are performance, durability, reliability, safety, and acceptable life-cycle costs. General design and construction requirements were established which are compatible with these considerations; they are summarized in Table 1-5.

1.3.2 Environmental Design Criteria

The collector subsystem is intended to be used with electric power and industrial process heat (IPH) plants located in the southwestern United States. Thus, the environmental design criteria are based, in part, on conditions expected in that region of the country; they are summarized in Table 1-6.

Table 1-2 Collector Subsystem Primary Performance Requirements

COMPONENT	REQUIREMENT ①
SYSTEM	o REFLECT 95% OF REDIRECTED ENERGY ON RECEIVER AT < 60° o FUNCTION DURING ALL PLANT STEADY-STATE MODES o POWER INCREMENTS IN TRACKING MODE OF ≤10% o EMERGENCY DEFOCUS TO < 3 % POWER IN 120 SECONDS
COLLECTOR FIELD	o AVERAGE STRUCTURAL SUPPORT STATIC DEFLECTIONS ≤ ± 1.7 MRAD FOR MIRROR NORMAL, EACH AXIS (12 M/S WIND; 0° - 50°C; ANY LOCATION; ALL ORIENTATIONS; NO GRAVITY; NO TEMPERATURE EFFECTS) o HEAT FLUX ON UNIRRADIATED PORTIONS OF RECEIVER ≤ 2500 W/M^2
HELIOSTAT	o 90% OF REFLECTED ENERGY WITHIN THEORECTICAL BEAM SHAPE + 1.4 MRAD FRINGE FOR 60 DAYS WITHOUT ALIGNMENT (0 M/S WIND; 0° - 50°C; GRAVITY; ALL ORIENTATIONS; ANY LOCATION; HELIOSTAT TRACKING) o BEAM POINTING ERROR ≤ ± 1.5 MRAD EACH AXIS (SAME CONDITIONS AS BEAM QUALITY) o STRUCTURAL DEFLECTION (EXCLUDING FOUNDATION) ≤ ± 1.2 MRAD (12 M/S WIND; 0° - 50°C; ALL ORIENTATIONS; ANY LOCATION; NO GRAVITY; NO WAVINESS; NO FACET MISALIGNMENT) o 2-POINT AIMING
FOUNDATION (2" ABOVE GROUND)	o TILT OR TORSIONAL ROTATION ≤ ± 0.5 MRAD (12 M/S WIND; PLASTIC DEFLECTION FROM 22 M/S WIND) o PLASTIC DEFLECTION ≤ ± 0.15 MRAD (SINGLE 22 M/S WIND)

① Tolerances are 1 sigma values.

Table 1-3 *Collector Subsystem Secondary Performance Requirements*

COMPONENT	REQUIREMENT
SYSTEM	o MEET PERFORMANCE @ 12 M/S WIND, 0° - 50°C, GRAVITY o TRACK WITH DEGRADED PERFORMANCE WHEN WIND IS 16 M/S o INITIATE STOW FROM EXTERNAL SIGNAL o INCORPORATE LIGHTNING PROTECTION o OPERATE FROM -9° - 50°C (PLUS INSOLATION ON UNPROTECTED COMPONENTS) o REQUIRE MINIMUM MAINTENACE o ANNOUNCE ANY COMPONENT FAILURE TO HAC o PROVIDE FAULT ISOLATION INFORMATION ON CRITICAL COMPONENTS o MINIMIZE HAZARDS TO OPERATIONS/ MAINTENANCE PERSONNEL AND THE PUBLIC
HELIOSTAT	o CAPABLE OF BEING POSITIONED FOR STOW, CLEANING OR MAINTENANCE ≤ 15 MINUTES (FROM ANY OPERATIONAL ORIENTATION)
CONTROLS	o CONTROL HELIOSTATS BY COMPUTER o SAFE BEAM CONTROL STRATEGY

Table 1-4 *Design Point Parameter Values*

Parameter	Design Point or Value/Description
Geographic Location	Latitude: 35°N Elevation: 0.65km
Soil Conditions	Based on soil at the DOE CRTF, Albuquerque, NM
Insolation	950 W/m^2
Day of Year	81
Aiming Strategy	Vertical flux distribution on receiver

Table 1-5 *Collector Subsystem Design and Construction Requirements*

COMPONENT	REQUIREMENT
SYSTEM	o 30 YEAR LIFE o COMMERCIAL DESIGN AND CONSTRUCTION STANDARDS (UBC/ 1976; AISCM/8TH EDITION; NATIONAL ELECTRIC CODE; NEMA AND MS-454 o OFF-THE-SHELF COMPONENTS o TOLERATE POWER TRANSIENTS o MINIMIZE SUSCEPTIBILITY TO AND GENERATION OF EMR o CORROSION PROTECTION ON ALL PARTS o COMPONENTS OR ASSEMBLIES TRANSPORTABLE BY TRUCK o WORKMANSHIP CONSISTENT WITH GOOD COMMERCIAL PRACTICE o ALL MAJOR ELEMENTS AND ASSEMBLIES TO HAVE NAMEPLATES o LIKE PARTS TO BE INTER-CHANGEABLE o DESIGN TO FACILITATE OPERATON AND MAINTENACE; USE MS-1472 AS GUIDE
COLLECTOR FIELD	o NOT BE VULNERABLE TO EXTENSIVE FIRE DAMAGE o HELIOSTATS NOT DIRECTLY ADJACENT TO A FIRE SHOULD NOT SPREAD TO OTHER PARTS OF THE FIELD
HELIOSTAT	o MAINTAIN STRUCTURAL INTEGRITY IN ANY POSITION IN A 22 M/S WIND o NO ELEVATION OR AZIMUTH DRIFT IN DRIVES o SURVIVE 19 MM HAIL @ 20 M/S IN ANY ORIENTATION o WITHSTAND AND/OR OPERATE WHEN SUBJECTED TO WIND-INDUCED VIBRATIONS o ENVIRONMENTALLY SEALED DRIVES o COST-EFFECTIVE STOWAGE o COST-EFFECTIVE REFLECTIVITY AND AREA

Table 1-6 Environmental Design Criteria for Production Collector Subsystem

Environmental Condition	Functional Capability Required When Subjected To Environmental Conditions of Values Shown While					
	Operating (1)				Not Operating (1)	
	Startup and Shutdown Per 3.2.6.2	Steering Per 3.2.6.2	Defocusing Per 3.2.3a	Stowing Per 3.2.2b and 3.2.6.3	Structural Integrity per 3.2.6.3 & 3.2.6.4 (Any Position)	Survival Per 3.2.6.3 (Stow Position)
Gravity	Local	Local	Local	Local	Local	Local
Earthquake	-	-	-	-	UBC Seismic Zone 3	UBC Seismic Zone 3
Wind						
Speed (Includes Gusts)	≤ 16 m/s	0 to 12 m/s	0 to 16 m/s	0 to 22 m/s	0 thru 22 m/s	0 thru 40 m/s
Rise RAte	0.01 m/s^2	0.01 m/s^2	0.01 m/s^2	0.01 m/s^2	0.01 m/s^2	0.01 m/s^2
Dust Devils (Cyclonic Winds)	0 to 16 m/s	0 to 12 m/s	0 to 17 m/s	0 to 17 m/s	0 to 17 m/s	0 to 17 m/s
Direction	Any	Any	Any	Any	Any	Any
Angle from Horizontal	±10°	±10°	±10°	±10°	±10°	±10°
Temperature (5)	-9 to 50°C	0 to 50°C	0 to 50°C	0 to 50°C	-30 to 50°C	-30 to 50°C
Precipitation						
Rain						
Annual Average	750 mm	-	-	750 mm	750 mm	750 mm
24-Hour Rate	≤ 75 mm	-	-	≤ 75 mm	≤ 75 mm	≤ 75 mm
Ice/Freezing Rain Thickness	≤ 50 mm	-	-	≤ 50 mm	≤ 50 mm	≤ 50 mm
Hail						
Diameter	-	-	-	≤ 20 mm	≤ 20 mm	≤ 25 mm
Speed	-	-	-	≤ 20 m/s	≤ 20 m/s	≤ 23 m/s
Special Gravity	-	-	-	0.9	0.9	0.9
Temperature	-	-	-	0 thru 6.7°C	0 thru 6.7°C	0 thru 6.7°C
Snow						
24-Hour Rate	0.3 m	-	-	0.3 m	0.3 m	0.3 m
Max. Loading	250 Pa	-	-	250 Pa	250 Pa	250 Pa
Insolation						
Max Flux	1100 w/m^2	1100 w/m^2	1100 w/m^2	1100 w/m^2	1100 $2/m^2$	1100 w/m^2
Rate of Change	(4)	(4)	(4)	(4)	(4)	(4)
Lightning						
Maximum Stroke	200,000 AMPS	200,000 AMPS	200,000 AMPS	200,000 AMPS	200,000 AMPS	200,000 AMPS
Direct Hit	Loss of 1 Helio ok	Loss of 1 Helio ok	Loss of 1 Helio ok	Loss of 1 Helio ok	Loss of 1 Helio ok	Loss of 1 Helio ok
Adjacent Hit (3)	Minimize Damage	Minimize Damage	Minimize Damage	Minimize Damage	Minimize Damage	Minimize Damage

Notes: (1) Paragraph references are to Sandia specification A10772, Rev. 6, 10-10-79

(2) A "Hail-Survival" stow position may be specified and may be distinct from "High Wind" stow position.

(3) Damage to be minimized subject to appropriate cost/risk limits (TBD).

(4) Collector shall be capable of performance indicated when subjected to flux changes associated with passage of opaque cloud; flux shall be assumed to drop from 1100 w/m^2 to 0 w/m^2 and return to 1100 w/m^2.

(5) For components installed in an uncontrolled environment.

1.3.3 Detail Design Requirements

1.3.3.1 Facet Requirements

Based on the system performance and design requirements, detail design requirements for the reflector were established. Some requirements were allocated to individual components; for the facet assembly, they are:

Reflective Surface Waviness: The installed facet shall not exhibit a surface waviness greater than 0.60 milliradians (mrad) over 90% of its reflective area when in a horizontal position relative to ground with no wind;

Reflective Surface Deflection: 99% of the facet's reflective area shall not exhibit a deflection greater than 0.6 mrad when oriented in a position which generates the highest loads in a 12 m/s wind. This deflection allowable includes thermal effects caused by ambient temperature variance, but does not include reflector surface waviness;

Reflectance: The facet reflective surface shall have a minimum solar specular reflectance of 0.94 based on an air mass 1-1/2 solar spectrum;

Hailstone Survival: The facet assembly shall not sustain significant damage when impacted by 19 mm hailstones striking it at 20 m/s when in any orientation; it shall survive and maintain structural integrity when impacted by 25 mm hail striking it at 23 m/s when in a special stow position; and,

Maintenance: The facet shall require minimum maintenance during its lifetime other than periodic cleaning of the reflective surface.

Design requirements were also levied on the frame assembly and complete reflector assembly; the most significant requirements concern the beam pointing error, beam quality, and structural deflections which are summarized in Table 1-2, and are not repeated here. The capability of alternate design configurations to satisfy the reflector/facet/frame requirements was evaluated by trade study, analyses and tests.

1.3.3.2 Attachment Bracket Requirements

The function of the attachment brackets is to maintain facet orientation and alignment, and provide load paths between the facets and support structure. Winds generate pressure gradients both over the surfaces and across the facets. These pressure loads are reacted normal to the facet faces with in-plane facet loads approximately zero. The only in-plane facet loads are due to gravity and earthquake. Therefore, the attachment brackets are required to prevent movement in the direction normal to the facet planes only. When the reflector is oriented in non-horizontal positions, the facets must be restrained by bottoming on the lower-most brackets. The spacing between opposing brackets must be greater than the width of the panel to allow thermal expansion/contraction of the support frame relative to the facet. The bracket design must also incorporate a joint to prevent moment loads between the bracket and facet. Finally, the bracket must incorporate a feature which would permit each facet to be canted.

1.3.3.3 Frame Assembly Requirements

A frame is required to react wind and gravity loads transmitted from the facets through the bracket assemblies. In addition, the frame is required to hold the facet assemblies in a fixed position while maintaining the canting angles required for the reflected beam.

1.3.3.4 Gimbal/Actuator Drive Assembly Requirements

The gimbal/actuator assembly is required to rotate the reflector assembly in azimuth and elevation so that the sunlight will be redirected onto the receiver. It must perform this function continuously during normal operation when supplied with electric power from the heliostat controller. The gimbal/actuator is also required to orient the reflector assembly in certain pre-determined positions, such as overnight stow, cleaning, high-wind stow, etc. In addition, it must be capable of rapidly slewing the reflector in response to emergency detargeting commands.

To perform these functions, the gimbal/actuator must be capable of:

a. Elevation travel of -3° to +93°. The azimuth travel will be at least ±165° governed only by the location of the limit switches;

b. Achieving an azimuth slew velocity to travel 180° in 15 minutes and an elevation slew velocity to travel 93° in 15 minutes in wind velocities $\leq$ 15 m/s;

c. Positioning the reflector to the commanded position in wind velocities (including gusts) $\leq$ 15 m/s (35 mph); and to horizontal stow in wind velocities $\leq$ 22 m/s (50 mph);

d. Positioning the reflector to the commanded position within 0.50 mrad standard deviation (1 sigma) for each gimbal axis while tracking in negligible wind and under normal operating conditions;

e. Positioning the reflector to the commanded position within 3.0 mrad/axis due to all effects in 12 m/s (27 mph) wind under the worst conditions of wind direction and heliostat orientation;

f. Withstanding loads imposed on it from the reflector assembly due to winds of $\leq$ 22 m/s when the reflector is in any position; and of $\leq$ 40 m/s when the reflector is in the horizontal (stowed) position; and

g. Interfacing with the reflector assembly and the pedestal assembly.

1.3.3.5 Drive Motor Requirements

Motors are required to rotate the input drive shafts of the elevation and azimuth assemblies. The motors are to be electric powered and of sufficient size to satisfy all operational input torque requirements. They must be capable of driving the elevation and azimuth assemblies so as to achieve elevation tracking rates of 6.2°/min; and azimuth tracking rates of 12°/min. The motors must be capable of driving the gimbal/actuator through 93° of elevation travel, and azimuth travel of 180°. Motors must be environmentally capable of operation for 30 years with no scheduled maintenance.

1.3.3.6 Sensors Requirements

a. Motor Shaft Revolution Counters

It is necessary to monitor and quantify motor shaft rotation. The quantization must be of sufficiently small increments that the gimbal/actuator can meet its pointing accuracy requirements. The motors must be controlled in a smooth and stable manner. In addition, the sensors must be compatible with the use of a microprocessor for closing the motor control loops; provide positive identification as being forward or reverse motion pulses; and provide correct sensing of motor shaft rotation regardless of shaft velocity.

b. Zero Reference Sensors

Because incremental revolution sensors were selected for the design, zero reference sensors are required on both axes to show when the unit passes a zero reference position. The zero reference sensor will be used to initialize or check the unit position count in the computer memory. Indication of the reference position must be repeatable within 0.01 milliradians when traveling in a specified direction across the point. The reference mark signal must also provide a proximity warning that the reference point is close enough to occur within 3.5 $\pm$0.5 seconds of time if the unit is moving at maximum slew rate.

1.3.3.7 Pedestal/Foundation Requirements

The pedestal/foundation consists of both the above-ground and below-ground structure required to support the gimbal drive and reflector assembly. The design requirements for the pedestal/foundation are summarized in Table 1-7. The requirement governing pedestal deflection reflects the BEC unified pedestal/foundation design approach, in constrast to composite designs which incorporate a separate foundation and pedestal. In addition, it was decided to tighten the deflection requirement for the pedestal in order to relax the performance requirements for the gimbal drive system.

Table 1-7 Pedestal/Foundation Design Requirements

Characteristic or Function	Design Requirement
Support Heliostat	Support 13,650 lbs. in specified soil conditions
Resist Bending Forces	Deflection at top of pedestal $\leq$ 0.9 mrad in 27 mph wind
Resist Plastic Deformation Forces and Rotation	Plastic deformation of pedestal in soil $\leq$ 0.45 mrad when subjected to 50 mph wind
Design Life	30 years with minimum maintenance

1.3.3.8 Heliostat Control Hardware Requirements

The prototype control components are required to: provide HAC, HFC and HC functions for two heliostats with an error contribution less than .4 mrad (1 sigma) per axis; provide protection against lightning strikes; and provide protection against 70% overvoltage surges on the power lines.

The principal functions which the prototype controls are required to perform are: startup (apply power, determine heliostat's status, and display status to operator); transition (bring reflected images to standby target position); track (move images to target and continuously direct heliostat image on target); defocus (bring heliostat images from target to standby position); stow (position heliostat reflectors in horizontal or other planned positions, e.g., for maintenance, overnight stow, etc.); shutdown (store all pertinent operating data on disk and exit control program). The prototype controller must also permit the operator to command the heliostat images to any selected position, and to locate the reference marks on each axis.

1.3.3.9 Control Software Requirements

Software design requirements were derived from the Sandia specification (reference 1-1), and the computer hardware selections. The requirements derived from the collector subsystem specification concerned primarily aiming accuracy; 15-minute stow/positioning; south-field gimbal lock resolution in 15 minutes; and a beam control strategy to protect personnel and property.

The requirements necessary to be compatible with the hardware design were primarily to provide a method of locating the reference marks and initializing the motor position counts; provide a method to protect the motors against burn-out due to stalling; and to assist in compensating for jack-screw non-linearity. In addition, methods were needed to compensate for gravity sag; correct non-verticality errors in the gimbal/actuator assembly mounting; compensate for non-orthogonality errors between the elevation axis and azimuth axis; and to provide for operator command to the control system.

APPENDIX B

Azimuth Drive/Bearing Assembly
Test Data

for

Gimbal/Actuator Drive Assembly

for

Boeing Second Generation Heliostat

APPENDIX B

AZIMUTH DRIVE/BEARING ASSEMBLY

TEST DATA

1.0 INTRODUCTION

This report describes the findings of tests performed at Winsmith on two identical prototype azimuth drive/bearing assemblies for the Ford Aerospace & Communications Division.

Tests were conducted on the period from July 21 through July 25, 1980.

2.0 CONCLUSION

The performance tests were successfully completed on the two prototype assemblies. No major problems developed during any part of the evaluation period. The units were partially inspected at the conclusion of the testing and were found to be in excellent condition.

Specifically unit #1 performed slightly better than Unit #2 by showing a higher operating efficiency, lower power consumption and lower gear mesh loss. Unit #2 showed larger torsional compliance... and this discrepancy is discussed elsewhere after retesting at FACC. The backlash was also very much less on Unit #2.

The following discussion was submitted by Winsmith.

3 DISCUSSION

3.1 DRIVES

The two drives tested are identical and identified as UNIT 1, serial number D651133-2D-1; and UNIT 2, serial number D651133-2D-2. Reference also to Winsmith Outline Drawing D651133-2 and Assembly Cross Section Drawing D651133-18. Both primary and secondary stages were filled to proper oil level with our synthetic gear lubricant, Mobil SHC 626, part number 51,001.

3.2 TEST PROCEDURES

Testing procedures were in compliance with those originally submitted by P. B. Nanava ti of Ford Aerospace dated 1/4/80 and an approved version by R. Zajac of Winsmith dated 6/5/80. (See Section B-5)

3.3 TEST SETUP *

3.3.1 GENERAL

The reducer is shown in Photographs 1 and 2 prior to being fixtured and instrumented for test purposes. All of the tests performed on both units were in an identical test setup, with the exception of the running torque and efficiency. UNIT 1 (S.N. D651133-2D-1) was mounted in a horizontal plane and loaded on the output by a disc brake dynomometer and ran continuously. UNIT 2 (S.N. D651133-2D-2) was mounted in a vertical plane 90 degrees to UNIT 1. The load was created by intermittently running the drive and raising a weight on an arm attached to the output flange. The lubricant was drained out of the secondary stage during this test.

The drive was powered by a 3/4 HP, 1750 RPM motor through the extension end of the input shaft on the primary stage. Many of the tests were performed two or three times to establish repeatability.

3.3.2 INSTRUMENTATION

Oil temperature in the primary stage was not able to be monitored because of the limited space to install a thermocouple or other sensing device.

Where the input torque was measured statically, a 0-6 in.-lb. torque wrench was used.

*Photographs referred to in this section are found in Appendix B-4, starting on page B-42.

A strain-gage type torque transducer was installed between the drive motor and input shaft to measure running torque. Photograph 3 and 4 show the calibration of the torque transducer and related readout instruments. A copy of the calibration curve is in Appendix B-6 . Photographs 8, 9, & 10 show the transducer installed.

Motor speed is determined electronically by determining the frequency at the shaft. A magnetic pickup is located near the motor shaft.

3.3.3 RUNNING TORQUE AND EFFICIENCY

In tests on UNIT 1, torque was applied in both directions of rotation by applying hydraulic pressure to a disc brake attached to the output flange of the drive. See Photographs 5, 7, & 8.

In tests on UNIT 2, torque was applied in only one direction by running the motor intermittently and raising a weighted arm attached to the output flange of the drive. Data was also collected on lowering various loads. See Photograph 14. The operating load is 3900 ft.-lbs. (46,800 in.-lb.) and the maximum load is 7800 ft.-lbs. (93,600 in.-lbs.)

3.3.4 BREAK LOOSE FRICTION TORQUE

This was measured in a static condition with no load on the drive. The drive motor was temporarily removed and a torque wrench installed on the torque transducer. This was also determined for a load condition in one direction.

UNIT 1 was floor mounted and UNIT 2 was side-wall mounted.

3.3.5 BACKLASH

Overall system backlash was determined for both units in a floor mounted position. This allowed the planetary frame element to be resting on the base and not on the ring gears.

A dial indicator was installed between the base and cover. Backlash was measured at the input shaft and expressed in degrees or number of turns.

Photograph 9 shows the graduated dial plate used to measure the rotation. Photographs 6, 11, and 12 show the position of the dial indicator.

3.3.6 TORSIONAL STIFFNESS

Static torsional loads were applied to the output flange on the base in both directions, and deflection was measured between base and cover. See Photographs 13 and 15. Maximum load applied in each direction was 2,300 ft.-lbs. or 27,600 in.-lbs.

The torque was applied by hanging a weight at the end of an arm connected to the output flange on the base of the drive. At the same point, a scale was attached and fastened to an overhead crane.

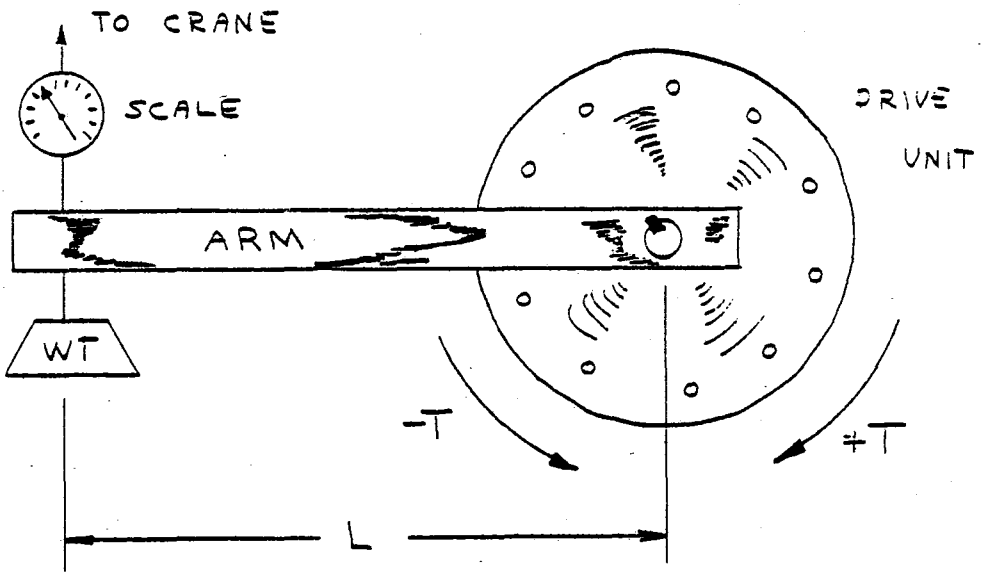

The torque applied in a downward direction or CCW caused by the weight is expressed:

$$-T = [(WT + ARM\ WT) - (SCALE\ READING)] \times L$$

When the scale reading is zero maximum negative torque is realized. When the scale reading equals the total weight of hanging weight plus arm weight, no torque is applied.

The torque applied in an upward direction or CW caused by the pull of the crane is expressed:

$$+T = [(SCALE\ READING) - (WT + ARM\ WT)] \times L$$

When the scale reading is twice the total weight plus arm weight, maximum positive torque is realized.

Distance from the centerline of the output flange and dial indicator is 12.7 inches and the angular deflection is shown in milliradians.

3.3.7 MOMENT STIFFNESS

A static elevation moment was applied to the drive in both directions. Dial indicators were located in top and bottom positions. With the drive side-wall mounted, an I-beam was attached to the flange on the cover. A weight was placed at the end of the beam. At that same point, a scale was attached and fastened to an overhead crane. Procedure is similar to the torsional stiffness test in 3.3.6. See Photographs 16 and 17.

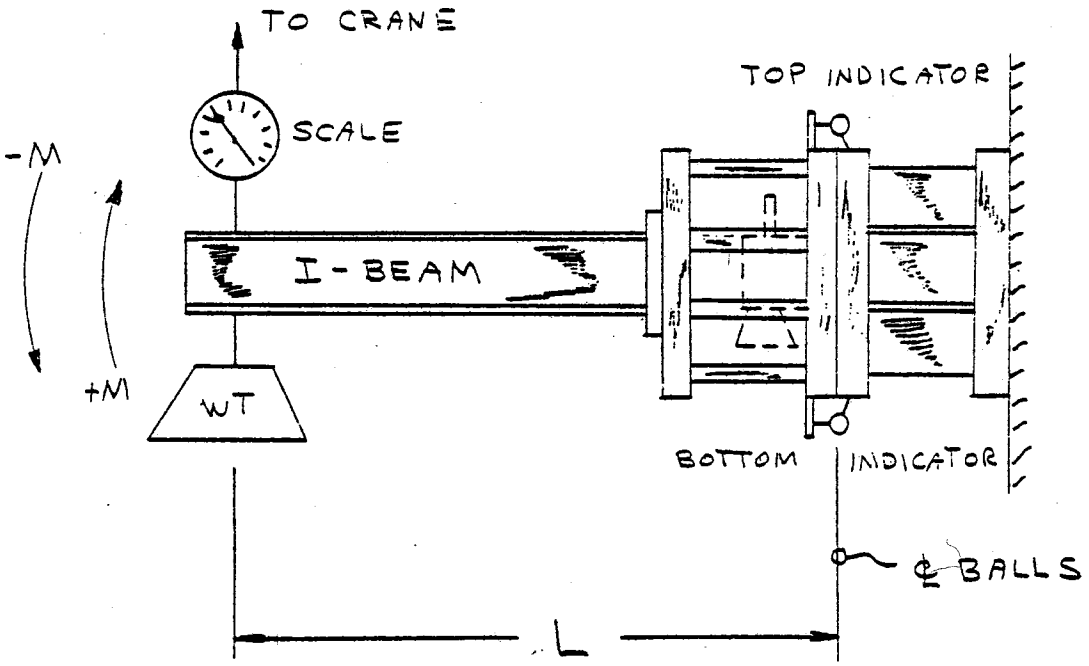

The moment applied in a downward direction caused by the weight is expressed:

$$-M = [(WT) - (SCALE\ READING)] \times L$$

The weight of the beam is neglected here.

The moment applied in an upward direction caused by the pull of the crane is expressed:

$$+M = [(SCALE\ READING) - (WT)] \times L$$

Deflection is expressed in total milliradians, the sum of the top and the bottom dial indicators. Distance between indicators is 25.63 inches.

3.3.8 BACKDRIVING

A 7,800 ft.-lb. or 93,600 in.-lb. load was applied to the drive to determine if backdriving would occur. A dial indicator was installed on the input shaft to determine any movement. The drive was side-wall mounted.

3.4 TEST RESULTS - UNIT 1

Tablulated data and graphical results are located in Appendix B-2 covering Unit 1.

3.4.1 TORQUE, HORSEPOWER, AND EFFICIENCY

Refer to Figures 1, 2, and 3. Test was performed in both directions of rotation, reference being made to the extension end of the input shaft.

"CCW" ROTATION

No load input torque	=	3.0 in. lbs.
No load input H. P.	=	0.0853 H. P.
No load input speed	=	1793 RPM
Efficiency @ 46,800 in.-lbs.	=	12.92%
Input torque @ 46,800 in.-lbs.	=	6.9 in.-lbs.
Input horsepower @ 46,800 in.-lbs.	=	0.1957 H. P.
Gear Mesh Loss @ 46,800 in.-lbs.	=	0.1104 H. P.

where: G.M.L. = Total Input - No Load Loss
G.M.L. = .1957 H. P. - .0853 H. P.
G.M.L. = 0.1104 H. P.

"CW" ROTATION

No load input torque	=	3.9 in.-lbs.
No load input H. P.	=	0.1110 H. P.
No load input speed	=	1793 RPM
Efficiency @ 46,800	=	12.73%
Input torque @ 46,800 in.-lbs.	=	7.0 in.-lbs.
Horsepower input @ 46,800 in.-lbs.	=	0.1986 H. P.
Gear Mesh Loss @ 46,800 in.-lbs.	=	0.0876 H. P.

where: G.M.L. = .1986 - .1110
G.M.L. = .0876 H. P.

Overall performance in both directions of rotation was very similar.

3.4.2 BREAK LOOSE FRICTION TORQUE

Break loose or friction drag torque was measured at 2.5 in.-lbs. at the input shaft and was very consistent in three positions. This was a no load condition. See Figure 4.

3.4.3 BACKLASH

Backlash at two positions showed 8-1/2 and 8-3/4 total turns at the input. A third position showed 5-1/4 turns. See Figure 5.

3.4.4 TORSIONAL STIFFNESS

Repeatability of data at three positions was very good. Figures 6, 7, and 8 show graphically test results. Figure 9 lists the tabulated data. Hysteresis was very low.

$$\text{TORSIONAL STIFFNESS} = \frac{2 \times 27{,}500 \text{ IN-LB}}{0.00182 \text{ RADIANS}}$$

$$\text{TORSIONAL STIFFNESS} = 0.302 \times 10^{8} \text{ IN-LB/RAD}$$

$$\text{TORSIONAL COMPLIANCE} = \frac{1}{0.302 \times 10^{8}}$$

$$\text{TORSIONAL COMPLIANCE} = 3.3 \times 10^{-8} \text{ RAD/IN-LB}$$

These graphs can also be used to estimate the backlash from torsional stiffness. The movement at zero torque is an indication of system backlash. Using Figure 6:

Backlash @ input = (1.6-0.6) milliradians = 1.0 milliradian = 0.001 radian.

0.001 rad. x57.3 = 0.0573 degrees x 52495.625 = 3008 degrees ÷360 = 8.35 turns.

This is very close to the actual backlash found in 3.4.3.

3.4.5 MOMENT STIFFNESS

Repeatability of data for two cycles tested was good. Figures 10 and 11 show clearly the linearity between deflection and load. hysteresis was very low.

The moment was applied in both directions.

$$\text{MOMENT STIFFNESS} = \frac{2 \times 23,850 \text{ IN-LB}}{0.000206 \text{ RADIANS}}$$

$$\underline{\text{MOMENT STIFFNESS} = 2.31 \times 10^{8} \text{ IN-LB/RAD}}$$

$$\text{MOMENT COMPLIANCE} = \frac{1}{2.31 \times 10^{8}}$$

$$\underline{\text{MOMENT COMPLIANCE} = 0.43 \times 10^{-8} \text{ RAD/IN-LB}}$$

3.4.6 BACKDRIVING

Applied a 7800 ft.-lb. or 93,600 in.-lb. load in both directions with no indication of the drive backdriving.

3.5 TEST RESULTS - UNIT 2

Tabulated data and graphical results are located in Appendix B-3 for Unit 2.

3.5.1 TORQUE, HORSEPOWER, AND EFFICIENCY

Refer to Figures 12, 13, and 14. These are results taken during tests to raise a load on an attached arm on the output.

"CCW" ROTATION (RAISE LOAD)

No load input torque	=	3.4 in.-lbs.
No load input H. P.	=	0.0967 H. P.
No load input speed	=	1793 RPM
Efficiency @ 46,800 in.-lbs.	=	10.49%
Input torque @ 46,800 in.-lbs.	=	8.5 in.-lbs.
Input horsepower @ 46,800 in.-lbs.	=	0.240 H. P.
Gear Mesh Loss @ 46,800 in.-lbs.	=	0.144 H. P.
where: G.M.L. = .2407 - .0967	=	
G.M.L. = .144 H. P.		

3.5.2 BREAK LOOSE FRICTION TORQUE

Figure 15 shows the break loose friction torque at the input shaft between 2.0 - 2.3 in.-lbs. in one direction and 2.5 - 3.0 in.-lbs. in the other direction. Data was consistent in three positions.

3.5.3 BACKLASH

See Figure 16. Backlash was checked at three positions and expressed in degrees of rotation at the input shaft. Results show 230, 280, and 270 degrees. This was much lower than found in Unit 1 (3.4.3).

3.5.4 TORSIONAL STIFFNESS

Two readings were taken at the same position. Figure 17 shows the results of the first reading. Indications are that some movement had occurred and even caused permanent slippage. The excessive deflection is noted when the torque changes direction. Hysteresis is very high.

Figure 18 shows results of the second reading, after bolt tightness was rechecked. The permanent deflection was nearly eliminated and the total deflection was reduced from 4.26 to 3.66 milliradians. However, the deflection was still about twice as much as had occurred on Unit 1. The source of the apparent movement is not known.

$$\text{TORSIONAL STIFFNESS} = \frac{2 \times 31{,}050 \text{ IN-LB}}{0.00366 \text{ RADIANS}}$$

$$\text{TORSIONAL STIFFNESS} = 0.169 \times 10^{8} \text{ IN-LB/RAD}$$

$$\text{TORSIONAL COMPLIANCE} = \frac{1}{0.169 \times 10^{8}}$$

$$\text{TORSIONAL COMPLIANCE} = 5.92 \times 10^{-8} \text{ RAD/IN-LB}$$

3.5.5 MOMENT STIFFNESS

Repeatability of data for two test readings was good. See Figures 20 and 21. Linearity between deflection and load was very good. Hysteresis is still small.

$$\text{MOMENT STIFFNESS} = \frac{2 \times 23{,}850 \text{ IN-LB}}{0.000234 \text{ RADIANS}}$$

$$\text{MOMENT STIFFNESS} = 2.04 \times 10^{8} \text{ IN-LB/RAD}$$

$$\text{MOMENT COMPLIANCE} = \frac{1}{2.04 \times 10^{8}}$$

$$\text{MOMENT COMPLIANCE} = 0.49 \times 10^{-8} \text{ RAD/IN-LB}$$

3.5.6 BACKDRIVING

A torque of 7800 ft.-lbs. or 93,600 in.-lbs. was applied to the output shaft without any movement on the input confirming the non-backdriving condition.

APPENDIX B-1

TEST SUMMARY CHART

TEST DATA SUMMARY CHART

FORD AEROSPACE AZIMUTH DRIVE - UNITS 1 & 2

ITEM	PARAMETER	UNIT 1	UNIT 2
1	NO LOAD INPUT TORQUE _____ IN-LB	3.45	3.40
2	" " " SPEED _____ RPM	1793	1793
3	" " " HORSEPOWER _____ HP	0.0981	0.0967
	AT LOAD TORQUE OF 46,800 IN-LB:		
4	EFFICIENCY _____ %	12.82	10.49
5	INPUT TORQUE _____ IN-LB	6.95	8.50
6	INPUT HORSEPOWER _____ HP	0.1971	0.240
7	GEAR MESH LOSS _____ HP	0.099	0.144
8	BREAK LOOSE FRICTION TORQUE _____ IN-LB	2.5	2.5
9	BACKLASH @ INPUT _____ DEGREES	3105	260
10	TORSIONAL STIFFNESS _____ IN-LB/RAD.	0.302×10^{8}	0.169×10^{8}
11	TORSIONAL COMPLIANCE _____ RAD./IN-LB	3.3×10^{-8}	5.92×10^{-8}
12	MOMENT STIFFNESS _____ IN-LB/RAD.	2.31×10^{8}	2.04×10^{8}
13	MOMENT COMPLIANCE _____ RAD./IN-LB	0.43×10^{-8}	0.49×10^{-8}
14	BACKDRIVING _____	NO	NO

DATA IS AVERAGED FOR EACH UNIT WHERE MULTIPLE DATA TAKEN

APPENDIX B-2

TEST RESULTS - UNIT 1

FIG 1 - INPUT HORSEPOWER AND TORQUE

FORD AEROSPACE AZIMUTH DRIVE S.N. D 65133-20-1

UNIT 1

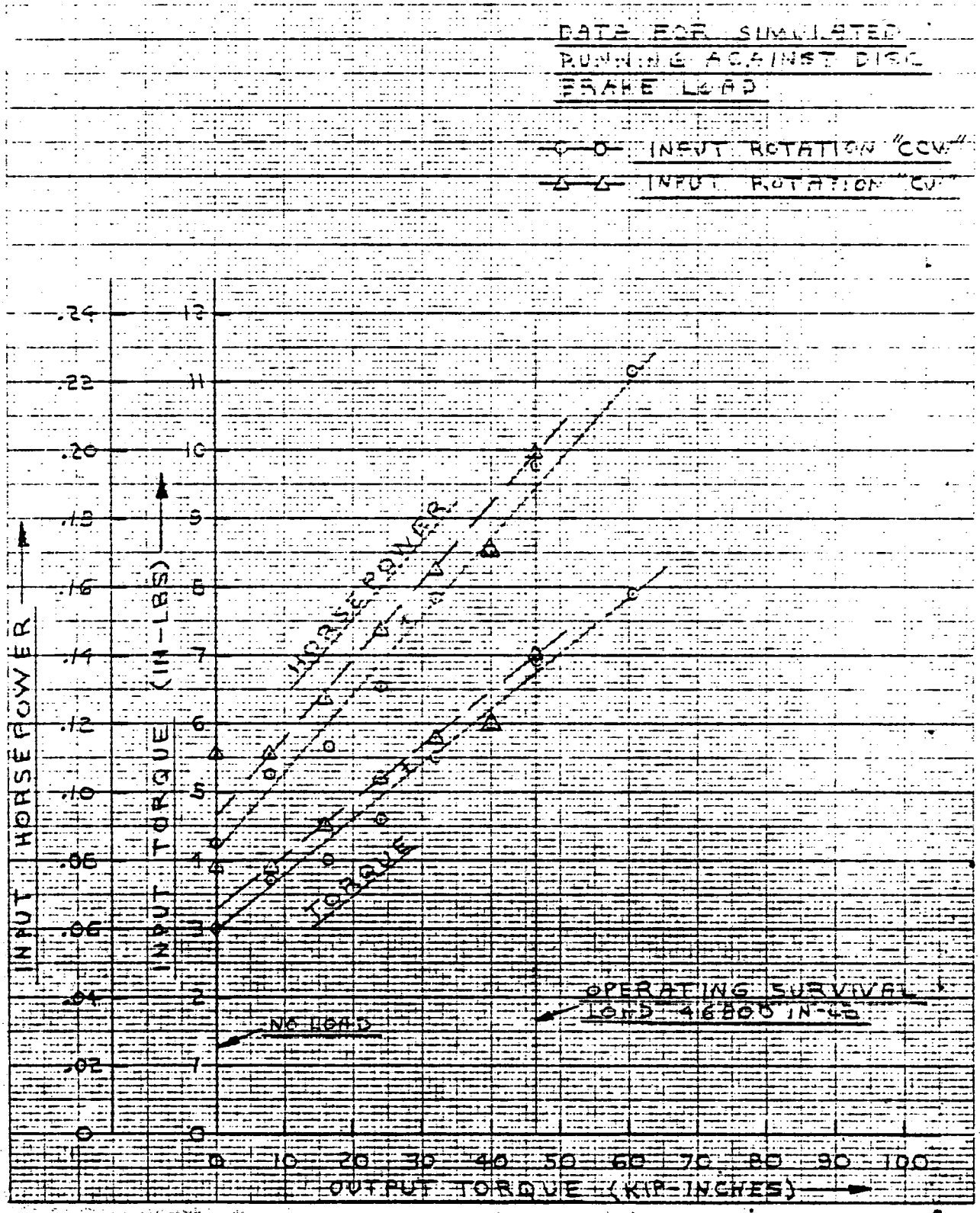

FIG 2 - EFFICIENCY

FORD AEROSPACE AZIMUTH DRIVE S.N. D651133-21-1

UNIT 1

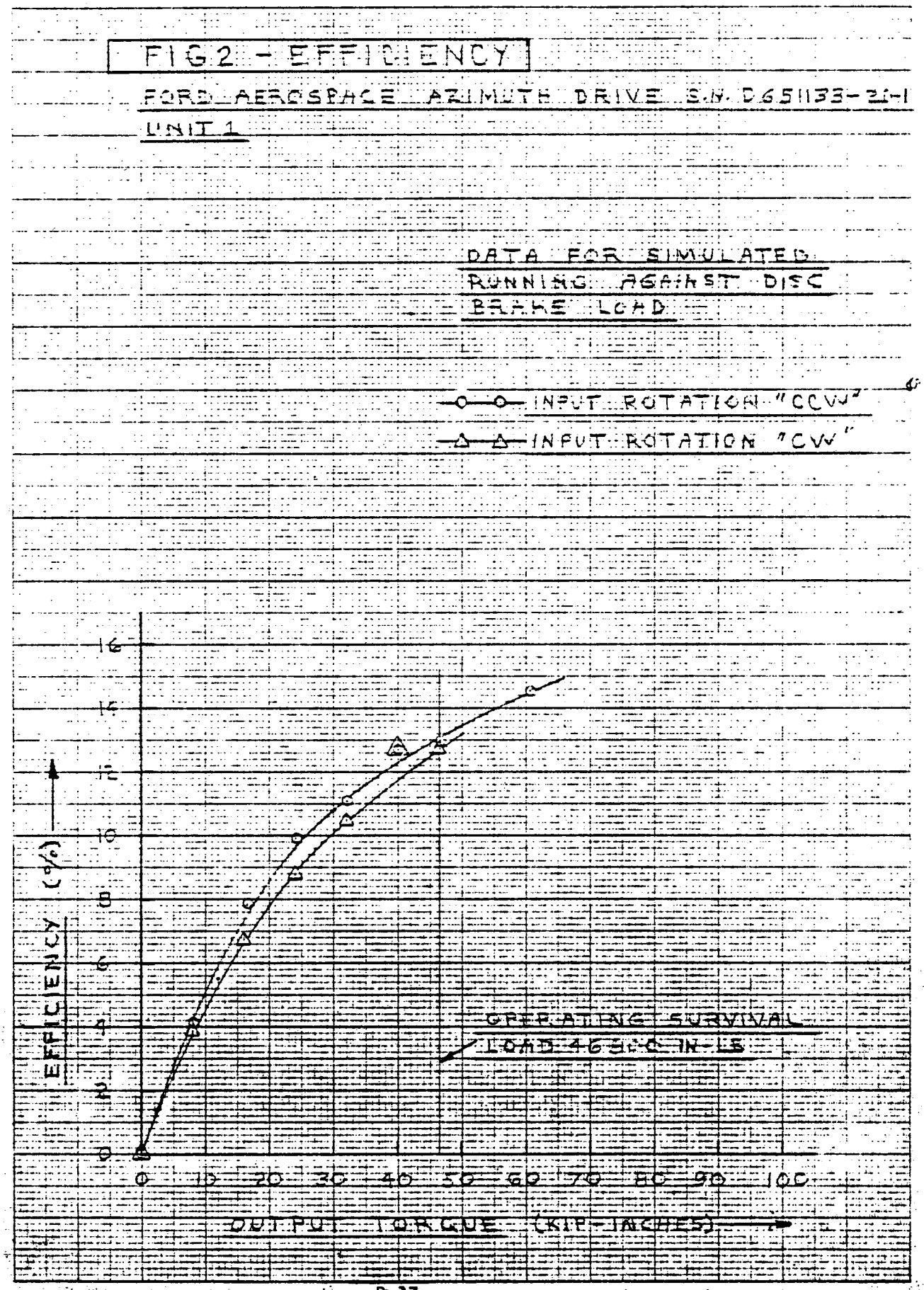

FIG 3 - EFFICIENCY DATA

FORD AEROSPACE AZIMUTH DRIVE S.N. DGS1133-2D-1 UNIT/1
DATA TAKEN UNDER SIMULATED RUNNING AGAINST A DISC-BRAKE LOAD UNIT FLOOR-MOUNTED

LOAD CONDTION	OUTPUT SCALE (LBS)	OUTPUT TORQUE (IN-LB)	OUTPUT H.P.	INPUT VOLTS (DCV)	INPUT TORQUE (IN-LB)	INPUT ROTATION	INPUT SPEED (RPM)	INPUT H.P.	EFF. (%)
NO LOAD →	0	0	0	.012	3.0	CCW	1793.11	.0853	—
	200	8000	.00433	.014	3.7		1792.31	.1052	4.119
	410	16400	.00886	.0155	4.0		1792.64	.1137	7.815
	600	24000	.01299	.017	4.6		1791.03	.1307	9.940
	800	32000	.01731	.020	5.5		1789.91	.1562	11.083
	1000	40000	.02162	.022	6.0		1788.84	.1702	12.706
OPERATING →	1170	46800	.02529	.024	6.9		1788.30	.1957	12.926
	1510	60400	.03259	.028	7.9		1785.22	.2237	14.562
	1750	70000		.033	9.2				
	2000	80000		.037	10.5	↓			
	2100	84000				CCW			
NO LOAD →	0	0	0	.009	3.9	CW	1793.92	.1110	—
	200	8000	.00433	.009	3.9		1792.85	.1109	3.907
	400	16000	.00866	.011	4.5		1791.12	.1278	6.773
	600	24000	.01298	.014	5.2		1789.88	.1476	8.792
	800	32000	.01730	.0155	5.8		1789.03	.1646	10.512
	1000	40000	.02162	.016	6.0		1788.99	.1703	12.699
OPERATING →	1170	46800	.02529	.0185	7.0		1788.42	.1986	12.735
	2000	80000		.029	10.0	CW			

FIG 4 – INPUT BREAKAWAY TORQUE

FORD AEROSPACE AZIMUTH DRIVE S.N. D651133-2D-1

UNIT 1

LOAD ON OUTPUT (IN-LB)	POSITION(1)	INPUT TORQUE(2)	
		CW (IN-LB)	CCW (IN-LB)
NONE	1	2.0	2.5
NONE	2	2.5	2.5
NONE	3	2.5	2.5
46800(3)	3	—	7.5

(1) ORIENTATION OF OUTPUT APPROX. 120° APART

(2) STATICALLY DETERMINED; 0–6 IN-LB TQ. WRENCH

(3) TORQUE MEASURED TO DRIVE LOAD

FIG 5 – BACKLASH

FORD AEROSPACE AZIMUTH DRIVE S.N. D651133-2D-1

UNIT 1

POSITION(1)	BACKLASH (TOTAL TURNS OF INPUT SHAFT)	BACKLASH(2) (DEGREES @ OUTPUT)
1	8 3/4 TURNS	0.0600°
2	8 1/2 "	0.0583°
3	5 1/4 "	0.0360°

(1) ORIENTATION OF OUTPUT APPROX. 120° APART

(2) BACKLASH = $\frac{(\text{TURNS ON INPUT}) \times 360^\circ}{52495}$

FIG 6 - TORSIONAL STIFFNESS

FORD AEROSPACE AZIMUTH DRIVE S.N. D65133-201

UNIT 1

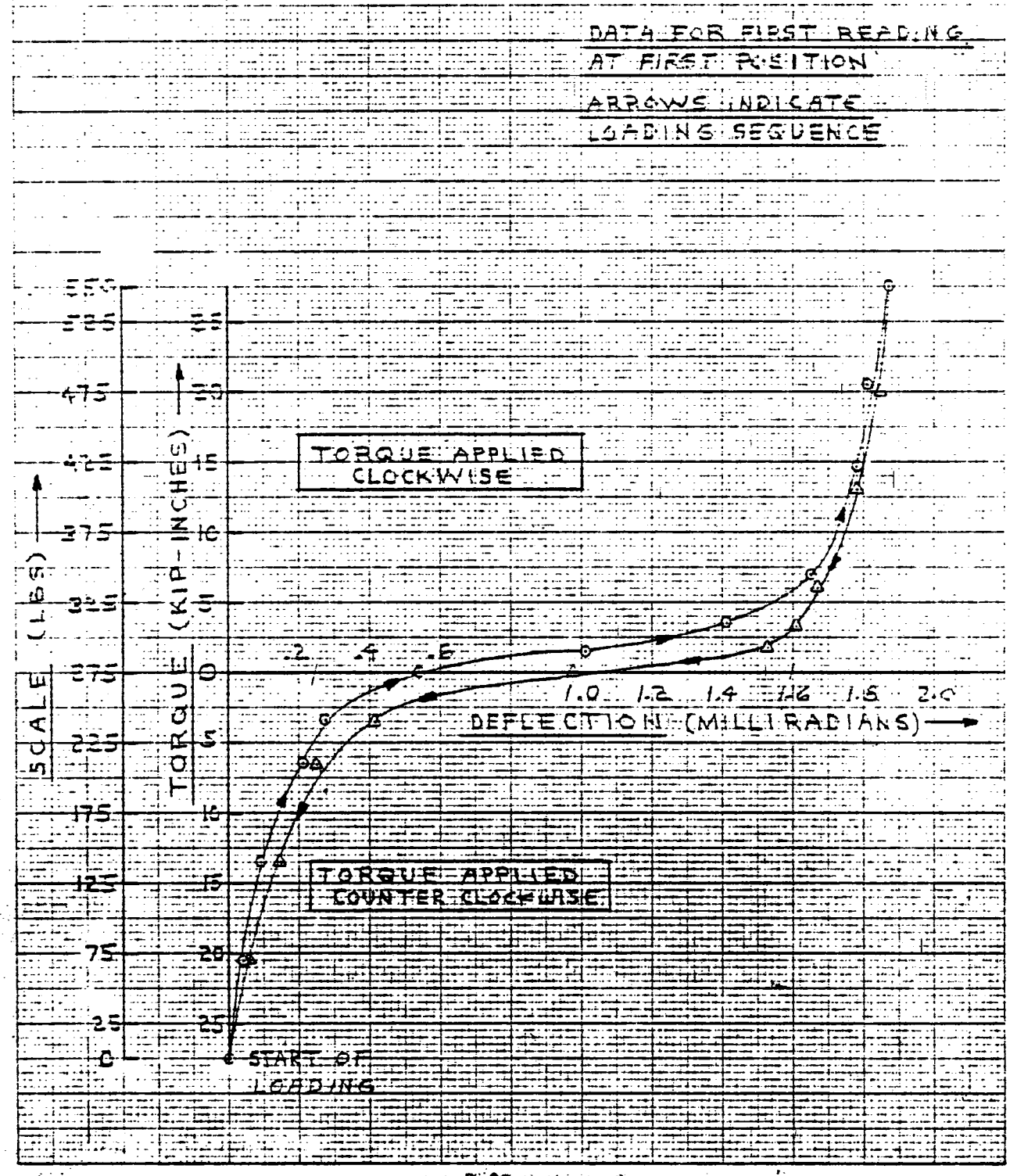

FIG 7 - TORSIONAL STIFFNESS

FORD AEROSPACE AZIMUTH DRIVE S.N. D65HZ8-2D-1

UNIT 1

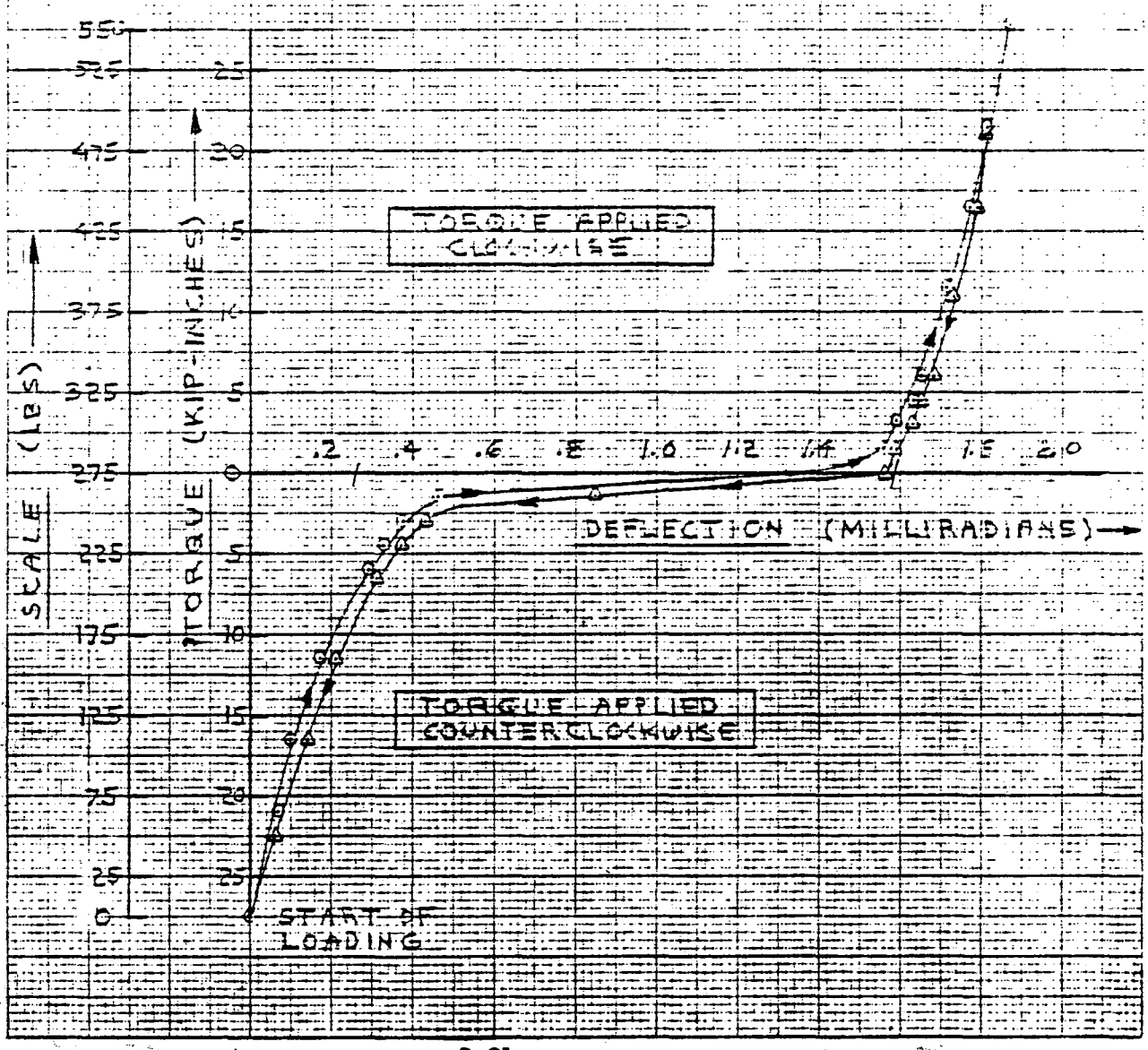

FIG 8 - TORSIONAL STIFFNESS

FORD AEROSPACE AZIMUTH DRIVE S.N. D6511B2-3D-1

UNIT 1

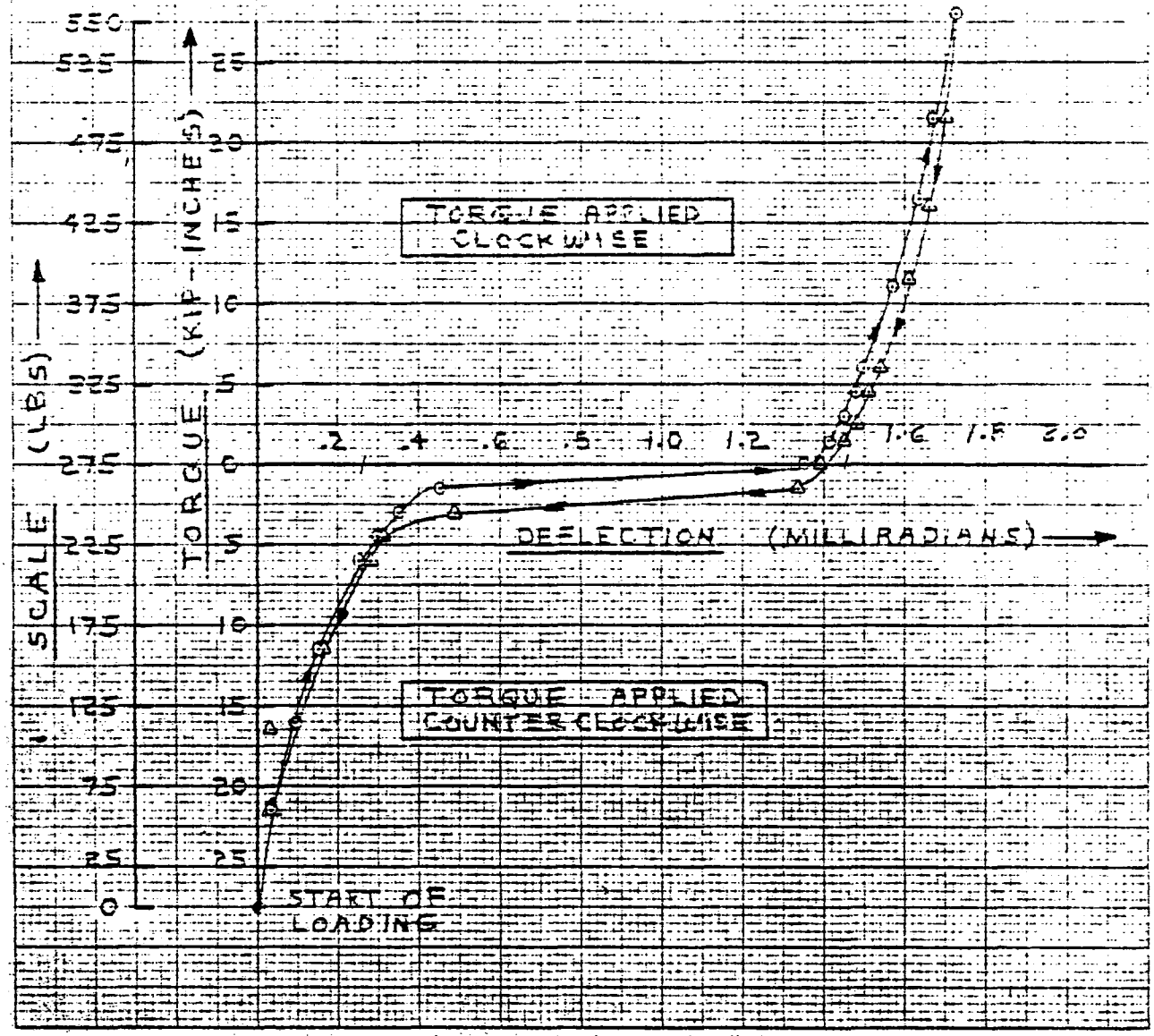

FIG 9 - TORSIONAL STIFFNESS

FORD AEROSPACE AZIMUTH DRIVE S.N. D651133-2D-1

UNIT 1

SCALE (1) (LBS)	DEFLECION (IN.)	SCALE (1) (LBS)	DEFLECTION (IN.)
1ST READING	1ST POSITION	2ND READING	1ST POSITION
0	0	0	0
70	.0005	70	.0005
140	.0012	140	.0014
210	.0027	215	.0030
242	.0035	240	.0038
276 (2)	.0069	270	.0076
290	.0129	290	.0155
310	.0180	310	.0196
345	.0210	339	.0207
421	.0226	410	.0221
480	.0230	480	.0230
550	.0238	550	.0237
475	.0235	480	.0233
405	.0227	405	.0224
335	.0212	340	.0213
308	.0205	311	.0205
292	.0195	290	.0190
276 (2)	.0125	270	.0100
240	.0053	240	.0050
210	.0032	208	.0030
140	.0019	140	.0018
70	.0008	70	.0005
0	0	0	-.0004

(1) SCALE ARM LENGTH = 100 IN.

TORQUE CHANGES DIRECTION AT A SCALE LOAD OF 276 LB

2) EFFECTIVE TORQUE ON UNIT IS ZERO

FIG 9 - TORSIONAL STIFFNESS

FORD AEROSPACE AZIMUTH DRIVE S.N. D631133-2D-1

UNIT 1

SCALE (1) (LBS)	DEFLECION (IN.)
1ST READING – 2ND POSITION	
0	0
65	.0008
110	.0013
160	.0022
215	.0037
230	.0041
245	.0048
260	.0059
275 (2)	.0169
290	.0198
308	.0202
320	.0208
335	.0210
390	.0218
440	.0225
490	.0230
554	.0238
485	.0231
440	.0228
384	.0220
335	.0213
320	.0210
305	.0208

SCALE (1) (LBS)	DEFLECTION (IN.)
290	.0202
275 (2)	.0198
260	.0105
245	.0055
230	.0048
210	.0039
160	.0027
110	.0018
60	.0008
0	–.0003
2ND READING – 2ND POSITION	
0	–.0005
65	.0004
112	.0010
160	.0020
215	.0033
230	.0038
245	.0045
260	.0055
275 (2)	.0157
290	.0198
305	.0204
330	.0210

(1) SCALE ARM LENGTH = 100 IN.
TORQUE CHANGES DIRECTION AT A SCALE LOAD OF 276

(2) EFFECTIVE TORQUE ON UNIT IS ZERO

FIG 9 - TORSIONAL STIFFNESS

FORD AEROSPACE AZIMUTH DRIVE S.N. D651133-2D-1

UNIT 1

SCALE (1) (LBS)	DEFLECION (IN.)
335	.0210
390	.0219
440	.0225
490	.0230
550	.0237
490	.0232
440	.0228
390	.0222
335	.0213
320	.0210
305	.0208
290	.0203
275 (2)	.0197
260	.0092
245	.0050
230	.0045
212	.0036
160	.0025
110	.0015
60	.0050
0	-.0005
1ST READING - 3RD POSITION	
0	0
60	.0004

SCALE (1) (LBS)	DEFLECTION (IN.)
114	.0012
160	.0019
215	.0032
230	.0038
245	.0044
260	.0058
275 (2)	.0172
290	.0180
305	.0184
320	.0189
335	.0191
390	.0200
440	.0208
490	.0213
555	.0220
490	.0216
440	.0211
390	.0205
335	.0196
320	.0192
300	.0188
290	.0185
275 (2)	.0177
260	.0171
245	.0050

(1) SCALE ARM LENGTH = 100 IN.

TORQUE CHANGES DIRECTION AT A SCALE LOAD OF 276 LE

(2) EFFECTIVE TORQUE ON UNIT IS ZERO

FIG 9 - TORSIONAL STIFFNESS

FORD AEROSPACE AZIMUTH DRIVE S.N. D651133-2D-1

UNIT 1

SCALE (1) (LBS)	DEFLECION (IN.)
230	.0039
215	.0036
160	.0021
110	.0004
60	.0002
0	-.0006
2ND READING - 3RD POSITION	
0	-.0006
60	-.0002
110	.0005
162	.0015
215	.0028
230	.0035
245	.0039
260	.0060
276 (2)	.0173
290	.0180
305	.0185
320	.0188
335	.0191
390	.0200
443	.0208
490	.0213
560	.0220

SCALE (1) (LBS)	DEFLECTION (IN.)
490	.0216
440	.0211
390	.0205
325	.0194
320	.0192
305	.0189
290	.0185
275 (2)	.0176
260	.0178
245	.0050
230	.0038
215	.0032
160	.0018
105	.0006
60	-.0002
0	-.0008

(1) SCALE ARM LENGTH = 100 IN.
TORQUE CHANGES DIRECTION AT A SCALE LOAD OF 276

(2) EFFECTIVE TORQUE ON UNIT IS ZERO

FIG 10 - MOMENT STIFNESS

FORD AEROSTACE AZIMUTH DRIVE S.N. DGE/82-20-1

UNIT 1

DATA FOR FIRST READING

ARROWS INDICATE LOADING SEQUENCE

EFFECTIVE MOMENT CHANGES DIRECTION AT 450 LB.

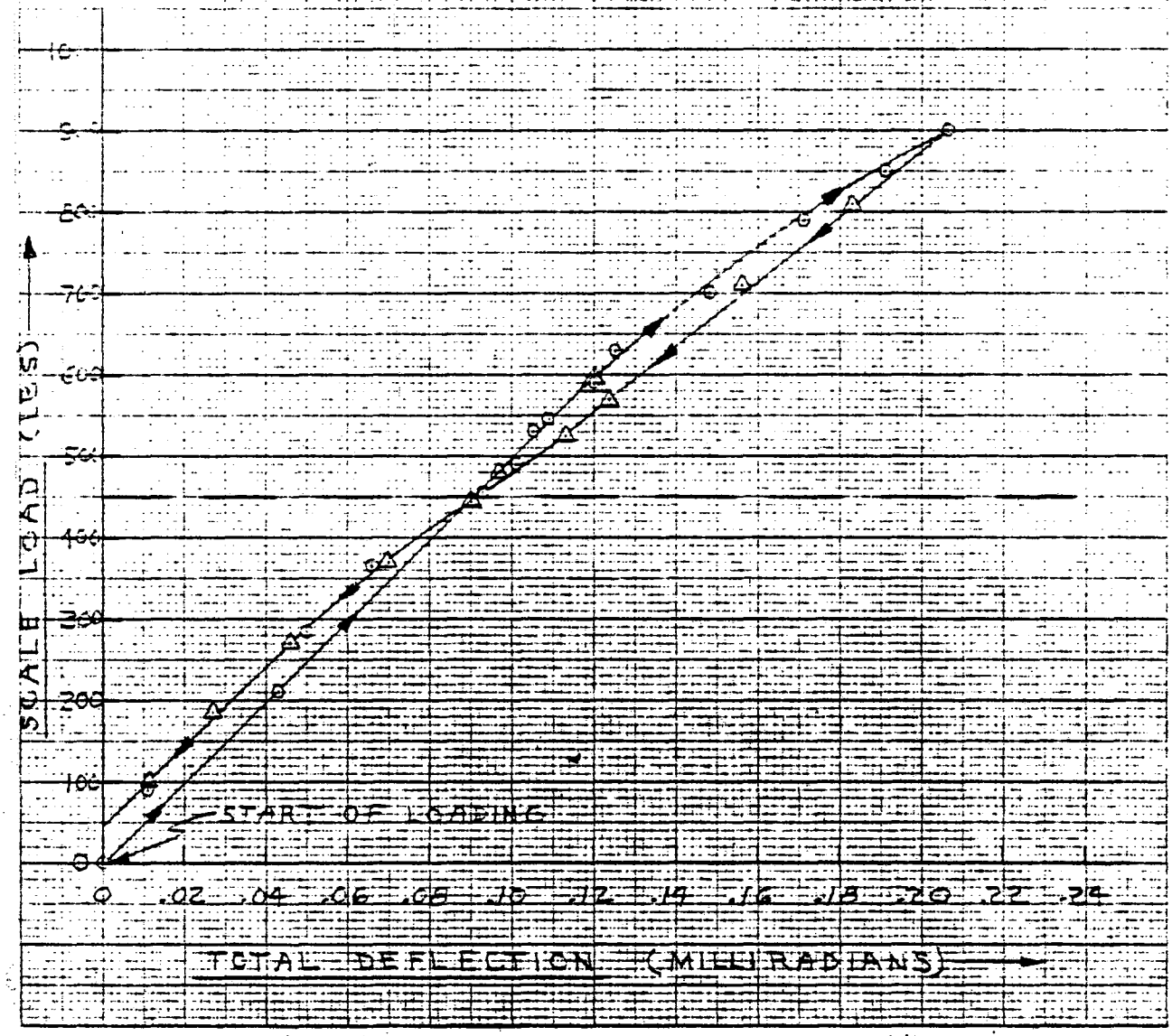

FIG 11 - MOMENT STIFFNESS

FORD AEROSPACE AZIMUTH DRIVE S.N. D651133-2D-1

UNIT 1

SCALE (1) (LBS)	TOP DEFLECTION (IN)	BOT. DEFLECTION (IN)
←	FIRST READING	→
0	0	0
90	0	−.0003
210	+.0002	−.0009
285	+.0003	−.0010
365	+.0005	−.0012
455 (2)	+.0007	−.0017
490	+.0008	−.0018
530	+.0008	−.0019
545	+.0008	−.0020
590	+.0009	−.0022
630	+.0009	−.0024
700	+.0010	−.0028
790	+.0011	−.0033
850	+.0012	−.0037
900	+.0013	−.0040
810	+.0012	−.0035
710	+.0010	−.0030
595	+.0008	−.0023
570	+.0009	−.0023
525	+.0008	−.0021
480	+.0007	−.0018
445	+.0006	−.0017

(1) SCALE ARM LENGTH = 53 IN.

(2) EFFECTIVE MOMENT ON UNIT IS ZERO AT 450 LB.

FIG 11 - MOMENT STIFFNESS

FORD AEROSPACE AZIMUTH DRIVE S.N. D651133-2D-1

UNIT 1

SCALE (1) (LBS)	TOP DEFLECTION (IN)	BOT. DEFLECTION (IN)
370	+.0005	-.0013
270	+.0003	-.0009
185	+.0002	-.0005
100	+.0001	-.0002
0	0	+.0001
←	SECOND READINGS	→
0	0	0
90	0	-.0003
180	+.0001	-.0006
300	+.0003	-.0010
350	+.0004	-.0012
450 (2)	+.0006	-.0015
555	+.0007	-.0020
630	+.0008	-.0023
755	+.0010	-.0031
850	+.0012	-.0038
910	+.0013	-.0042
850	+.0013	-.0038
715	+.0009	-.0030
580	+.0007	-.0022
500	+.0006	-.0019
430	+.0005	-.0016
315	+.0003	-.0011

(1) SCALE ARM LENGTH = 53 IN.

2) EFFECTIVE MOMENT ON UNIT IS ZERO AT 450 LB.

FIG 11 - MOMENT STIFFNESS

FORD AEROSPACE AZIMUTH DRIVE S.N. D651133-2D-1

UNIT 1

SCALE (1) (LBS)	TOP DEFLECTION (IN)	BOT. DEFLECTION (IN)
220	+.0002	-.0008
115	+.0000	-.0003
0	-.0001	+.0001

(1) SCALE ARM LENGTH = 53 IN.

APPENDIX B-3

TEST RESULTS - UNIT 2

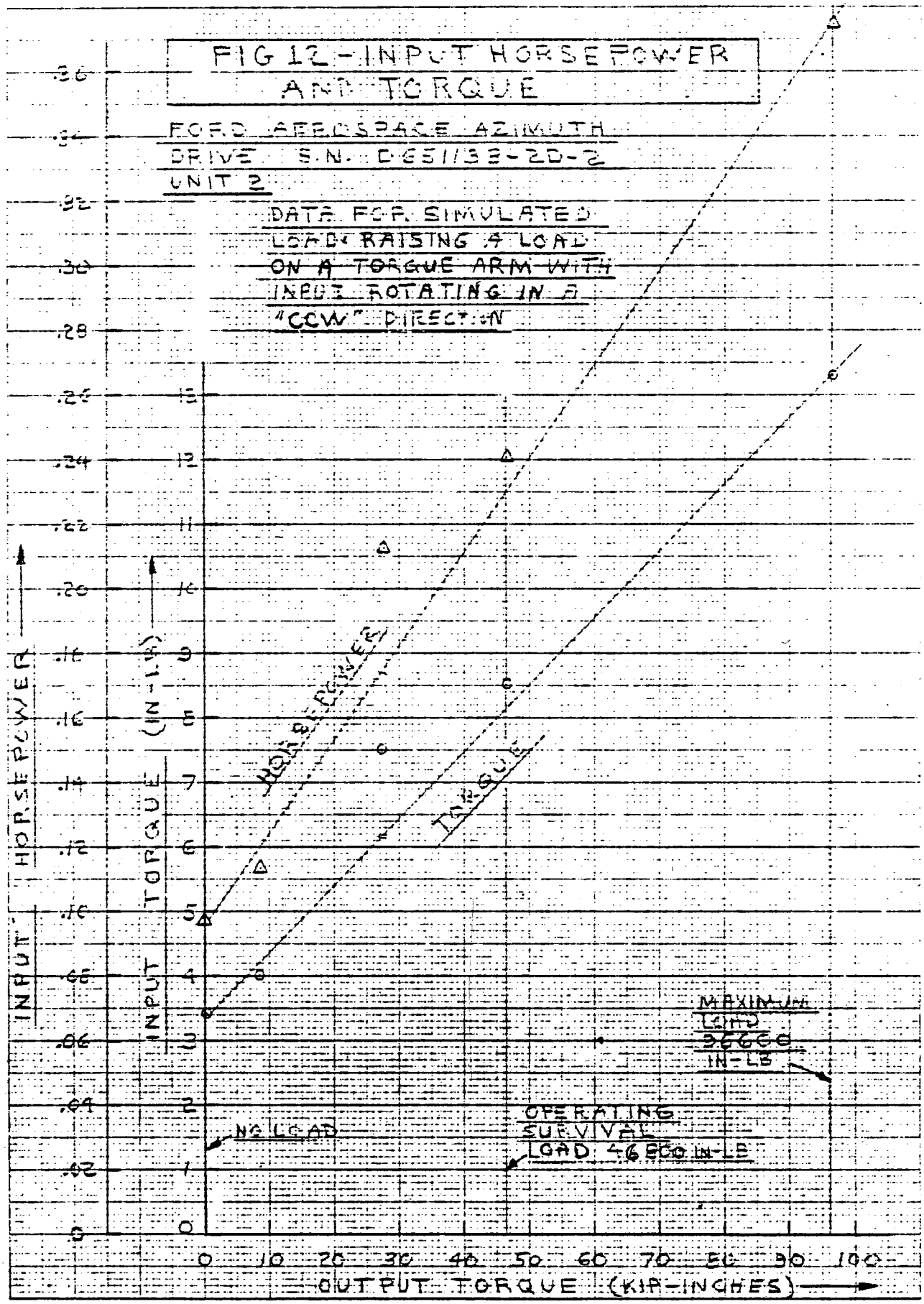

FIG 13 - EFFICIENCY

FORD AEROSPACE AZIMUTH DRIVE S.N. D65/1FE-2D-2
UNIT 2

DATA TAKEN UNDER SIMULATED LOAD: RAISING F LOAD ON A TORQUE ARM WITH INPUT ROTATING IN A "CCW" DIRECTION.

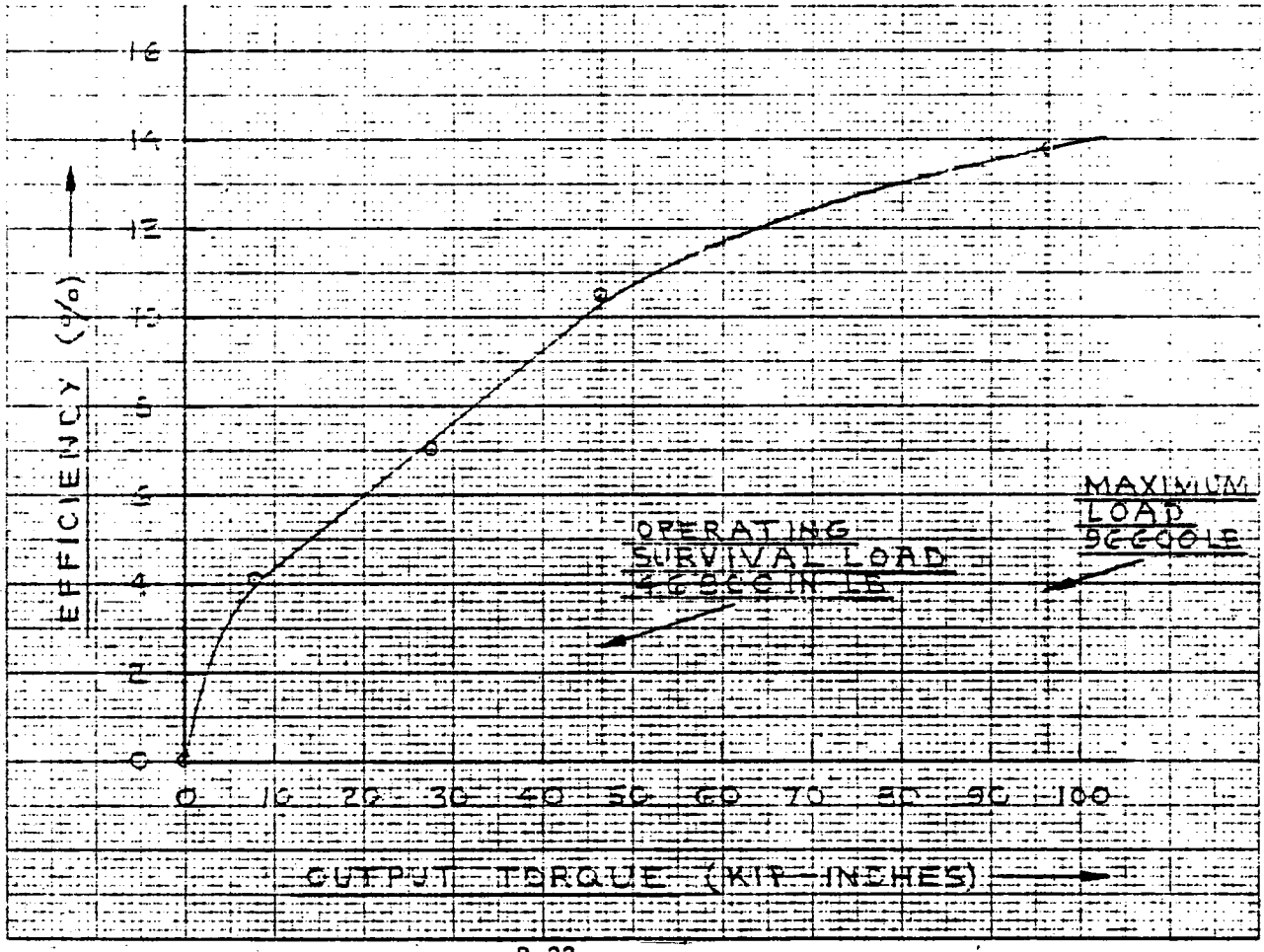

FIG 14 - EFFICIENCY DATA

FORD AEROSPACE AZIMUTH DRIVE S.N. DGS1133-2D-2 UNIT 2
DATA TAKEN UNDER SIMULATED LOAD RAISING WEIGHTS ON A TORQUE ARM WITH UNIT WALL MOUNTED

LOAD CONDITION	LOAD[1] WEIGHT (LB)	TORQUE ARM (IN)	OUTPUT[2] TORQUE (IN-LB)	OUTPUT H.P.	INPUT VOLTS (VDC)	INPUT TORQUE (IN-LB)	INPUT[3] ROT.	INPUT SPEED (RPM)	INPUT h.p.	EFF. (%)
NO LOAD	0	0	0	0	.013	3.4	CCW[3]	1792.94	0.0967	—
	0	90	8550	0.00463	.015	4.0		1792.59	0.1137	4.07
	450	42.33	27600	0.01492	.027	7.5		1789.25	0.2129	7.01
OPERATING	450	85	46800	0.02525	.0305	8.5		1785.38	0.2407	10.49
MAXIMUM	930	94.6	96600	0.05187	.0465	13.3	CCW	1776.67	0.3749	13.83
NO LOAD	0	0	0	0	.011	4.5	CW[3]	1793.70	0.1280	—
	0	90	8550	0.00463	.009	4.0		1793.90	0.1138	4.07
	450	42.33	27600	0.0149	.005	2.7		1794.24	0.0768	19.47
OPERATING	450	85	46800	0.0253	.009	4.0		1793.48	0.1138	22.28
MAXIMUM	930	94.6	96600	0.05234	.011	4.5	CW	1792.80	0.1280	40.89

(1) LOAD WEIGHT ADDED ON END OF TORQUE ARM
(2) TOTAL TORQUE IS SUM OF LOAD WEIGHT AND WEIGHT OF ARM (8550 IN-LB)
(3) "CCW" ROTATION RAISES LOAD WHILE "CW" LOWERS LOAD

FIG 15 - INPUT BREAKAWAY TORQUE

FORD AEROSPACE AZIMUTH DRIVE S.N. D651133-2D-2
UNIT 2

LOAD ON OUTPUT (IN-LB)	POSITION(1)	INPUT TORQUE(2)	
		CW (IN-LB)	CCW (IN-LB)
NONE	1	2.0	2.5
NONE	2	2.0	3.0
NONE	3	2.3	3.0
31050(3)	3	—	6.0

(1) ORIENTATION OF OUTPUT APPROX. 120° APART
(2) STATICALLY DETERMINED
(3) TORQUE TO RAISE UP LOAD

FIG 16 - BACKLASH

FORD AEROSPACE AZIMUTH DRIVE S.N. D651133-2D-2
UNIT 2

POSITION(1)	BACKLASH (DEGREES AT INPUT)	BACKLASH(2) (DEGREES AT OUTPUT)
1	230°	0.00438°
2	280°	0.00533°
3	270°	0.00514°

(1) ORIENTATION OF OUTPUT APPROX. 120° APART

(2) BACKLASH = $\frac{\text{BACKLASH @ INPUT}}{52495}$

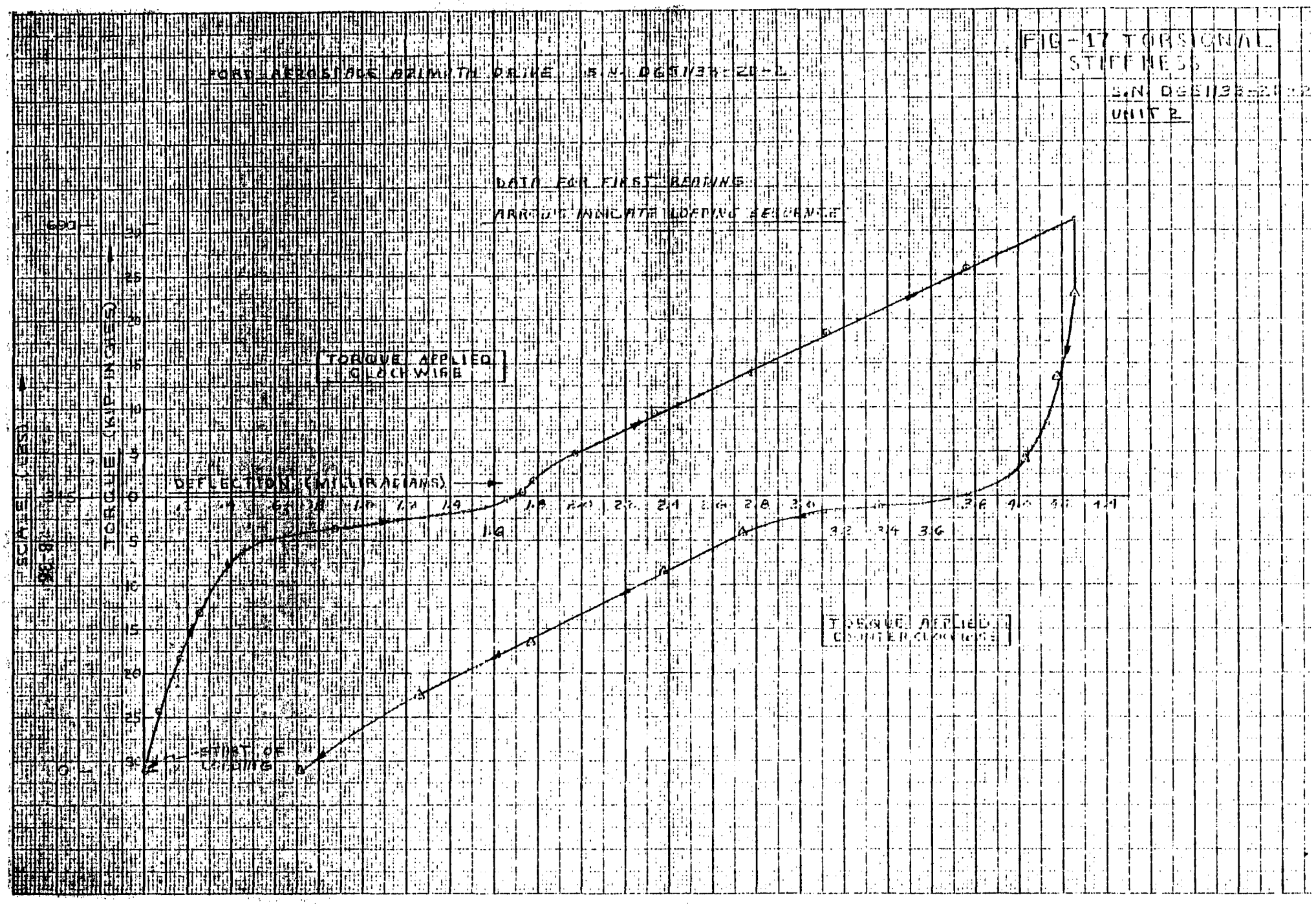
FIG-17 TORSIONAL STIFFNESS
FORE AEROBALLS AZIMUTH DRIVE S/N 0651132-201-L
UNIT 2
DATA FOR FIRST REVERSE
ARROW INDICATES LOADING SEQUENCE
TORQUE APPLIED CLOCKWISE
TORQUE APPLIED COUNTERCLOCKWISE
TORQUE (KIP-INCHES)
DEFLECTION (MILLIRADIANS)
SCALE 25-8
START OF LIMITING

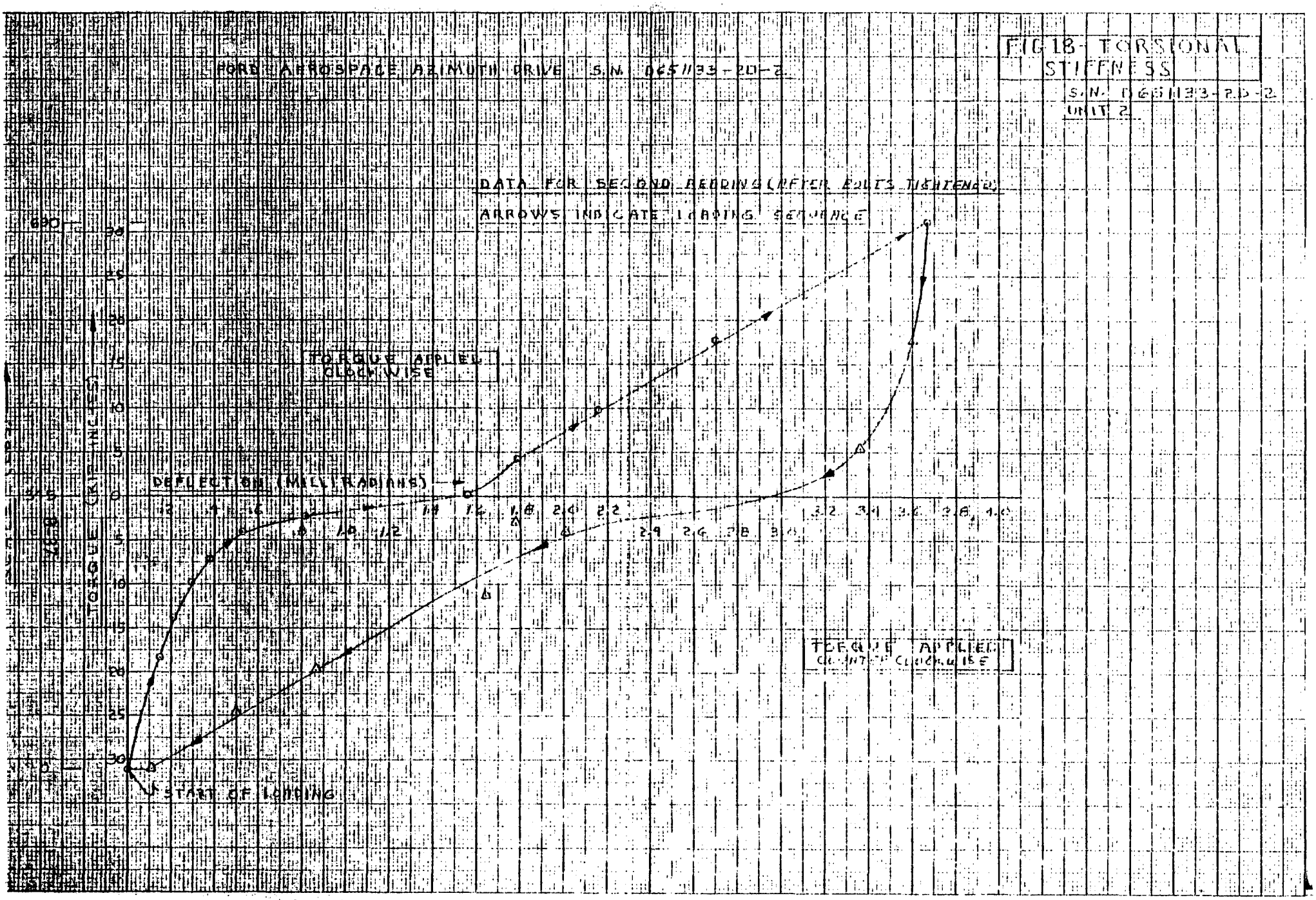
FIG 18- TORSIONAL STIFFNESS
S.N. 065133-20-2
UNIT 2
FORE AEROSPACE AZIMUTH DRIVE S.N. 065133-20-2
DATA FOR SECOND READING (AFTER BOLTS TIGHTENED)
ARROWS INDICATE LOADING SEQUENCE
TORQUE APPLIED CLOCKWISE
TORQUE APPLIED COUNTER CLOCKWISE
DEFLECTION (MILLIRADIANS)
TORQUE (FOOT POUNDS)
TORQUE (INCH POUNDS)
START OF LOADING

FIG 19 - TORSIONAL STIFFNESS

FORD AEROSPACE AZIMUTH DRIVE S.N. D651133-2D-2

UNIT 2

SCALE (1) (LBS)	DEFLECION (IN.)	SCALE (1) (LBS)	DEFLECTION (IN.)
← FIRST	READING →	← SECOND	READING (3) →
0	0	0	0
75	.0008	140	.0019
140	.0021	190	.0026
200	.0032	235	.0038
260	.0049	265	.0048
305	.0086	300	.0067
340	.0211	320	.0104
350 (2)	.0220	345 (2)	.0199
365	.0226	390	.0228
400	.0250	455	.0275
450	.0296	540	.0343
500	.0354	600	.0395
550	.0397	690	.0462
630	.0478	540	.0457
690	.0542	405	.0427
600	.0542	310	.0227
495	.0531	300	.0263
390	.0512	220	.0196
330	.0428	125	.0110
300	.0348	70	.0063
250	.0302	0	.0075
160	.0225		
95	.0161		
0	.0092		

(1) SCALE ARM LENGTH = 90 IN.

TORQUE CHANGES DIRECTION AT A SCALE LOAD OF 345 LB

(2) EFFECTIVE TORQUE ON UNIT IS ZERO

(3) CHECKED ALL MOUNTING BOLTS FOR TIGHTNESS FIRST

FIG 20 - MOMENT STIFFNESS

FORD AEROSPACE AZIMUTH DRIVE S.N. DGE/83-20-2 UNIT 2

DATA FOR FIRST READING

ARROWS INDICATE LOADING SEQUENCE

EFFECTIVE MOMENT CHANGES DIRECTION AT 45° LE.

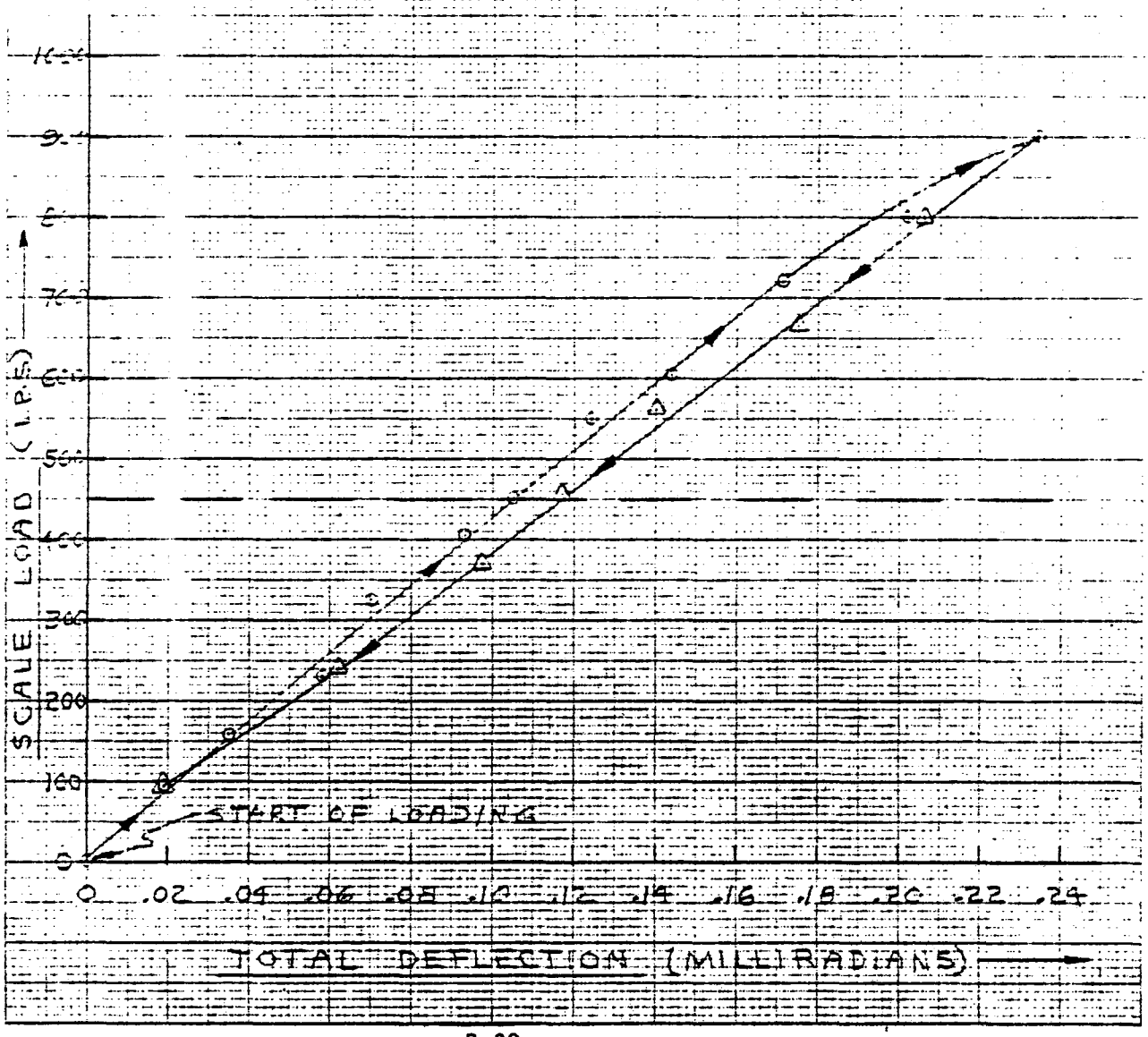

FIG 21 - MOMENT STIFFNESS

FORD AEROSPACE AZIMUTH DRIVE S.N. D651133-20-2

UNIT 2

SCALE (1) (LBS)	TOP DEFLECTION (IN)	BOT. DEFLECTION (IN)
←	FIRST READING	→
0	0	0
90	+.0003	-.0002
160	+.0005	-.0004
230	+.0007	-.0008
325	+.0008	-.0010
405	+.0011	-.0013
450 (2)	+.0012	-.0015
550	+.0013	-.0019
605	+.0016	-.0021
720	+.0018	-.0026
800	+.0021	-.0031
900	+.0023	-.0037
800	+.0021	-.0032
665	+.0018	-.0027
560	+.0015	-.0021
455 (2)	+.0012	-.0018
370	+.0011	-.0014
240	+.0007	-.0009
95	+.0003	-.0002
0	+.0001	+.0002

(1) SCALE ARM LENGTH = 53 IN.

(2) EFFECTIVE MOMENT ON UNIT IS ZERO AT 450 LB.

FIG 21 - MOMENT STIFFNESS

FORD AEROSPACE AZIMUTH DRIVE S.N. D651133-20-3
UNIT 2

SCALE (1) (LBS)	TOP DEFLECTION (IN)	BOT. DEFLECTION (IN)
←	SECOND READINGS	→
0	0	0
110	±.0003	−.0003
300	±.0008	−.0011
460 (2)	±.0012	−.0016
595	±.0015	−.0021
760	±.0018	−.0028
910	±.0022	−.0038
450 (2)	±.0012	−.0017
0	0	±.0001

(1) SCALE ARM LENGTH = 53 IN.

(2) EFFECTIVE MOMENT ON UNIT IS ZERO AT 450 LB.

APPENDIX B-4

PHOTOGRAPHS OF TEST UNIT

All photographs typical for Units 1 & 2 except #14 - Unit 2 only.

INDEX TO PHOTOGRAPHS

IN APPENDIX B-4

PHOTOGRAPH 1: Unit 1, prior to installation of test fixturing and instrumentation.

PHOTOGRAPH 2: Unit 1, another view of basic drive.

PHOTOGRAPH 3: Static dead-weight calibration of torque transducer used on input shaft torque measurements.

PHOTOGRAPH 4: Instrumentation used during testing.

PHOTOGRAPH 5: Unit 1, shown fully instrumented in a test stand. A disc brake assembly provides a means of dynamically loading the drive.

PHOTOGRAPH 6: Unit 1, closeup of the drive with motor removed. The dial indicator is used to determine backlash. No-load torque and breakaway torque are determined here also using a torque wrench.

PHOTOGRAPH 7: Unit 1, technician monitors backlash test.

PHOTOGRAPH 8: Unit 1, another view of the overall test stand and drive unit.

PHOTOGRAPH 9: Unit 1, closeup view of the torque transducer and graduated dial plate used in backlash measurements.

PHOTOGRAPH 10: Unit 1, closeup view of drive.

PHOTOGRAPH 11: Unit 1, similar to above.

PHOTOGRAPH 12: Unit 1, another overall look at drive with more detail to disc brake loading device.

PHOTOGRAPH 13: Unit 1, showing the test stand inverted 90°. An output arm is attached to the drive to provide a means of torsionally loading for stiffness tests.

PHOTOGRAPH 14: Unit 2, shown being readied to raise the attached weight load in an efficiency test.

PHOTOGRAPH 15: Unit 1, measurement of torsional deflection can be seen. Note the attached weighted arm and dial indicator.

PHOTOGRAPH 16: Unit 1, technician keeps an eye on tests to determine moment or elevation stiffness.

PHOTOGRAPH 17: Unit 1, a closer look at the two dial indicators used to determine moment stiffness.

PHOTOGRAPH 1

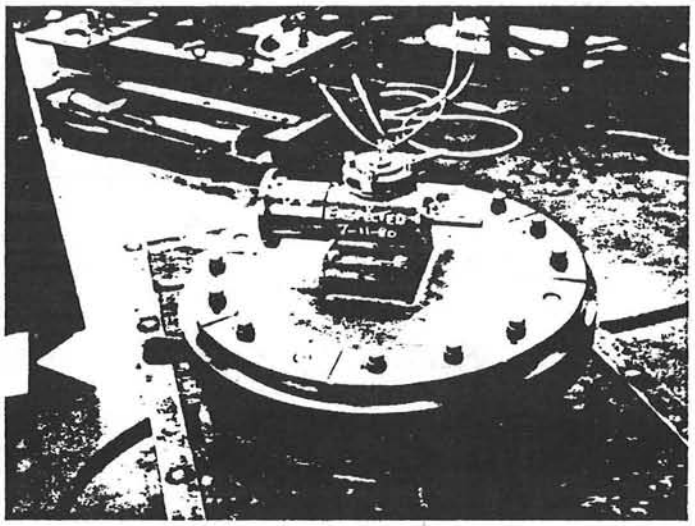

PHOTOGRAPH 2

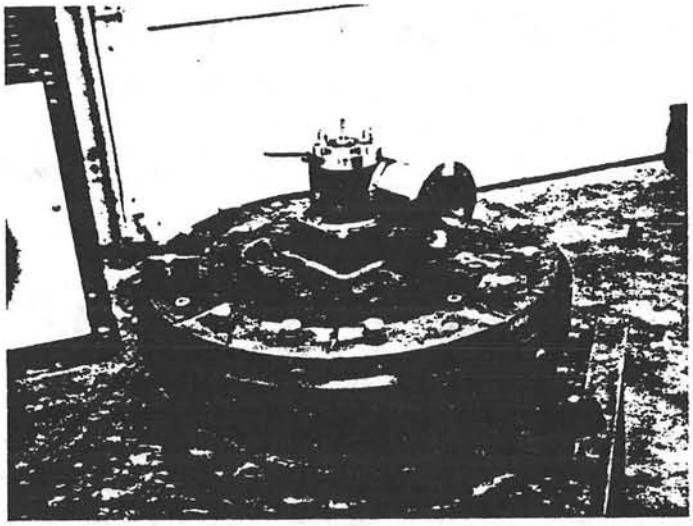

PHOTOGRAPH 3

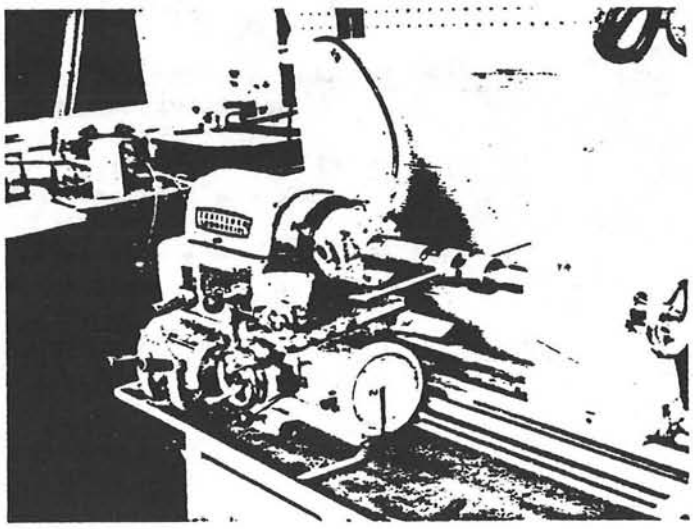

PHOTOGRAPH 4

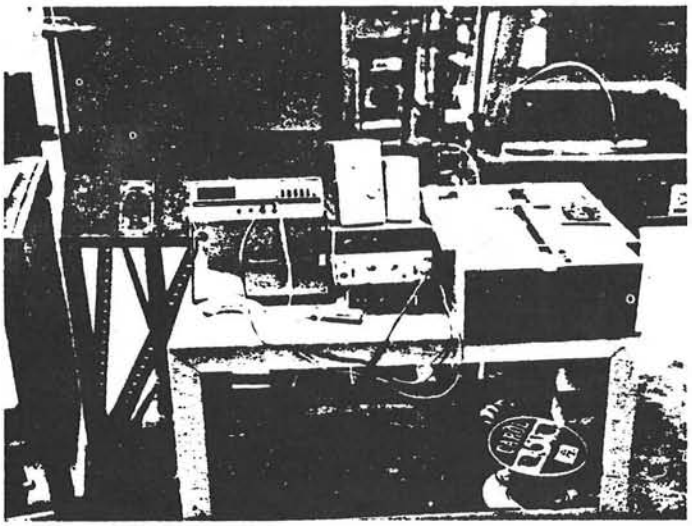

PHOTOGRAPH 5

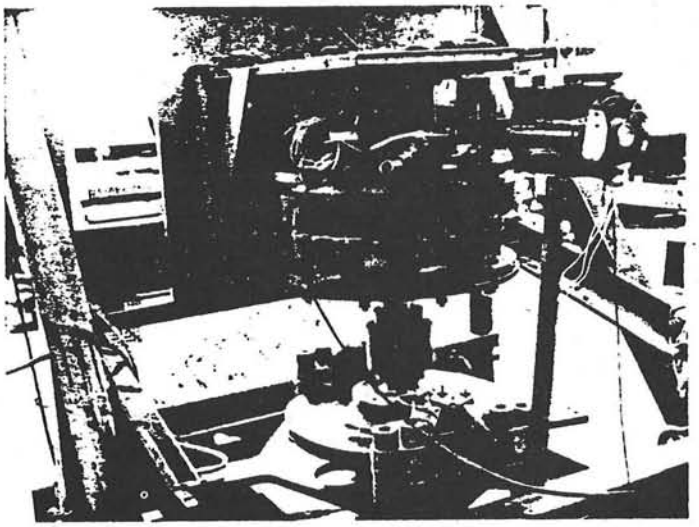

PHOTOGRAPH 6

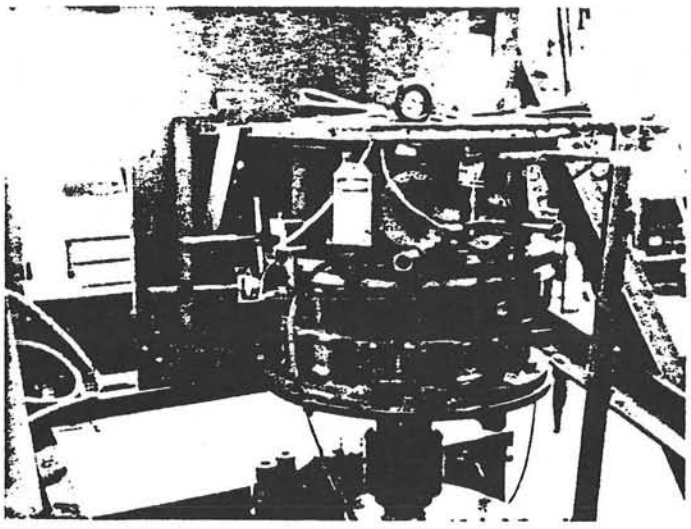

PHOTOGRAPH 7

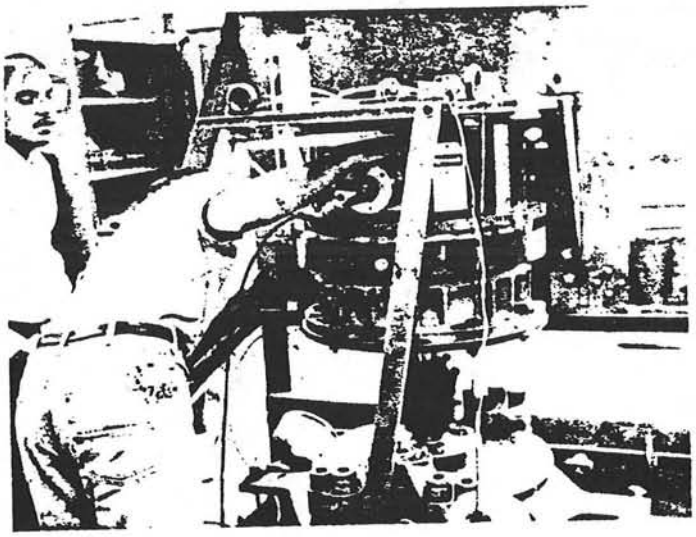

PHOTOGRAPH 8

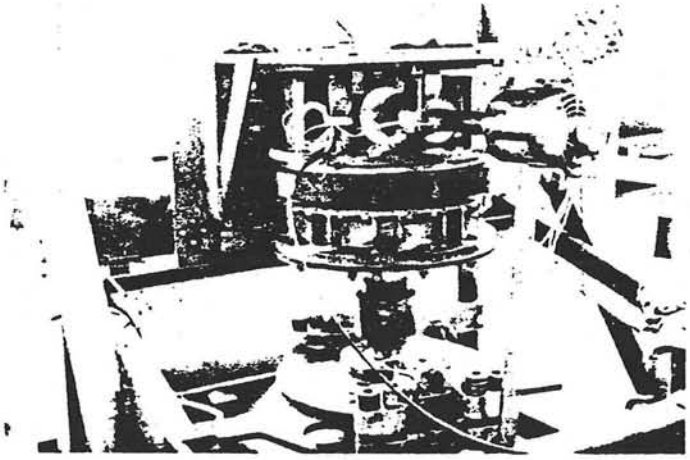

PHOTOGRAPH 9

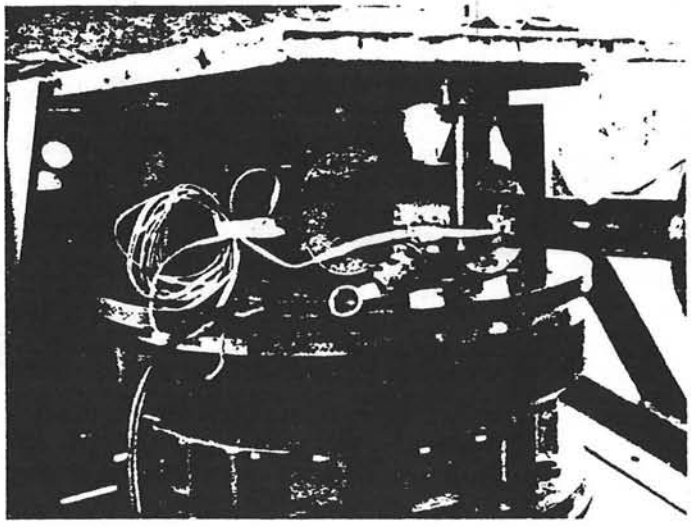

PHOTOGRAPH 10

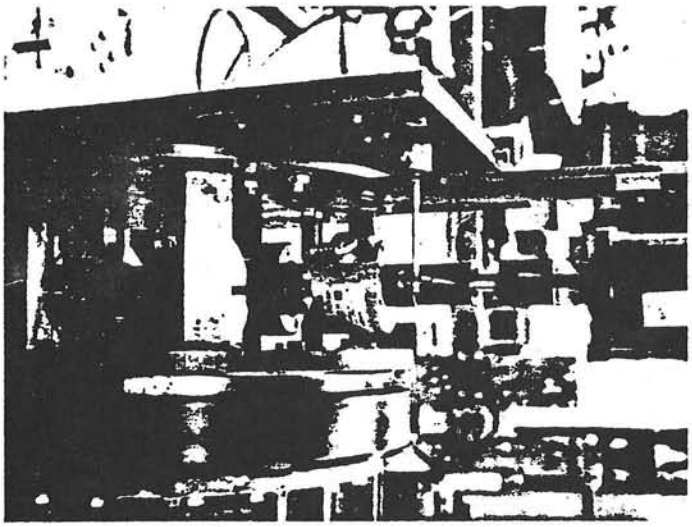

PHOTOGRAPH 11

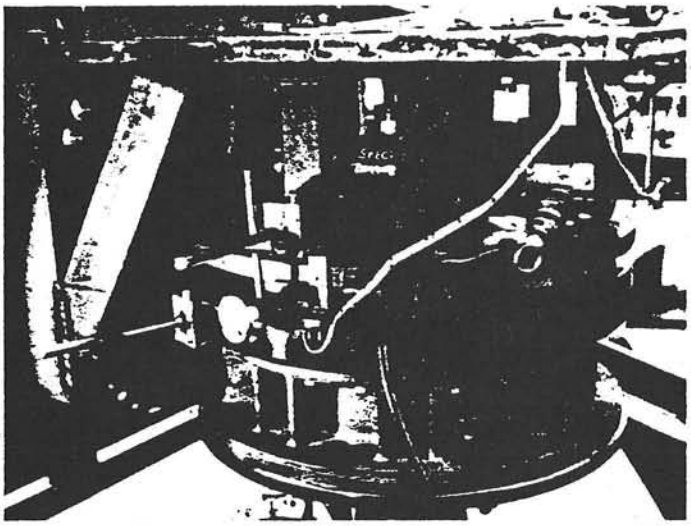

PHOTOGRAPH 12

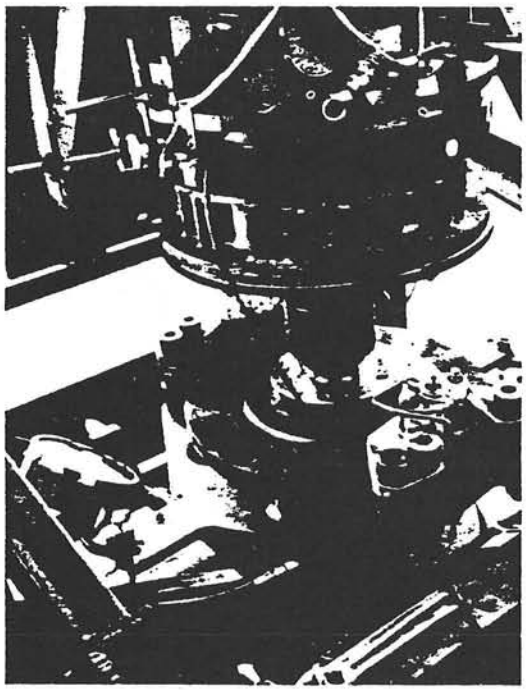

PHOTOGRAPH 13

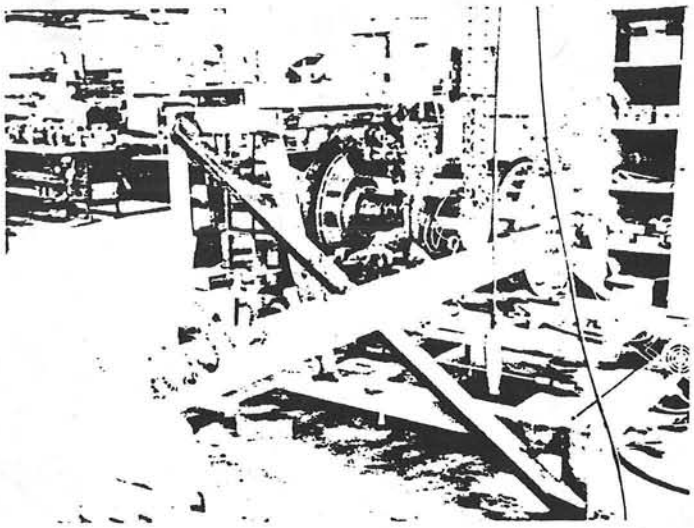

PHOTOGRAPH 14

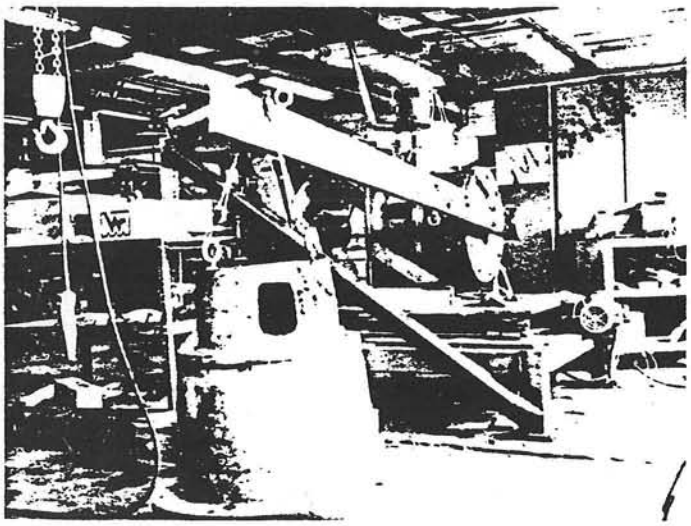

PHOTOGRAPH 15

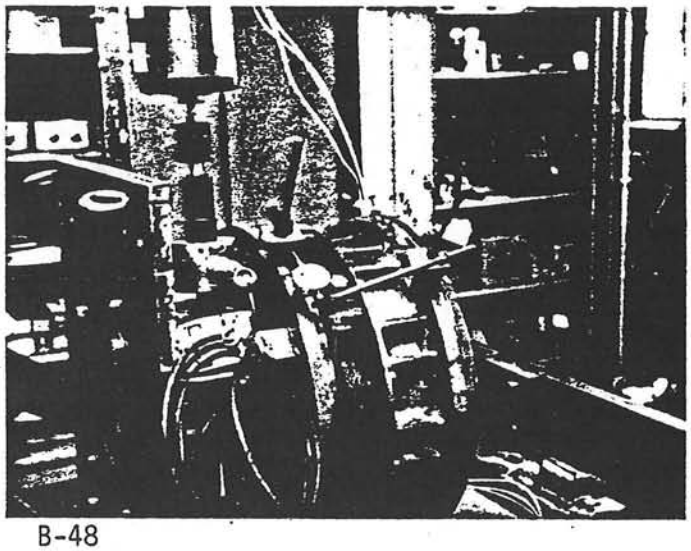

PHOTOGRAPH 16

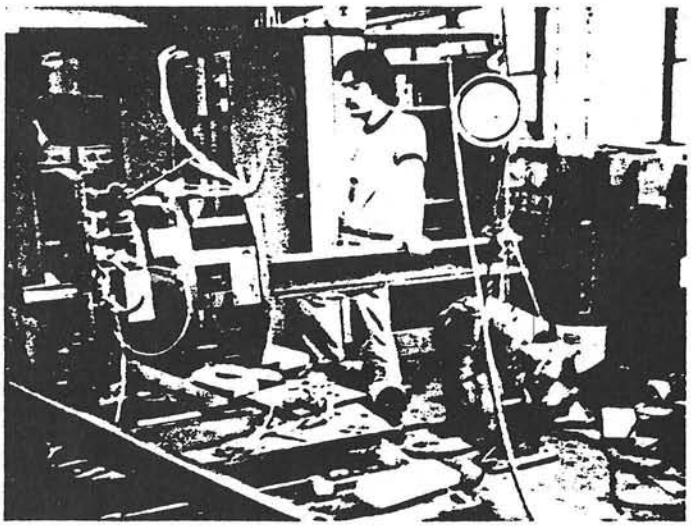

PHOTOGRAPH 17

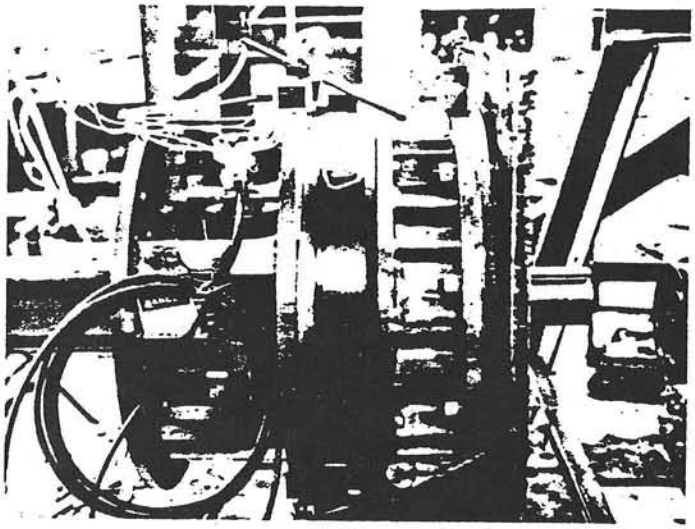

APPENDIX B-5

TEST PROCEDURES

Refer to Appendix E-11 of Second Generation Heliostat Design Report, Volume 1 - Appendices II: "Azimuth Drive/Bearing Test Procedures".

APPENDIX B-6

TORQUE TRANSDUCER CALIBRATION CURVE

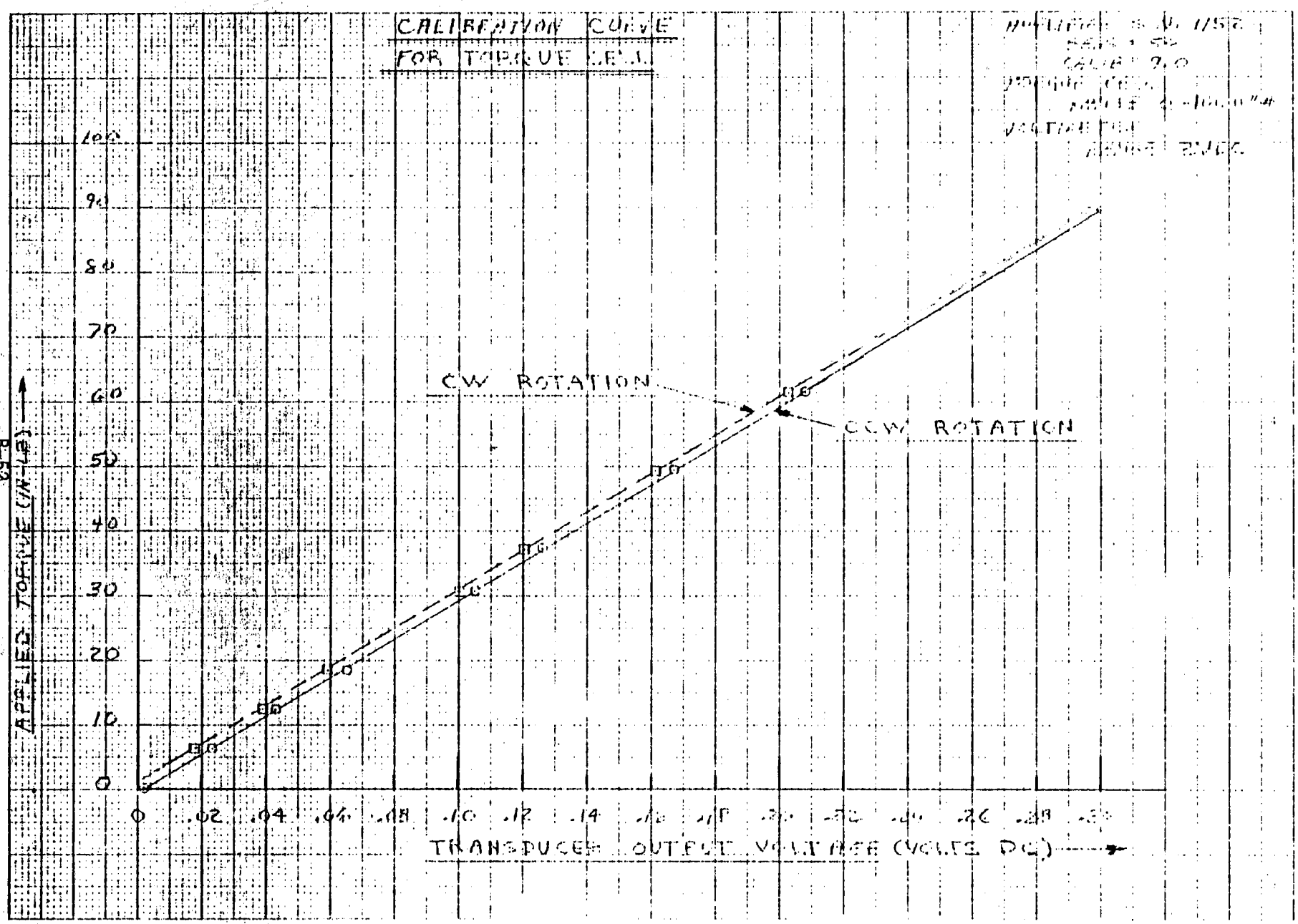

APPENDIX C

Assembled Gimbal/Actuator Drive Assembly
Test Data

for

Gimbal/Actuator Drive Assembly

for

Boeing Second Generation Heliostat

APPENDIX C

ASSEMBLED GIMBAL/ACTUATOR DRIVE ASSEMBLY

TEST DATA

Attached test results are data sheets referencing Test Procedures for the Gimbal/Actuator Drive Assembly issued as Appendix E-12 of **Appendices II.** All tests pertain to Unit #2 unless noted.

Ford Aerospace &
Communications Corporation
Western Development
Laboratories Division

3939 Fabian Way
Palo Alto, California 94303

Code Ident. No. 11530

5.0 DATA SHEETS

5.1 Azimuth and Elevation Axis Orthogonality

(a) Initial reading of dial indicator a = 0 inches

(b) Final reading of dial indicator b = +0.0002 inches

(c) Distance between two points, where dial indicator touches, ℓ = 16.75 inches

(d) Axes non-orthogonality

$= \frac{a-b}{\ell}$ Radians

$= 1.19 \times 10^{-5}$ Radians

$= 1.19 \times 10^{-5}$ Radian * 57.296

= 0.0007 Degrees

NOTE: READING ON ELEVATION ABSOLUTE ENCODER SIDE IS HIGHER

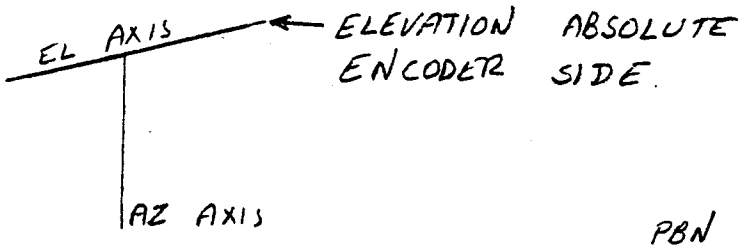

PBN 8/6/80

Ford Aerospace &
Communications Corporation
Western Development
Laboratories Division

3939 Fabian Way
Palo Alto, California 94303

Code Ident. No. 11530

5.0 DATA SHEETS

5.1 Azimuth and Elevation Axis Orthogonality

(a) Initial reading of dial indicator a = + 0.0006 inches

(b) Final reading of dial indicator b = + 0.0162 inches

(c) Distance between two points, where dial indicator touches, ℓ = 16.75 inches

(d) Axes non-orthogonality

$= \frac{a-b}{\ell}$ Radians

$= 93 \times 10^{-5}$ Radians

$= 93 \times 10^{-5}$ Radian * 57.296

= 0.0534 Degrees

NOTE: READING ON ELEVATION ABSOLUTE ENCODER SIDE IS HIGHER.

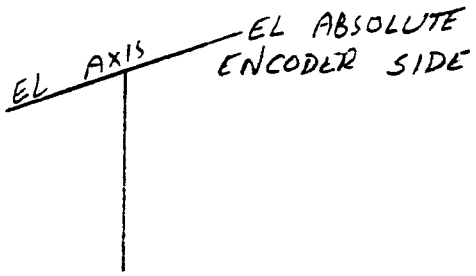

PBN 8/8/80

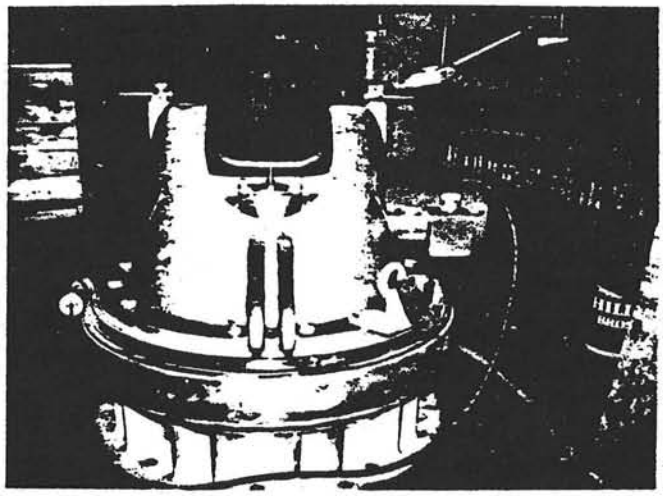

ORTHOGONALITY TEST

Ford Aerospace &
Communications Corporation
Western Development
Laboratories Division

3939 Fabian Way
Palo Alto, California 94303

Code Ident. No. 11530

5.2 Dimensional Verification

Items (a.i) and (a.ii) shall be verified at FACC/WDL. Items (a.iii), (a.iv), (c), and (d) shall be verified at the torque tube subcontract facility. Items (a.v) shall be verified at the gimbal subcontract facility. Items of (b) shall be verified at the pedestal subcontract facility. All items verified at subcontract facilities shall be recorded in this section.

a. Overall dimensions

i) Height of elevation axis over base flange (21.50 ± 0.100) = 21.499

ii) Offset between elevation and azimuth axes (4.50 ± 0.100) = 4.53

iii) Distance between elevation axis and torque tube center line..... = } Per Drawing

iv) Distance between elevation axis and upper pivot point of actuator..... = }

v) Distance between elevation axis and lower pivot point of actuator..... = 19.292 INCH

b. Interface dimensions to pedestal

i) Mounting hole diameter..... = 0.882 TO 0.884 INCH

ii) Distance between adjacent holes ..... = TRUE WITHIN 0.030"

iii) Bolt circle diameter..... = 20.233 INCH

c. Interface dimension to torque tube flanges

i) Mounting hole diameter ..... = }

ii) Distance between adjacent holes ..... = } Per Drawings

iii) Bolt circle diameter..... = }

iv) Location of bolt holes with respect to elevation bearing and actuator pivot is located correctly = }

Ford Aerospace &
Communications Corporation
Western Development
Laboratories Division

3939 Fabian Way
Palo Alto, California 94303

Code Ident. No. 11530

d. Perpendicularity of torque tube flanges and parallelism of flange axis to the elevation axis.

i) Torque tube flanges are parallel within = } Per Drawing

ii) Flanges are perpendicular to elevation axis within..... = }

e. Clearance and accessibility (record findings)

i) Azimuth motor

ACCEPTABLE. MOTOR IS OVER THE OIL FILL PLUG. FUTURE DRIVES WILL HAVE FILL PLUG ON DIAMETRICALLY OPPOSITE SIDE.

ii) Azimuth motor revolution sensors

ACCEPTABLE

iii) Azimuth zero reference sensor

ACCEPTABLE

iv) Elevation motor

ACCEPTABLE

Ford Aerospace &
Communications Corporation
Western Development
Laboratories Division

3939 Fabian Way
Palo Alto, California 94303

Code Ident. No. 11530

v) Elevation motor revolution sensors

ACCEPTABLE

vi) Elevation zero reference sensor

ACCEPTABLE

5.3 Azimuth Survival Loading

List here any abnormalities observed during or after the test.

None. No slippage at the torque tube flanges. Drive operated subsequent to survival loads. No effect of survival loading.

5.4 Azimuth Drive Motor Capability Under Maximum Operational Loads

Can the motor drive against maximum operational torque without stalling?

(YES or NO) _____

Record comments or findings if any. THIS TEST WAS NOT PERFORMED AT FINAL ASSEMBLY. INPUT TORQUE REQUIRED FOR VARIOUS OUTPUT TORQUE WAS TESTED AT AZIMUTH DRIVE VENDOR DURING RUNNING TORQUE AND EFFICIENCY TESTING. INPUT TORQUE REQUIRED TO DRIVE AGAINST OUTPUT TORQUE FOR 35 MPH WIND WAS 8.5 IN-LBS, (FIRST UNIT, THIS WAS 7.0 IN-LBS.) AND FOR 50 MPH WIND WAS 13.3 IN-LBS. THE RATED TORQUE FOR 1/6 H.P. MOTOR IS 6.0 IN-LBS, WHICH INDICATES AN OVERLOAD OF 40% FOR 35 MPH WIND AND 120% FOR 50 MPH WORST DIRECTION WIND VELOCITIES. AS THESE MOTORS CAN BE OVERLOADED BY ABOUT 200% FOR SHORT TIME DURATION, THIS 120% OVERLOAD WILL NOT HARM MOTOR PERFORMANCE.

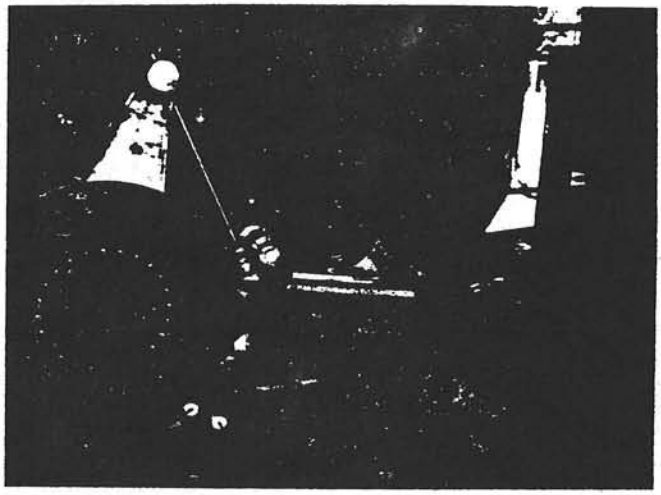

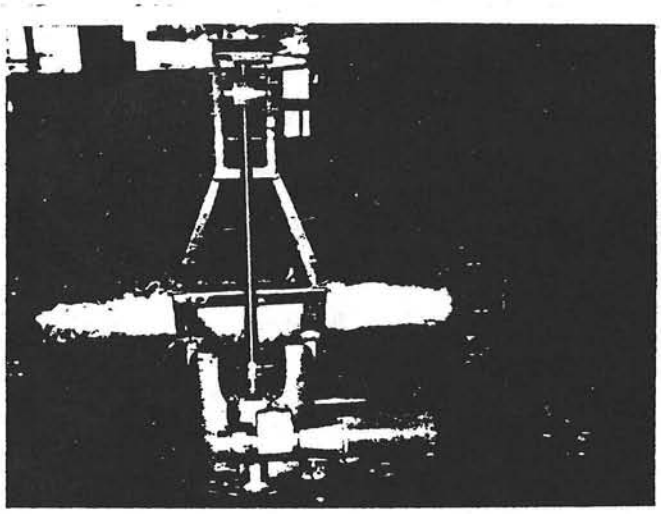

AZIMUTH SURVIVAL LOADING

Ford Aerospace &
Communications Corporation
Western Development
Laboratories Division

3939 Fabian Way
Palo Alto, California 94303

Code Ident. No. 11530

5.5 Azimuth Stiffness

Torque Induced (ft-lb)	Force (lb)	Dial Indicator Reading (Inches) #1	Dial Indicator Reading (Inches) #2	Reading Sum (1) (Inches)	Rotational Angle (2) (Milliradians)
0	0	0	0	0	0
173	35	-9.5	-11.0	-20.5	-0.37
346	70	-15.0	-15.5	-30.5	-0.55
494	100	-19.0	-19.5	-38.5	-0.70
800	162	-26.0	-26.0	-52.0	-0.95
1234	250	-33.5	-28.5	-62.0	-1.13
1605	325	-38.0	-33.0	-71.0	-1.29
2024	410	-42.8	-37.5	-80.3	-1.46
2311	468	-45.2	-40.0	-85.2	-1.55
2024	410	-43.0	-40.0	-83.0	-1.51
1605	325	-39.2	-40.0	-79.2	-1.44
1224	248	-36.0	-37.3	-73.3	-1.33
800	162	-32.0	-33.0	-65.0	-1.18
479	97	-28.2	-29.0	-57.2	-1.04
370	75	-26.8	-27.5	-54.3	-0.99
247	50	-25.0	-26.0	-51.0	-0.93
123	25	-20.8	-22.0	-42.8	-0.78
0	0	-10.0	-11.0	-21.0	-0.38
-123	-25	-4.5	-5.8	-10.3	-0.19
-272	-55	+3.0	+1.0	+4.0	+0.07
-370	-75	+7.2	+5.0	+12.2	+0.22
-494	-100	+10.1	+7.5	+17.6	+0.32
-800	-162	+15.9	+12.8	+28.7	+0.52
-1308	-265	+24.0	+20.5	+44.5	+0.81
-1605	-325	+28.0	+25.0	+53.0	+0.96
-2000	-405	+33.7	+30.5	+64.2	+1.17
-2321	-470	+37.1	+34.0	+71.1	+1.29
-2000	-405	+34.2	+31.5	+65.7	+1.19
-1605	-325	+30.4	+27.5	+57.9	+1.05
-1062	-215	+25.0	+22.0	+47.0	+0.85
-790	-160	+21.1	+18.0	+39.1	+0.71
-469	-95	+16.1	+13.3	+29.4	+0.53
-370	-75	+13.8	+10.9	+24.7	+0.45
-173	-35	+9.1	+5.2	+14.3	+0.26
0	0	+2.1	+0	+2.1	+0.04

Ford Aerospace &
Communications Corporation
Western Development
Laboratories Division

3939 Fabian Way
Palo Alto, California 94303

Code Ident. No. 11530

5.5 Azimuth Drive Stiffness

Torque Induced (ft-lb)	Force (lb)	Dial Indicator Reading (Inches) #1	Dial Indicator Reading (Inches) #2	Reading Sum[1] (Inches)	Rotational Angle[2] (Milliradians)
148	30	-6.3	-9.0	-15.3	-0.28
272	55	-11.0	-14.0	-25.0	-0.45
395	80	-15.5	-18.0	-33.5	-0.61
543	110	-19.0	-21.0	-40.0	-0.73
800	162	-25.0	-26.0	-51.0	-0.93
1210	245	-32.8	-29.0	-61.8	-1.12
1605	325	-37.0	-34.0	-71.0	-1.29
2000	405	-41.4	-38.0	-79.4	-1.44
2321	470	-45.0	-41.0	-86.0	-1.56 MIN
2000	405	-42.2	-41.0	-83.2	-1.51
1605	325	-39.0	-41.0	-80.0	-1.45
1210	243	-35.2	-37.7	-72.9	-1.33
800	162	-31.2	-33.5	-64.7	-1.18
494	100	-28.0	-30.0	-58.0	-1.05
346	70	-25.8	-27.7	-53.5	-0.97
183	37	-21.8	-23.8	-45.6	-0.83
0	0	-13.0	-15.0	-28.0	-0.51
-123	-25	-8.8	-11.0	-19.8	-0.36
-262	-53	+4.2	+2.0	+6.2	+0.11
-370	-75	+8.8	+6.0	+14.8	+0.27
-494	-100	+11.2	+8.7	+19.9	+0.36
-800	-162	+17.7	+14.0	+31.7	+0.58
-1224	-248	+24.0	+20.0	+44.0	+0.80
-1605	-325	+28.6	+25.0	+53.6	+0.97
-2000	-405	+33.8	+31.0	+64.8	+1.18
-2321	-470	+37.2	+34.2	+71.4	+1.30 MAX
-1975	-400	+34.5	+31.6	+66.1	+1.20
-1580	-320	+30.9	+27.8	+58.7	+1.07
-1185	-240	+27.0	+23.8	+50.8	+0.92
-790	-160	+22.0	+18.4	+40.4	+0.73

Procedure No.

Ford Aerospace &
Communications Corporation
Western Development
Laboratories Division

3939 Fabian Way
Palo Alto, California 94303

Code Ident. No. 11530

Torque Induced (ft-lb)	Force (lb)	Dial Indicator Reading (Inches) #1	Dial Indicator Reading (Inches) #2	Reading Sum (1) (inches)	Rotational Angle (Milliradians)
494	100	+17.2	+14.0	+31.2	+0.57
370	75	+14.7	+11.2	+25.9	+0.47
247	50	+11.5	+8.7	+20.2	+0.37
0	0	+5.0	+2.3	+7.3	+0.13

(Pointing error Angle = .5 X (Maximum Angle - Minimum Angle) = 1.43 Milliradians

(1) Reading Sum = Reading, Indicator #1 + Reading, Indicator #2

(2) Rotational Angle (in milliradians) = $\frac{\text{Reading Sum}}{\text{Distance between indicators (in inches)}}$ X 1000

NOTE: 1. DISTANCE BETWEEN DIAL INDICATORS = 55 INCH

2. DISTANCE BETWEEN FORCE APPLYATION POINTS = 59.25 INCH

AZIMUTH STIFFNESS: PLOT OF ROTATIONAL ANGLE VS TORQUE INDUCED

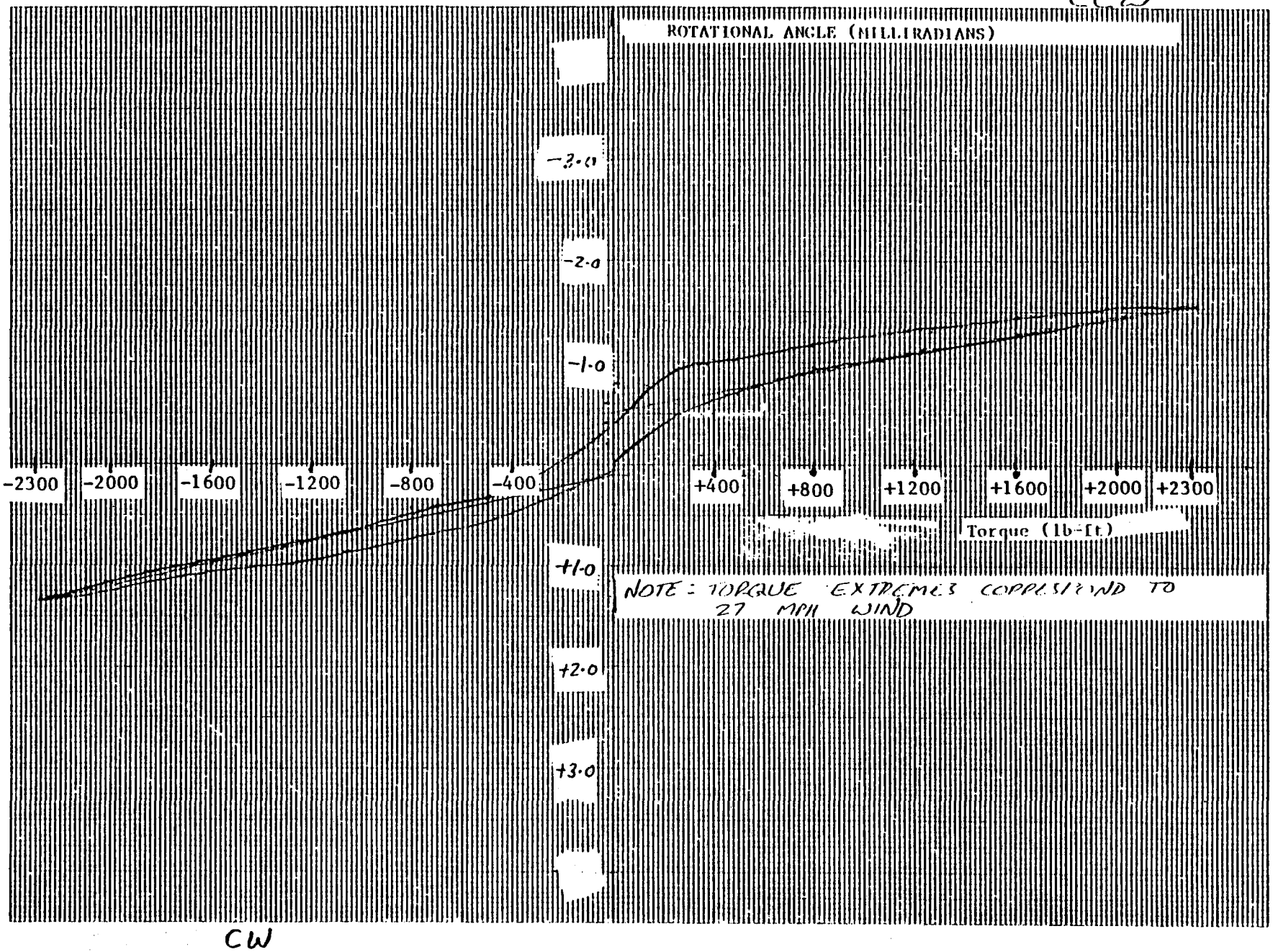

Because of the stiffness discrepancy found at Winsmith for unit 2, the gimbal actuator assembly using unit 2 was selected for all the tests run at FACC. During torsional compliance testing of the whole assembly at FACC, torsional compliance of just the Winsmith drive was also tested. In addition, unit 1 was also tested at FACC. Test results for unit 1 and unit 2 are plotted on the following page. From this plot and figure 6 of Winsmith test report, it can be observed that total angular rotation of unit 1 at Winsmith was same as total angular rotation of unit 1 at FACC. But when this plot is compared to Figure 18 of Winsmith test report, it is observed that Winsmith test result showed much higher angular rotation for unit 2. The plot on the following page shows that results for testing of both units at FACC were similar and only difference was due to different backlash of 2 units. At FACC, tests were performed by using pure torques in azimuth drives proper orientation (i.e., vertical azimuth axis). While at Winsmith, tests were performed with horizontal azimuth axis and without pure torque. From this, it can be concluded that somehow the instrumentation for unit 2 provided erroneous results.

RUN #1 9/15/65

AT DRIVE #1 RUN AT M.055

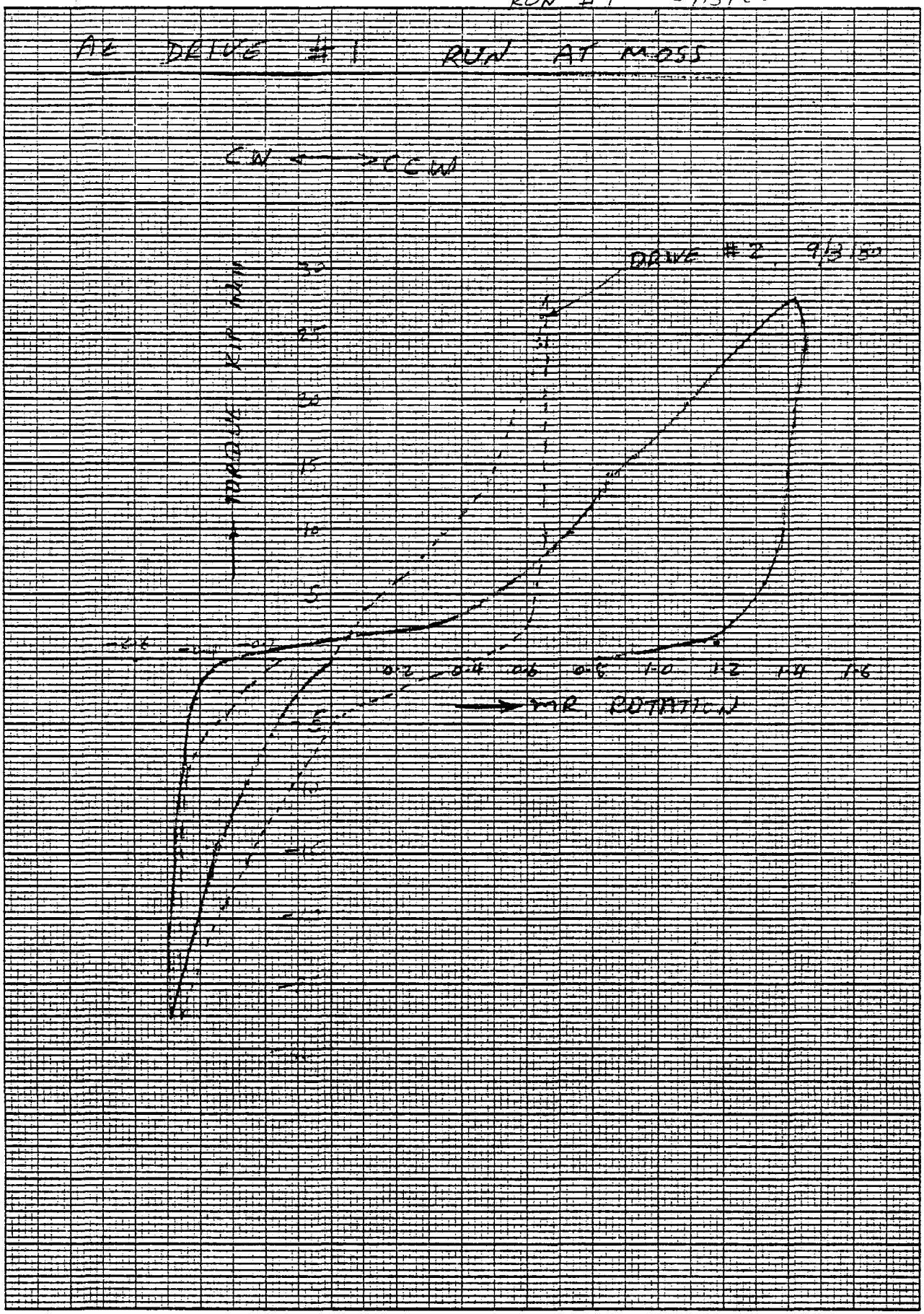

Ford Aerospace &
Communications Corporation
Western Development
Laboratories Division

3939 Fabian Way
Palo Alto, California 94303

Code Ident. No. 11530

Procedure No.

5.6 Azimuth Drive Travel Limits

Overall travel limits - UNLIMITED TRAVEL. LIMITED ONLY BY CABLES.

+_____ degrees to -_____ degrees

Record comments if any.

5.7 Elevation Drive Emergency Operation of Elevation Drive

Is it possible to drive elevation drive with drill motor? YES (Yes or No)

Record comments if any. NONE

Ford Aerospace &
Communications Corporation
Western Development
Laboratories Division

3939 Fabian Way
Palo Alto, California 94303

Code Ident. No. 11530

Procedure No. 531676

5.8 Elevation Drive Capability Under Maximum Operational Loads

Output Torque Induced (lb-ft)	Elevation Angle (degrees)	Does the motor stall? (Yes or No)
7080	0°	NO
10920	30°	NO
11750	60°	NO
6330	90°	NO

Record comments, if any.

MAXIMUM OPERATIONAL TORQUE APPLIED BY HANGING WEIGHTS AT A MOMENT ARM. DRIVE WAS OPERATED FOR ABOUT 2 MINUTES IN EACH CASE. NO OVERHEATING PROBLEMS.

Ford Aerospace &
Communications Corporation
Western Development
Laboratories Division

3939 Fabian Way
Palo Alto, California 94303

Code Ident. No. 11530

5.9 Elevation Stiffness

NOTE: Include the unbalance effect of tooling fixture. - NEGLIGIBLE.

5.9.1 Elevation Angle 0° (Vertical Mirror)

Torque Induced	Force (lb)	DIAL INDICATOR ~~Level~~ Readings x 0.001 INCH δ_1	δ_2	δ_3	δ_4	Rotational Angle (Milliradians)
3880	776	0	0	0	0	0 - MIN
4000	800	+ 0.2	+3.8	+3.2	+0.4	0.20
4200	840	+ 1.2	+6.0	+7.5	+1.8	0.30
4400	880	+ 2.2	+10.4	+12.2	+1.6	0.55
4600	920	+3.5	+ 15.5	+16.6	+2.1	0.77
4800	960	+4.1	+ 20.0	+20.5	+2.9	0.98
5000	1000	+5.2	+ 25.0	+25.2	+3.5	1.21
5200	1040	+6.2	+ 29.8	+27.0	+4.3	1.35
5340	1068	+8.0	+ 36.9	+35.7	+ 5.1	1.74 MAX
5200	1040	+ 6.8	+ 34.7	+32.8	+ 4.9	1.63
5000	1000	+ 6.1	+ 30.9	+ 29.2	+ 4.6	1.44
4800	960	+ 5.2	+ 26.9	+25.8	+ 4.1	1.27
4600	920	+ 4.4	+ 23.0	+ 22.1	+ 3.6	1.09
4400	880	+ 3.5	+ 19.2	+ 18.3	+ 3.2	0.90
4200	840	+ 2.7	+ 15.1	+ 14.8	+ 2.6	0.72
4000	800	+ 1.8	+ 10.2	+ 10.6	+ 2.2	0.49
3880	776	+ 1.2	+ 8.4	+ 9.4	+ 1.7	0.43
4000	800	+ 1.8	+ 10.0	+ 11.2	+ 2.4	0.50
4200	840	+ 2.6	+ 12.5	+ 14.5	+ 2.6	0.64
4400	880	+ 3.3	+ 16.4	+ 18.1	+ 3.2	0.82
4600	920	+ 4.2	+ 20.5	+ 22.0	+ 3.9	1.01
4800	960	+ 5.1	+ 24.4	+ 25.2	+ 4.4	1.17
5000	1000	+ 5.9	+ 29.1	+ 27.2	+ 4.9	1.33
5200	1040	+ 7.0	+ 33.2	+ 32.2	+ 5.5	1.55
5340	1068	+ 7.8	+ 37.2	+ 36.2	+ 6.0	1.71
5200	1040	+ 6.9	+ 35.9	+ 34.8	+ 5.7	1.70
5000	1000	+ 6.1	+ 31.9	+ 30.8	+ 5.3	1.50
4800	960	+ 5.2	+ 27.9	+ 26.8	+ 4.6	1.31
4600	920	+ 4.8	+ 23.9	+ 23.1	+ 4.2	1.11
4400	880	+ 3.8	+ 20.1	+ 20.1	+ 4.0	0.95
4200	840	+ 3.0	+ 16.8	+ 16.0	+ 3.4	0.77
4000	800	+ 1.9	+ 12.8	+ 12.1	+ 2.9	0.59
3880	776	+ 1.4	+ 9.8	+ 9.5	+ 2.4	0.45

Ford Aerospace &
Communications Corporation
Western Development
Laboratories Division

3939 Fabian Way
Palo Alto, California 94303

Code Ident. No. 11530

Pointing Error Angle = .5 X (maximum angle - minimum angle) = 0.87 Milliradians.

DISTANCE BETWEEN DIAL INDICATORS = 17.1 INCH

$$\text{ROTATIONAL ANGLE} = \frac{-d_1 + d_2 + d_3 - d_4}{2 \times \text{DISTANCE BETWEEN DIALS}}$$

DISTANCE BETWEEN FORCES = 30 INCHES

FORCES APPLIED AT 2 PLACES ON EACH FLANGE.

NOTE: 1. DIALS 1 & 2 ON ONE FLANGE & 3 & 4 ON THE OTHER FLANGE.
COMPUTED ROTATIONAL ANGLE IS AVERAGE OF ROTATIONS AT BOTH FLANGES.

2. POSITIVE ROTATION CAUSES -VE DIAL INDICATOR READINGS FOR DIALS 1 & 4 & +VE READINGS FOR DIALS 2 & 3.

ELEVATION STIFFNESS; & ELEVATION ANGLE, 0^{o} (VERTICAL MIRROR)

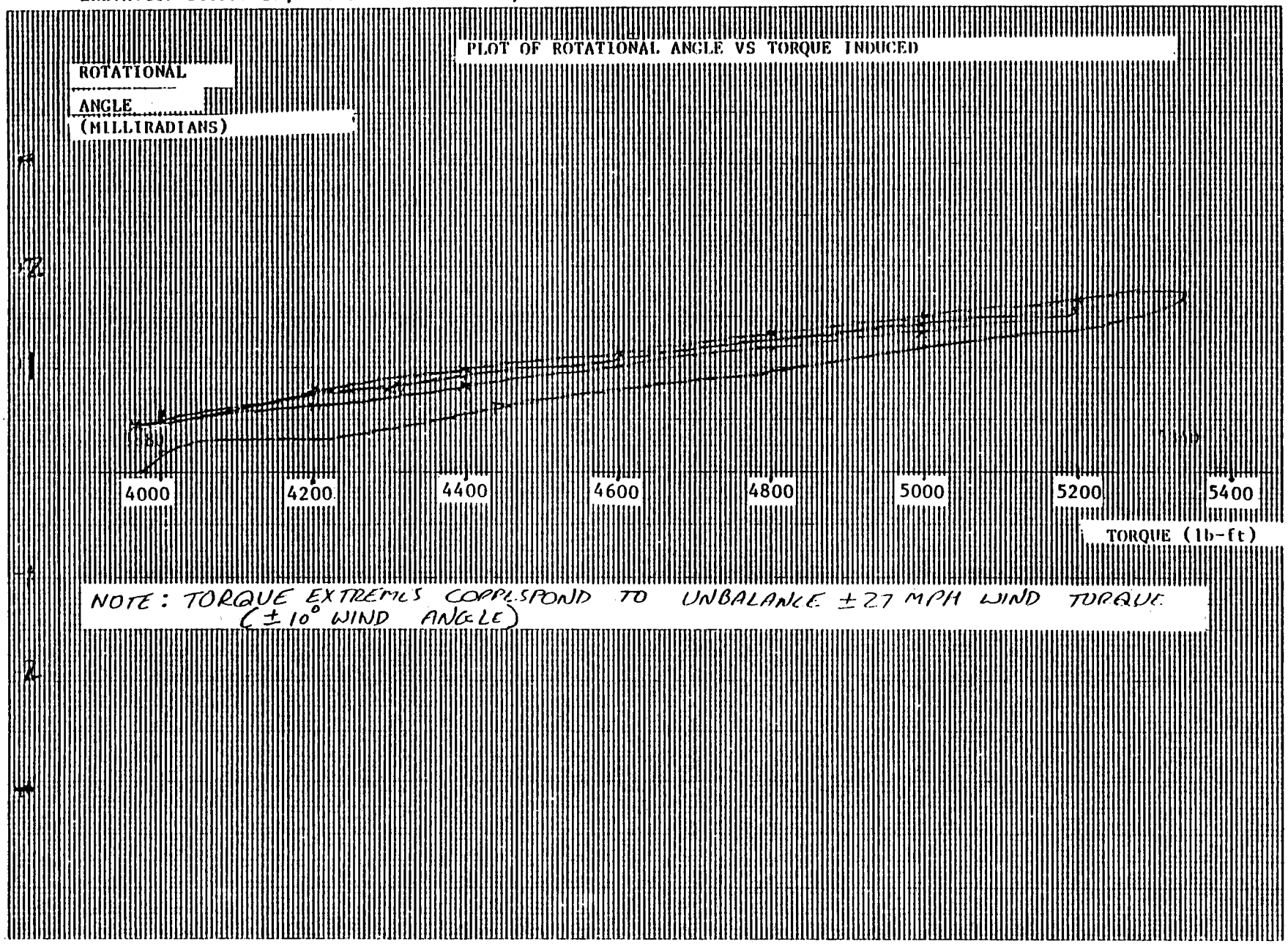

Ford Aerospace &
Communications Corporation
Western Development
Laboratories Division

3939 Fabian Way
Palo Alto, California 94303

Code Ident. No. 11530

NOTE: Include the unbalance effect of tooling fixture.- NEGLIGIBLE.

5.9.2 Elevation Angle of 90° (horizontal mirror)

Torque Induced FT LB	Force (lb)	DIAL INDICATOR ~~Inch~~ Readings X 0.001" δ_1	δ_2	δ_3	δ_4	Rotational Angle (milliradians)
0	0	0	0	0	0	0
300	60	0	+1.2	−1	+1.5	0.11
600	120	−0.8	+4	−3	+2.5	0.30
900	180	−1.8	+6.1	−5	+3.6	0.48
1200	240	−2.2	+8.8	−6.9	+5.5	0.68
1500	300	−2.7	+12.0	−8.9	+7.0	0.90
1810	362	−3.1	+14.0	−10.0	+7.9	1.03 - MAX
~~1400~~ ~~1500~~	~~250~~ ~~300~~	−2.5	+12.8	−8.0	+7.2	0.89
~~1100~~ ~~1200~~	220 ~~240~~	−2.2	+10.2	−6.2	+7.2	0.73
~~500~~ ~~900~~	170 ~~180~~	−1.9	+9.0	−4.9	+6.0	0.64
600	120	−1.1	+5.9	−3.2	+5.0	0.45
300	60	−0.3	+2.9	−0.9	+4.2	0.25
0	0	+0.3	+0.2	+0.9	+2.0	0.03
-300	-60	+1.5	−3.0	+5.0	+1.3	−0.24
-600	-120	+2.1	−5.2	+7.5	+1.1	−0.40
-900	-180	+2.1	−8.8	+9.1	−0.5	−0.60
-1200	-240	+1.8	−12.2	+10.4	−2.2	−0.78
-1500	-300	+1.1	−15.7	+12.0	−3.6	−0.95
-1810	-362	+1.2	−18.2	+13.9	−4.6	−1.10 - MIN
~~1250~~ ~~1500~~	~~-250~~ ~~300~~	+1.2	−16.8	+11.0	−3.5	−0.95
~~1200~~	~~240~~					
-900	-180	+0.8	−14.2	+9.1	−2.6	−0.78
-600	-120	+1.2	−10.5	+7.2	−1.0	−0.58
-300	-60	+1.2	−6.2	+6.0	+1.4	−0.35
0	0	0	−4.8	+2.4	+1.5	−0.17
600 300	120 60	−1.1	+0.2	+1.2	+3.4	+0.11
900	180	−1.9	+2.5	−0.8	+3.3	+0.25
1200	240	−2.9	+5.0	−2.8	+5.0	+0.46
1500	300	−3.1	+7.5	−5.0	+6.3	+0.64
1810	362	−3.9	+8.0	−6.5	+7.0	+0.74
~~1400~~ ~~1500~~	~~280~~ ~~300~~	−4.5	+10.9	−8.9	+9.5	+0.99
1200	240	−4.2	+10.0	−7.0	+8.2	+0.86
900	180	−4.2	+8.6	−6.1	+7.5	+0.77
~~600~~	~~120~~	−3.6	+6.2	−4.2	+6.9	+0.61
300	60	−1.9	+0.5	+0.2	+3.5	+0.17

Ford Aerospace &
Communications Corporation
Western Development
Laboratories Division

3939 Fabian Way
Palo Alto, California 94303

Code Ident. No. 11530

DIAL INDICATOR

Torque Induced (ft-lb)	Force (lb)	~~Level~~ Readings X 0.001" δ_1	δ_2	δ_3	δ_4	Rotational Angle (milliradians)
0	0	−1.7	−1.2	+1.5	+2.5	+0.04
-300	-60	−0.2	−4.0	+5.8	+2.0	−0.22
-600	-120	0	−7.2	+8.1	+2.0	−0.39
-900	-180	+0.2	−10.0	+10.1	+1.3	−0.56
-1200	-240	−0.8	−14.0	+11.5	−0.8	−0.75
-1500	-300	−0.2	−16.5	+14.1	−1.2	−0.92
-1810	-362	0	−19.2	+15.2	−2.3	−1.07
−1500	−300	−0.2	−19.0	+13.0	−2.2	−0.99
−1200	−240	−0.8	−18.0	+11.3	−1.9	−0.89
−900	−180	−0.9	−15.0	+9.5	−0.9	−0.72
−300	−60	−0.9	−8.6	+6.0	+1.4	−0.37
0	0	−2.0	−6.5	+3.0	+2.0	−0.16

DISTANCE BETWEEN DIAL INDICATORS = 17.1 INCH

$$\text{ROTATIONAL ANGLE} = \frac{-\delta_1 + \delta_2 - \delta_3 + \delta_4}{2 \times \text{DISTANCE BETWEEN DIALS}}$$

Pointing Error Angle = .5 X (Maximum Angle - Minimum Angle)

= 1.12 Milliradians

DISTNCE BETWEEN FORCES = 30 INCHES.
FORCES APPLIED AT 2 PLACES ON EACH FLANGE.

NOTE: 1. DIALS 1 & 2 ON ONE FLANGE & 3 & 4 ON THE OTHER FLANGE.
COMPUTED ROTATIONAL ANGLE IS AVERAGE OF ROTATIONS AT BOTH FLANGES.

2. POSITIVE ROTATION CAUSES −VE DIAL INDICATOR READINGS FOR DIALS 1 & 3 & +VE READINGS FOR DIALS 2 & 4

ELEVATION STIFFNESS: ELEVATION ANGLE, 90° (HORIZONTAL MIRROR)

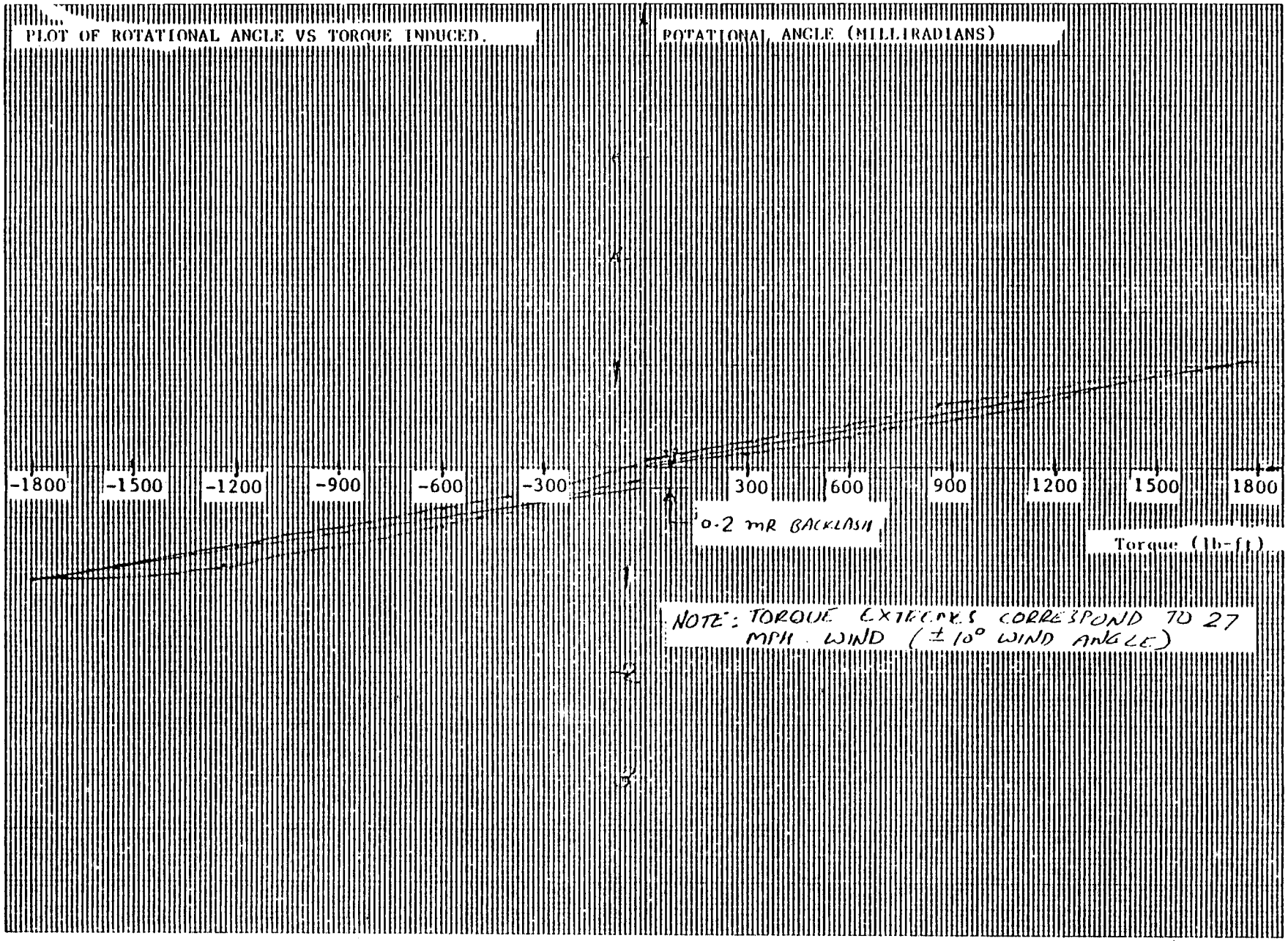

Ford Aerospace &
Communications Corporation
Western Development
Laboratories Division

3939 Fabian Way
Palo Alto, California 94303

Code Ident. No. 11530

5.10 Elevation Drive Survival Loading

List here any abnormalities observed during or after the test.
NONE. NO SLIPPAGE AT THE TORQUE TUBE FLANGES. DRIVE OPERATED SUBSEQUENT TO SURVIVAL LOADS. NO EFFECT OF SURVIVAL LOADING

5.11 Elevation Drive Backdriving

Is the input shaft rotation observed when survival output torque is applied at elevation axis: NO (yes or no)

Record comments, if any.

5.12 Elevation Drive Travel Limits

+ 93.0 degrees to - 2.94 degrees

Record comments, if any.
AT +93.0 DEGREES THERE IS ABOUT 0.25" GAP BETWEEN THE ACTUATOR NUT & STOP. AT -2.94 DEGREES THERE IS ALMOST NO GAP BETWEEN THE ACTUATOR NUT & STOP.

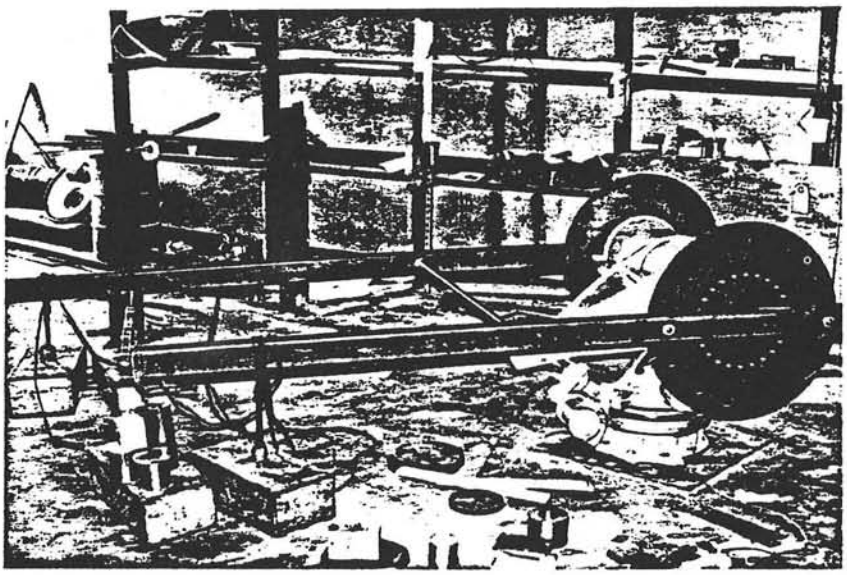

ELEVATION SURVIVAL LOADING

APPENDIX D

ACTUATOR SCREW AND NUT

TEST REPORT

FOR

GIMBAL/ACTUATOR DRIVE ASSEMBLY

FOR

BOEING SECOND GENERATION HELIOSTAT

OCTOBER 31, 1980

Reference: FACC TM23

Ford Aerospace &
Communications Corporation

TABLE OF CONTENTS

1.0 SUMMARY

1.1 Scope

This document identifies the test procedure and results for determining the durability of the stainless steel screw/non-lubricated nut elevation drive system proposed for use on the Boeing Heliostat Program.

1.2 Conclusions

- A non-lubricated bronze nut on a stainless steel screw has no chance of fulfilling the expected service life.
- Under identical service conditions, Delrin "AF" polymeric has better wear characteristics than Turcite "A" polymeric.
- Actual service nut wear values would be better than test results for the following reasons:
  (a) The pitch line velocity for the thread in actual operation is about 1/5 of the test case. Therefore, the generated heat due to friction will be less and the screw and nut materials will be operating at a much cooler temperature, allowing polymeric nuts to operate within their specified temperature range.
  (b) The actual load on the nut thread will not be constant as simulated in the test (maximum gravity condition). Therefore, threads will see less average pressure than was subjected during testing.
- The maximum thread wear rate occurred when sand and water were applied simultaneously. The probability of this occurring at frequencies or durations long enough to be harmful is considered to be unlikely. Therefore, the nuts during testing were exposed to a more severe environment than they would normally experience in actual operation.
- The stainless steel actuator screw did not show any significant measurable wear ($<$.001").

- Crack initialization occurred at the tip of the polymeric nut thread (See Figure 1).

1.3 Recommendations

(a) Delrin "AF" should be used as the material for the Boeing actuator nut.

(b) The thread should be relieved at both ends per Figure 2 to avoid overstressing this area.

(c) Other candidate polymeric materials should be tested along with new Delrin "AF" nuts. Screw speed should be reduced to keep nut temperature lower to avoid having to conjecture about temperature vs. life effects.

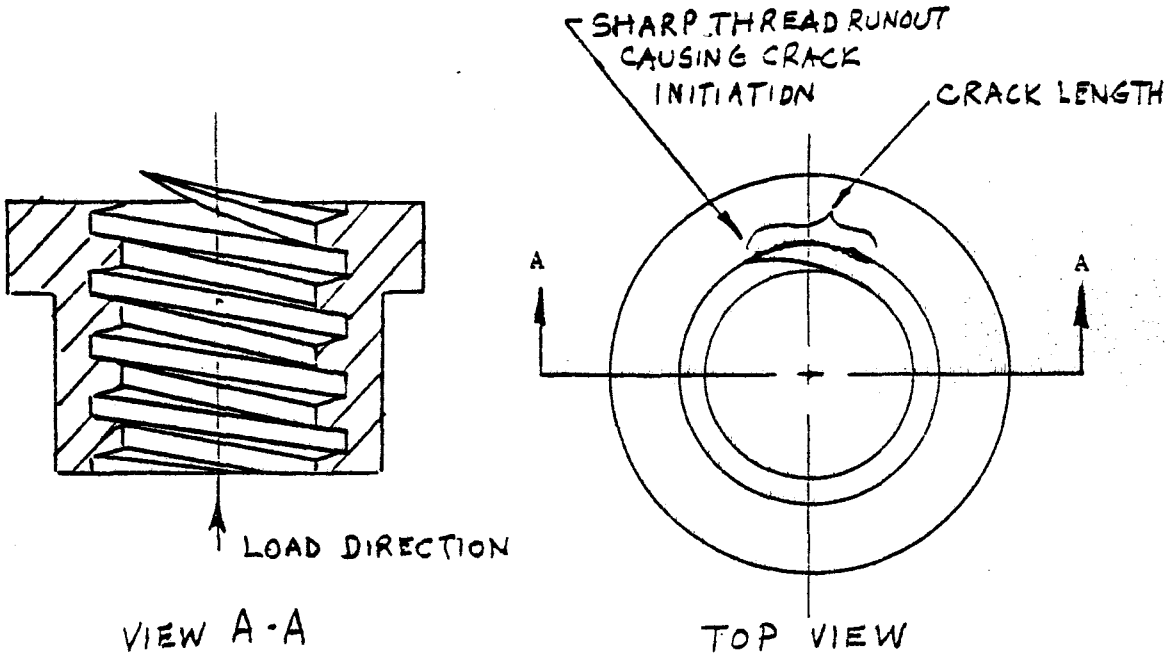

FIG. 1 NUT THREAD END CRACK

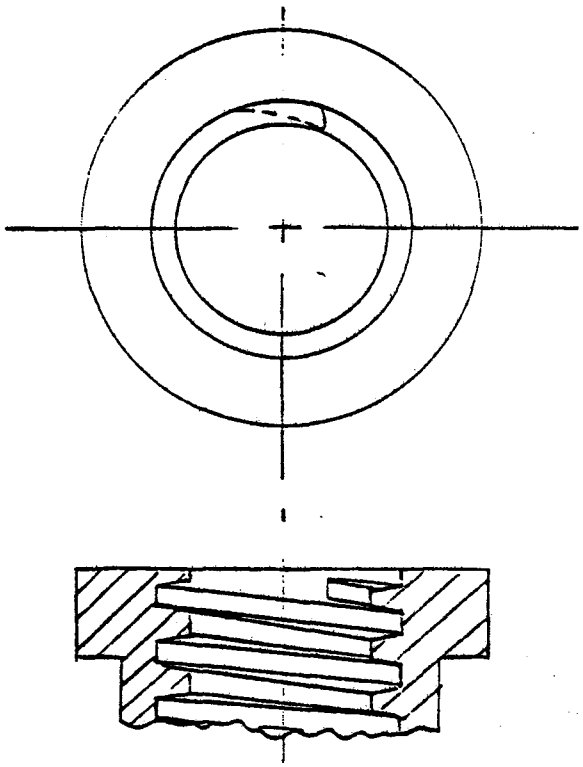

FIG. 2 PROPOSED METHOD OF THREAD RELIEF

2.0 TEST PROCEDURE

The test plan was to test a variety of nut materials on a stainless steel actuator screw on an accelerated basis to simulate actual service conditions. The test set-up, as shown in Figure 3, has the following features:

The test actuator is a Duff-Norton 2-ton traveling nut type with 65 inches of screw length. The screw material is type 304 stainless steel with a tooth surface finish of approximately 63 RMS microinches. Nut materials and their properties are listed below in Table 1 and are shown in Figure 4. The screw is mounted vertically, secured to the test fixture and driven by an AC motor through a 5:1 speed reducer. Electrical limit switches are installed to provide redundant control at each end of the stroke. Further, the motor is current limited so should the mechanism jam, the locked rotor motor current will cause a circuit breaker to trip before mechanical damage occurs. The fixture was tested to verify this feature pior to the operational portion of the test.

Table 1

Tested Nut Materials

	Delrin "AF"	Turcite "A"	Bronze "Dynalloy"
Approximate tensile yield strength (psi)	6,900	5,500	40,000
Static Coefficient of Friction on Steel (non-lubricated)	.08	.075	.3
Approximate operating temperature range (^{o}F)	-50 to 250	-50 to 170	-

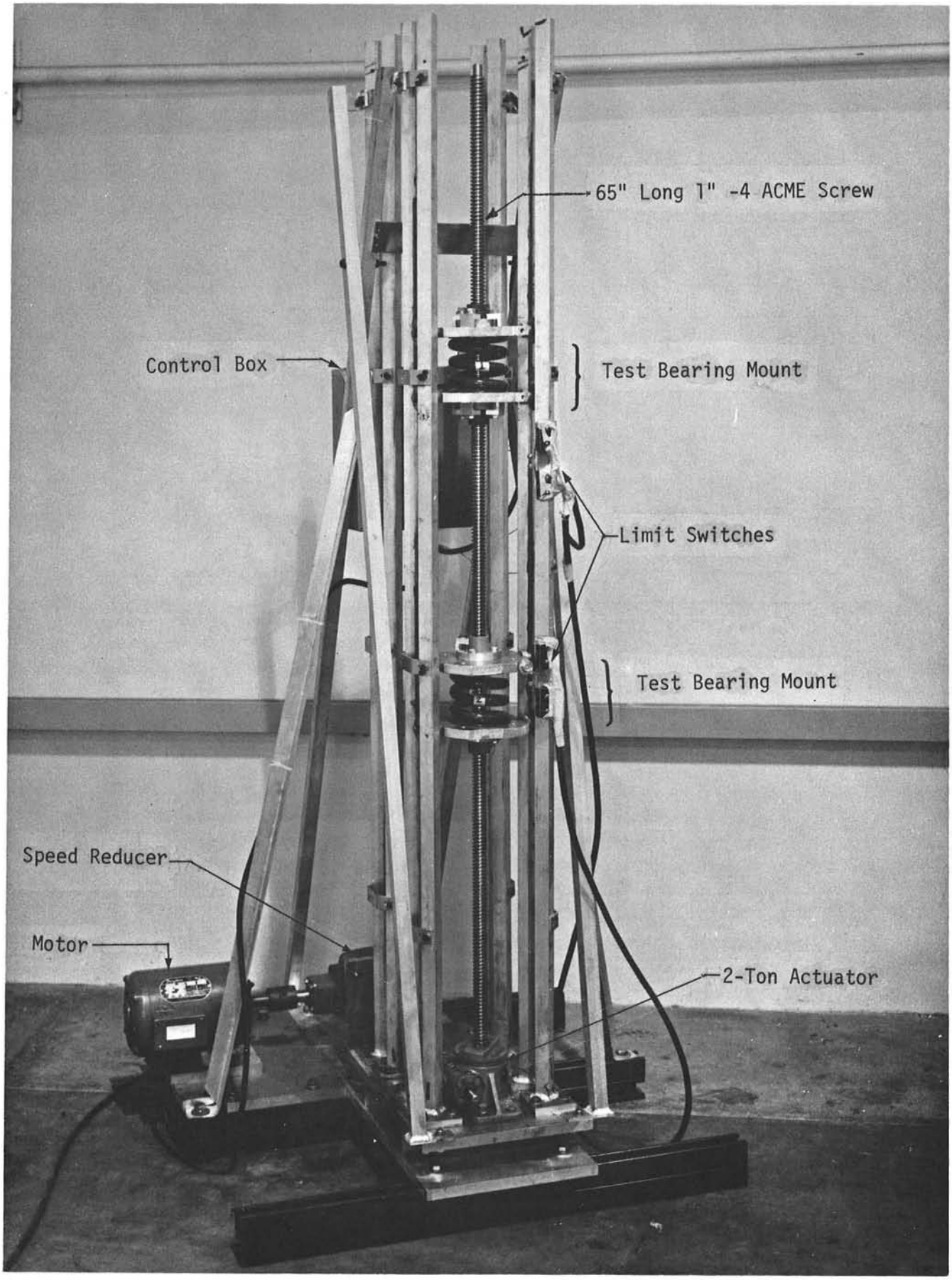

Figure 3 Test Setup

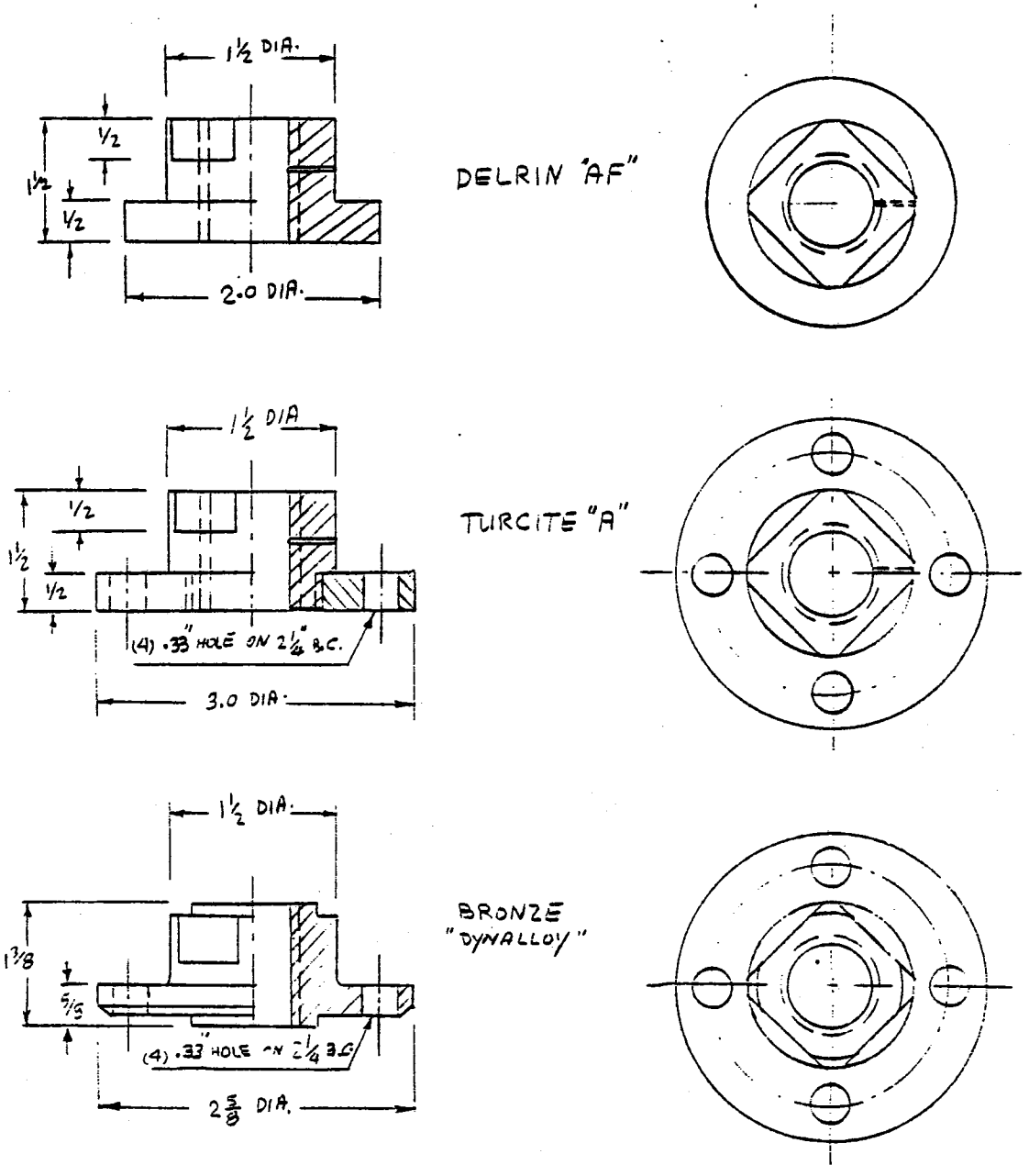

ACME TEST NUTS

FIGURE - 4

The screw and all parts that contact the screw/nut threads were wiped clean with a pure solvent to remove oil and cutting fluids. The nuts were all inspected for pits, burrs, etc., and these defects corrected or noted prior to the start of testing. Each nut and load spring was numbered and identified for future reference.

The first half of the test was conducted indoors for a period equivalent to 15 years of linear travel, and the second half was conducted outdoors, where screw and nuts were exposed to the natural sun and dust environment in addition to the purposely induced sand and water spray. The test was run round the clock, seven days/week, except for brief downtime periods for measurements or repair.

The test set-up represents a scaled down version of the actual elevation drive system designed for use on the Boeing Heliostat Program. Basically, the test was conducted using a two ton drive unit with corresponding screws and nuts in lieu of the full sized five ton assembly being proposed for use. The differences between the test set-up and the actual unit have been summarized in Table 2.

2.1 Pre-Assembly Measurements

Prior to assembly of the nut sets on the screw, the following measurements were made:

2.1.1 Backlash of Each Nut

The backlash of each nut was measured using a dial indicator to determine axial play between the nut and screw.

TABLE 2

COMPARISON OF DESIGN AND TEST PARAMETERS

No	ITEM DISCRIPTION	DESIGN	TEST
1	MINIMUM LIFE (YEARS)		
	— LINEAR TRAVEL	30	30
	— CIRCUMFERENTIAL TRAVEL	30	19
2	LUBRICATION	NONE	NONE
3	ACTUATOR CAPACITY	5	2
4	ACTUATOR REDUCTION RATIO	240:1	6:1
5	ACTUATOR INPUT SPEED (RPM)	1750	345
6	ACTUATOR SCREW:		
	— THREAD TYPE	ACME	ACME
	— OUTSIDE DIA. (inches)	1.500	1.000
	— PITCH DIA. (inches)	1.375	.875
	— ROOT DIA. (inches)	1.250	.750
	— PITCH (inches/thread)	.250	.250
	— TOOTH AREA (sq. inches/thread)	.540	.344
7	NUT:		
	LENGTH (inches)	3.2	1.5
	No. OF THREADS PER NUT LENGTH	12.8	6.0
8	OPERATING LOAD ON NUT (tons)	2.5 (gravity)	.747 (SPRING)
9	TOOTH PRESSURE (PSI)	723	723
10	AVERAGE NUT STROKE (inches)	28	13
11	MAXIMUM NUT SPEED (RPM)	7.29	57.50
12	STROKE TIME (seconds)	900	120
13	PITCH LINE VELOCITY (inches/second)	.525	2.634
14	No. OF CYCLES PER DAY (24 hours)	1	700
15	NUT TOTAL TRAVEL (INCHES)		
	- LINEAR	613200	613,200
	- CIRCUMFERENTIAL	10,595000	5,742,000
16	TOTAL No. OF CYCLES	10,950	23,585
17	TOTAL No. OF DAYS	10,950	33

2.1.2 Screw Thread Size (Refer to Appendix D-1)

The screw thread thickness was measured, using the three wire method, both before and after the test, to determine the amount of screw thread wear.

2.2. Assembly

2.2.1 Nut Set Assembly

The nut sets were installed back-to-back on the screw, and spring loaded as shown in Figures 5 and 6 to simulate the maximum elevation gravity unbalance load which the actual nut will see during operation.

The three nut set assemblies were positioned on the actuator screw in such a way that each set would travel over one section of the screw without going over the travel zone of the adjacent nut assembly.

The unloaded assembly height was measured (from nut-end to nut-end) and using two C-clamps over the end-plates, the springs were compressed to the required displacement. (Refer to Figure 7 for spring load-displacement curve.) The nuts were then rotated until they snugly contacted the plates and the C-clamps removed.

2.2.2 Torque Required/Nut for Motor Sizing (Refer to Appendix D-2)

The torque required to move each nut was calculated using published values of friction coefficients. Subsequently, the actual required torque was measured using a wrench and a spring scale. The test results indicated that the coefficient of friction of the two plastic materials is .09, very close to the published value of .08.

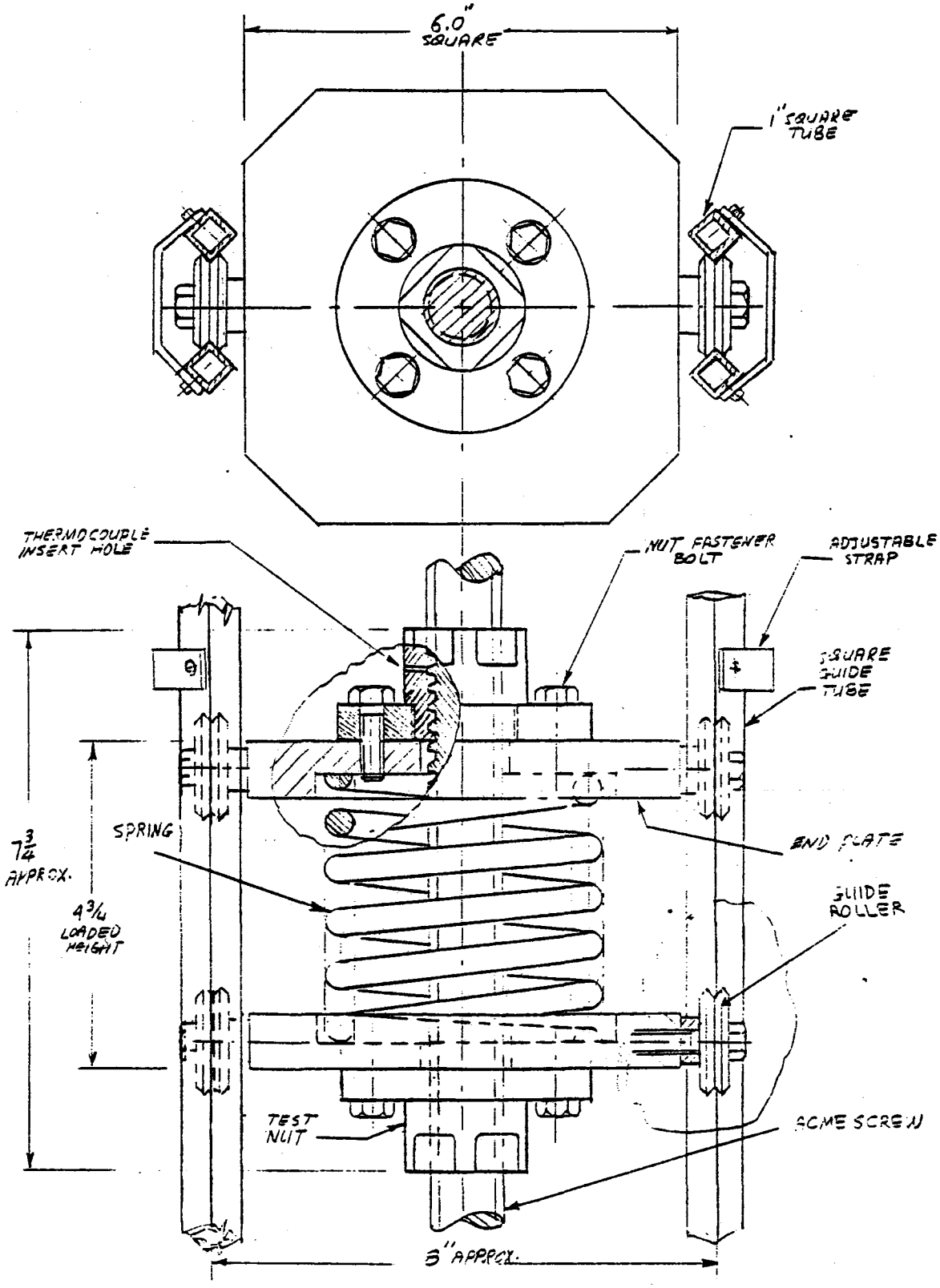

LOADED NUT ASSEMBLY

FIGURE 5

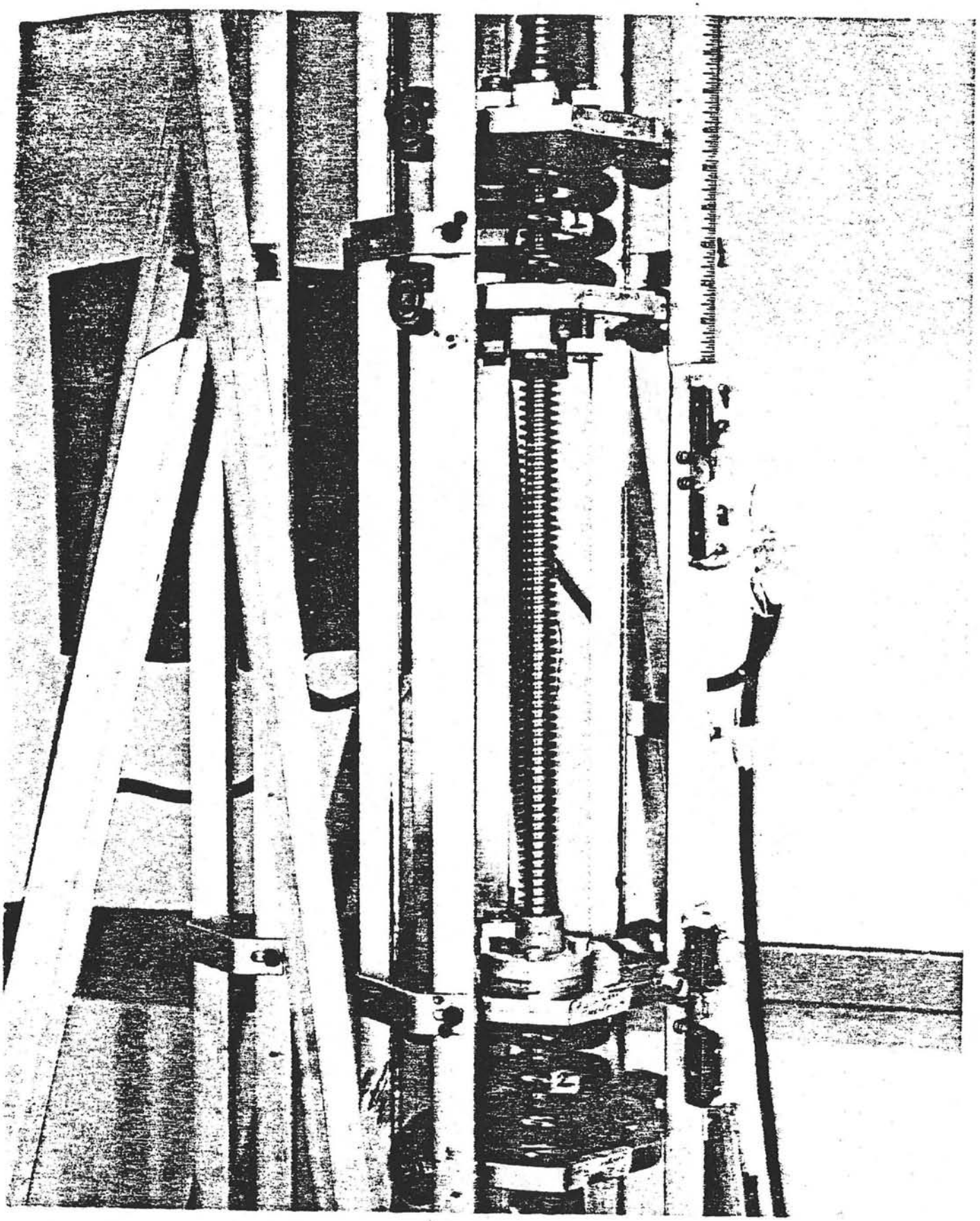

FIGURE 6 LOADED NUT ASSEMBLY

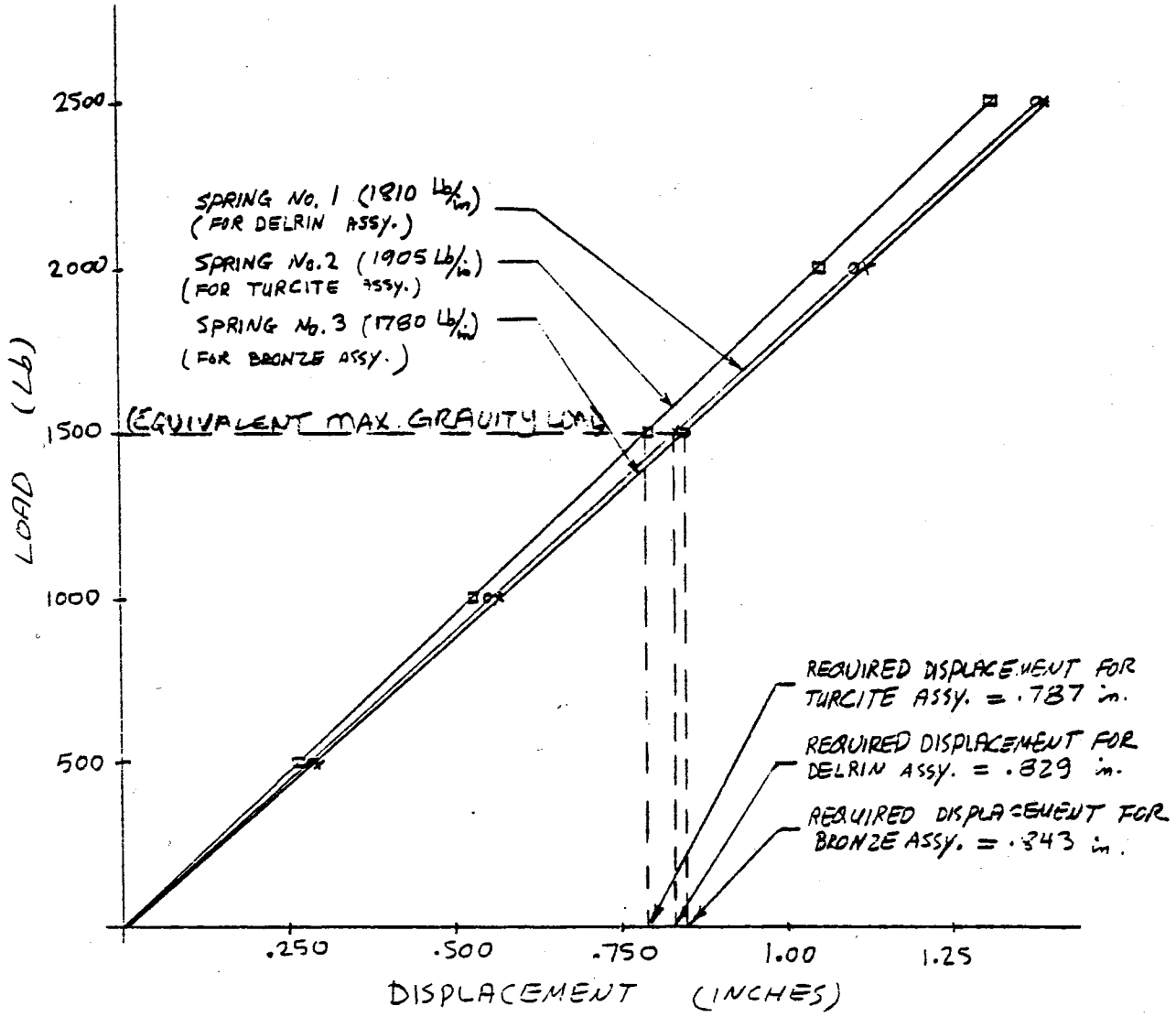

LOAD-DISPLACEMENT CURVE

FOR EACH COIL SPRING

FIGURE 7

2.2.3 Blowers

Compact blowers were installed on each end-plate of the nut assembly to dissipate the heat from the screw. This was found to be necessary because the screw speed during the accelerated life test was 8 times the heliostat screw RPM at slew and operating step speed, causing the nut temperature to approach the upper limit of allowable material temperature.

2.3 Test Conditions

The first half of the test was run free of dust or water in an indoor enviroment. The second half of the test was conducted outdoors to simulate sandstorms, dust and rain.

On the actual heliostat, the elevation drive screw is located at a height of approximately 10 feet off the ground. At this elevation, particles in the air are mainly light dust with very little sand. According to the Typical Meteorological Year (TMY) weather data for Albuquerque, the wind is greater than or equal to 10 mph only about 1.2% of the time. This wind velocity can cause dust and sand particles to lift. Thus the test set-up had sand and dust introduced by a blower once per workday during the second half of the test for a duration equal to (24 hrs) (60 min) $(1.2\%)\ \frac{(7\ \text{days})}{5\ \text{days}} = 24.2$ min/workday. Weather data shows that rain occurs in Albuquerque approximately once per week, therefore a heavy rain was simulated by applying water to the fixture on the 16th, 22nd and 28th day of testing. All simulated contaminants were applied while the test was running.

The dust used in this test was a fine sand (97-99 percent by weight SiO_2) of angular structure, with the following size distribution by weight, using the U.S. standard sieve series:

a. 100% shall pass through a 100-mesh screen

b. 98% shall pass through a 140-mesh screen

2.4 Test Measurements

2.4.1 Daily Measurements

The test was run continuously except for a brief period each workday in order to perform the following measurements:

- o Overall height of each set to the nearest .001".
- o Temperature of nut and screw thread surface while the nut was traveling over the screw.

2.4.2 Post Test Measurements

2.4.2.1 Measurements Before Cleaning

The torque required to turn each set of nuts was measured. This measurement was made without modification to the fixture after shutting down the test.

2.4.2.2 Measurements After Air Cleaning

The fixture was thoroughly cleaned by blowing compressed air on it to remove any clinging particles. The height of each nut set and the endplate-to-endplate height were measured and recorded.

2.4.2.3 Measurements After Disassembly and Cleanup

The nut sets were removed from the screw and all parts were thoroughly cleaned using air or water. All parts were visually inspected and nut thread wear measurements were made using ball measurement technique described in Appendix D-3.

3.0 TEST RESULTS

3.1 Bronze Nut

The first test was done using only the bronze "Dynalloy" nut assembly on the bottom part of the actuator screw. After the first hour of this test, the nuts and their traveled portion on the screw became severely worn and damaged (see Figures 8 and 9). The temperature on the screw surface and the nut was estimated (although not measured) to be in excess of 300°F. Therefore, it was decided to conclude testing of the bronze nut.

The key results from the testing of the bronze "Dynalloy" nut are as follows:

- The non-lubricated bronze nut severely damaged the stainless steel screw threads. Sharp corners of the threads were rounded and bronze particles were bonded to screw threads due to excessive heat generated by friction.
- Average nut thread wear as measured by three different methods was .080 after 2500 inches of linear travel (equivalent to 45 days of actual service life). This is illustrated in Figure 10.

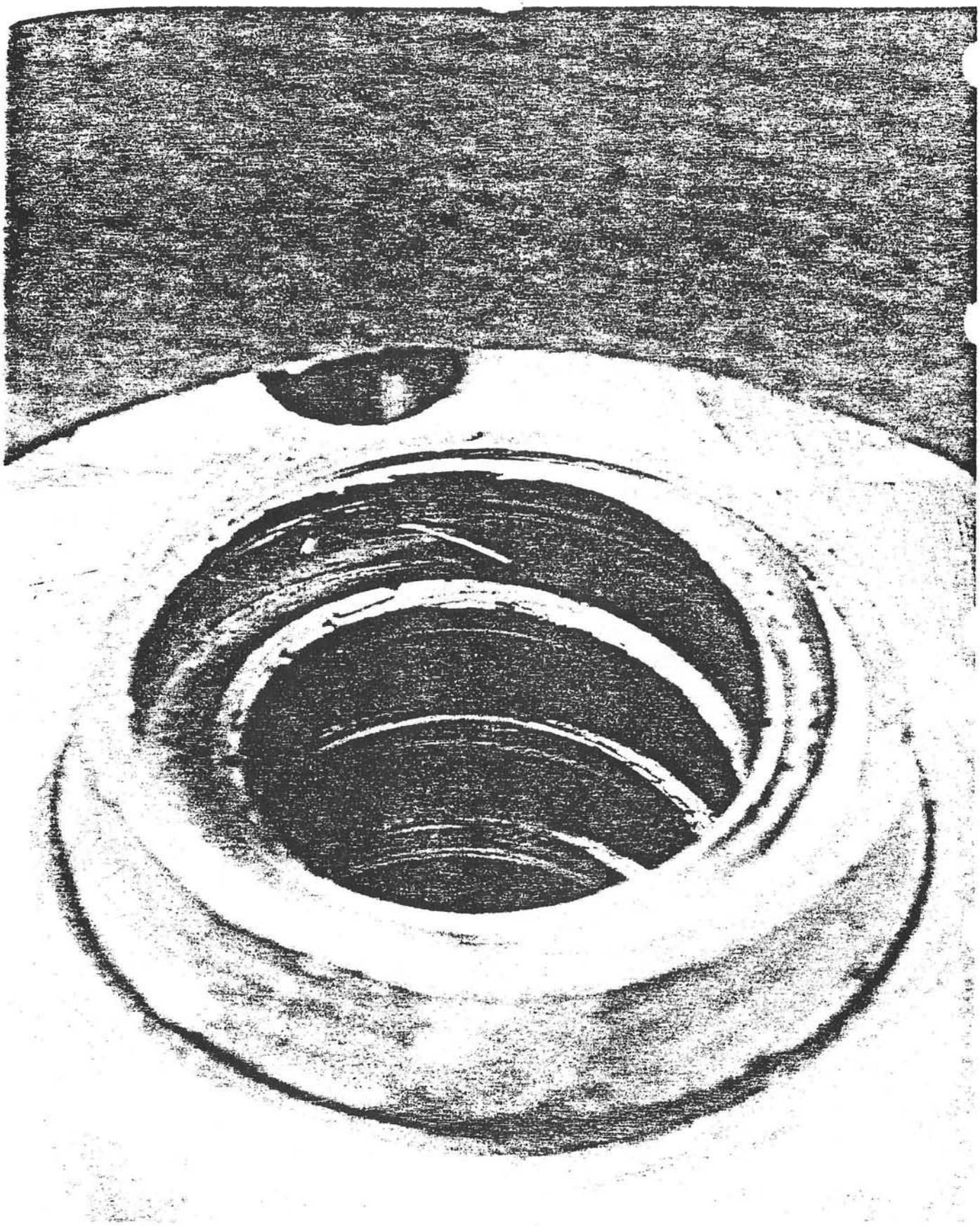

FIGURE 8 BRONZE NUT WEAR

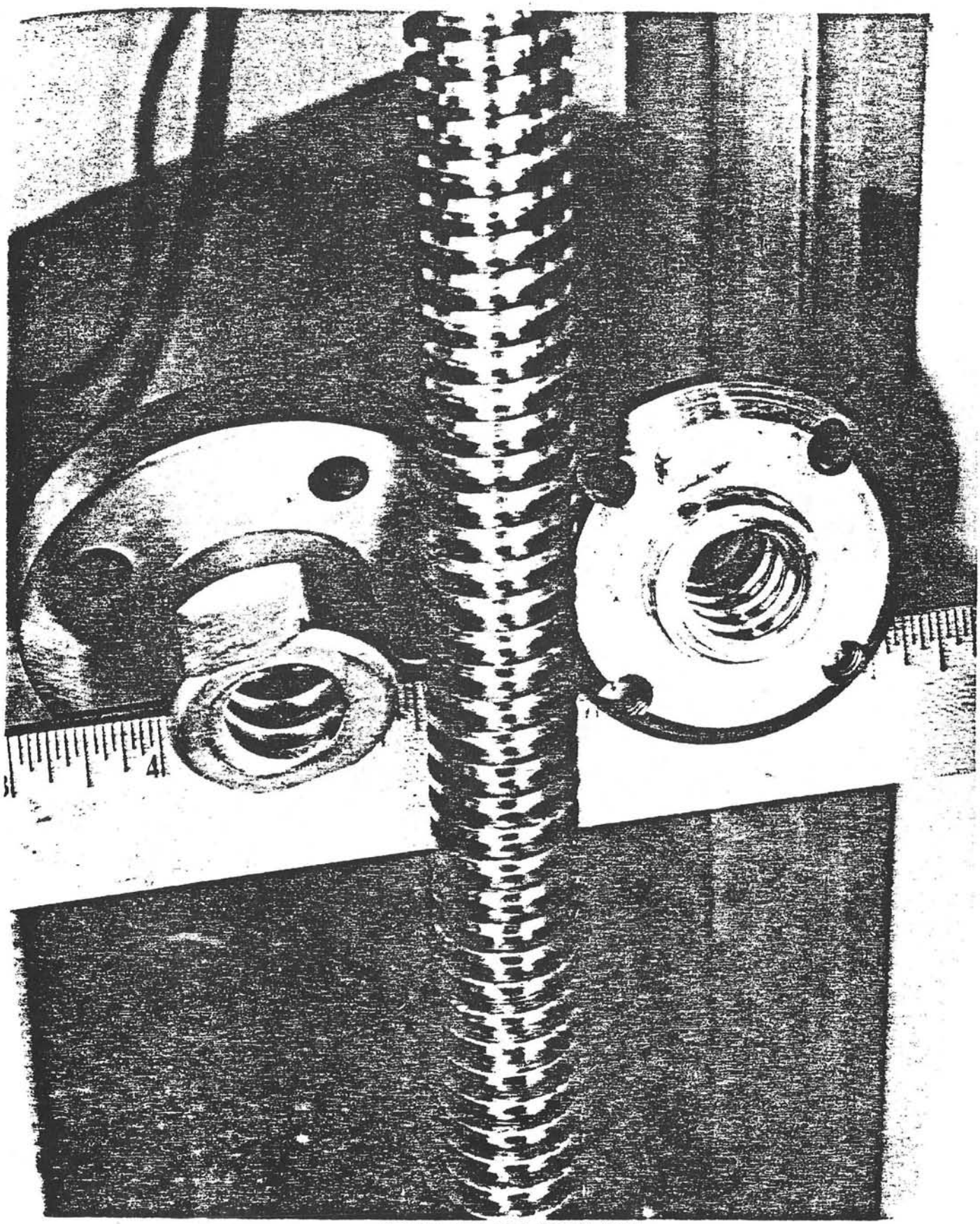

FIGURE 9 BRONZE NUT AND SCREW WEAR

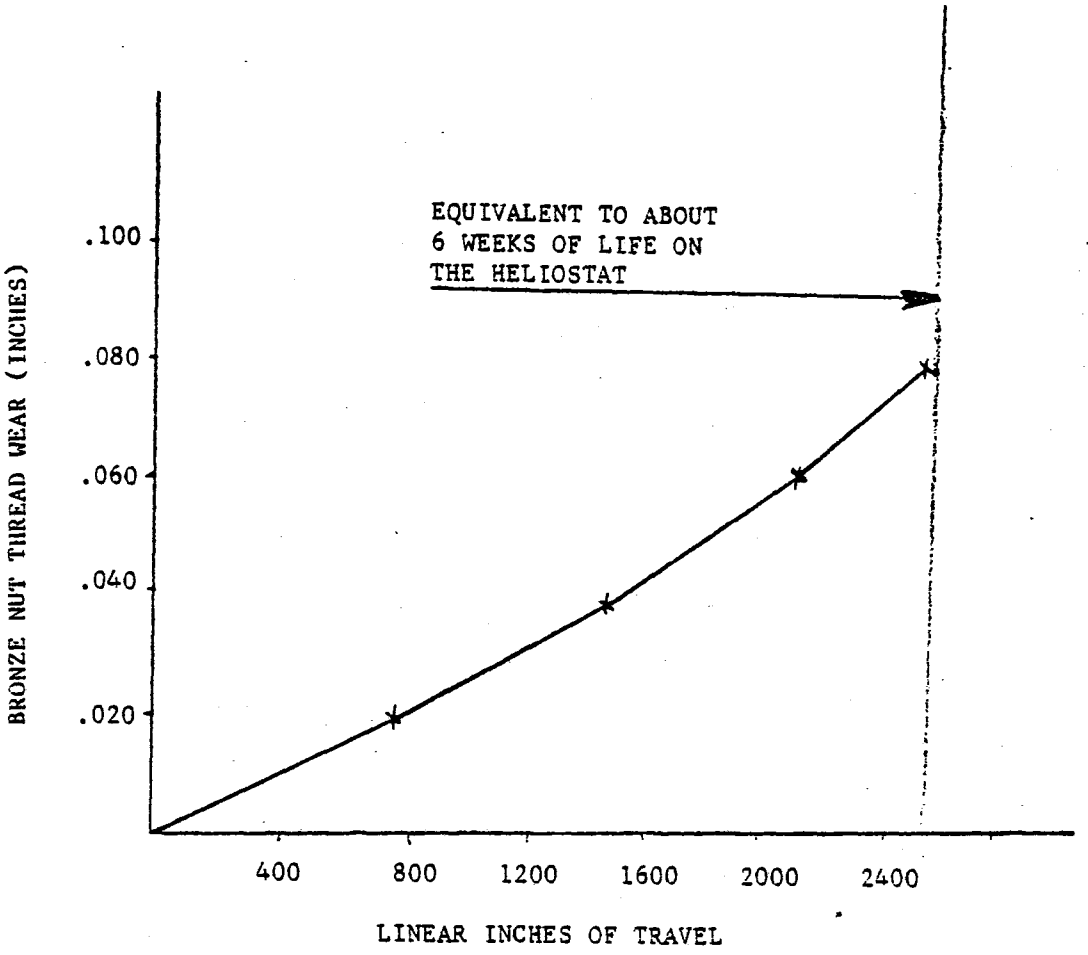

Nut Wear vs Total Travel

Figure 10.

3.2 Polymeric Nuts

Due to the accelerated traveling rate in the test set-up, the temperature on the screw surface was measured to be approximately 180°F. This was much higher than expected and not typical of the actual operation. To dissipate the heat, blowers were installed on each end-plate. The temperature of the nut thread was then measured to be approximately 120°F with these blowers directed on each nut.

Nut wear data taken during this test is shown in Figure 11, tabulated in Table 3 and summarized in Table 4. For the first 15 years of simulated running, the specimens were not exposed to sand and water. The wear rates were essentially linear and the Turcite rate was about twice the Delrin rate.

After the equivalent of 16 years, water and sand were applied for three years and the wear rate sharply increased. From 19 to 26 years, water or sand was not applied, and the Delrin rate returned to its original rate, whereas Turcite rate continued to be high, until finally the threads sheared at about 21 years of equivalent life.

The test was continued on the Delrin sample adding water only for the number of days equivalent to 26 to 29 years and sand only from 29 to 32 years. No significant change in wear rate occurred during the period from the 21st to the 32nd year.

Key results from the polymeric nut testing is summarized below:

- Nut thread wear was measured by three different methods with the average result shown below:
  - (a) .090 in. for Turcite "A" after 400,000 in. of linear travel (20 years).
  - (b) .040 in. of Delfin "AF" after 600,00 in. of linear travel (30 years).

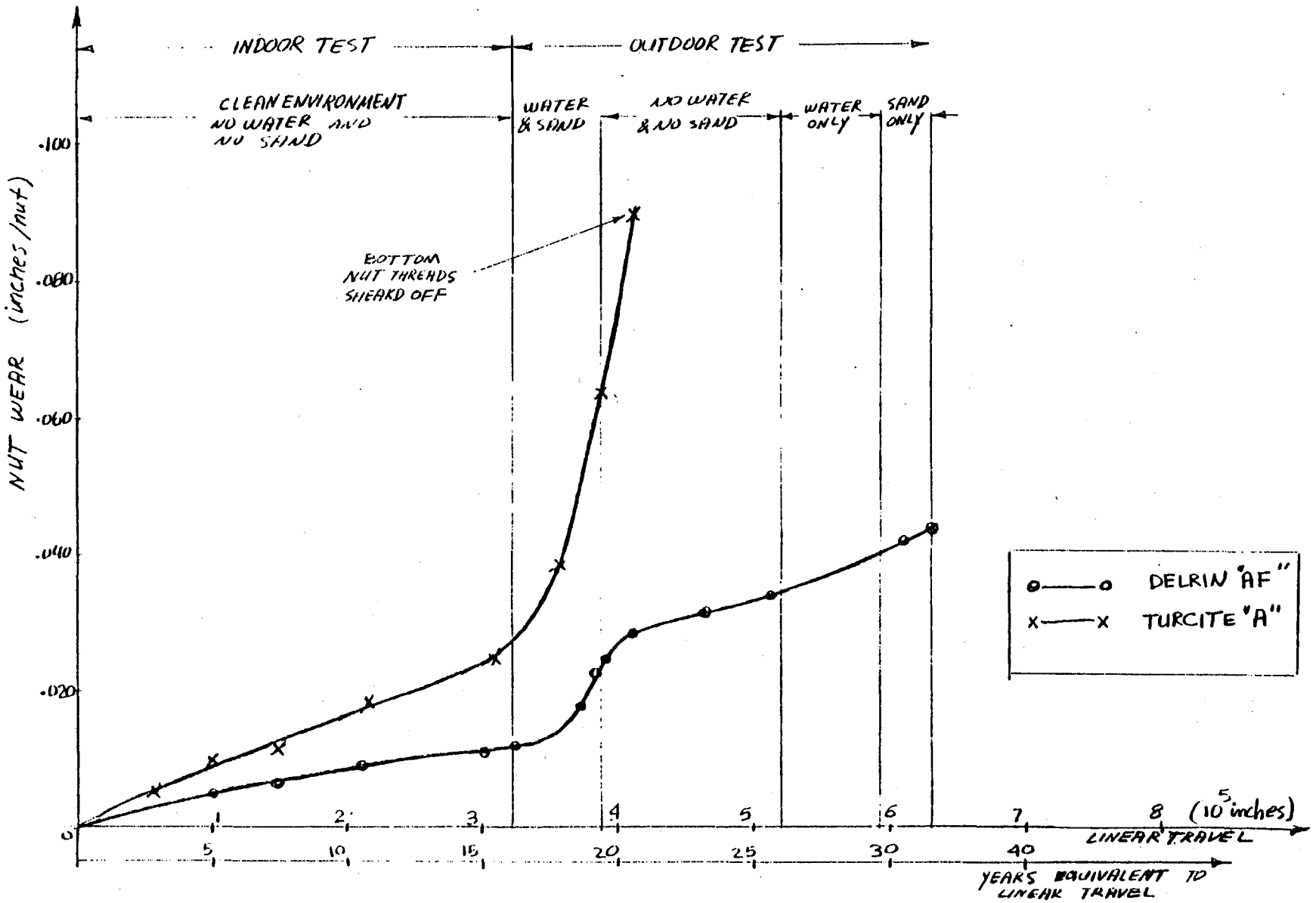

FIGURE 11 NUT WEAR VS. LIFE

TABLE 3

ENVIRONMENT	SCREW WEAR	No. OF CYCLES	EQUIVALENT LINEAR TRAVEL (inches)	ASSEMBLY HEIGHT (inches)		NUT WEAR (inches/NUT)		ENVIRONMENT	
				DELRIN "AF"	TURCITE "A"	DELRIN "AF"	TURCITE "A"	WATER	SAND
SUMMARY OF TEST MEASURED DATA									
INDOOR (CLEAN)	NO INDICATION OF SCREW THREAD WEAR	0	0	7.924	7.886	0	0	NO	NO
		2351	61126	7.932	7.894	.004	.004		
		3834	99684	7.935	7.902	.0055	.008		
		3908	101608	7.934	7.905	.005	.0095		
		4827	125502	7.936	7.906	.006	.010		
		5696	148096	7.937	7.909	.0065	.0115		
		6453	167778	7.940	7.914	.008	.014		
		7100	184600	7.941	7.918	.0085	.016		
		5379	217854	7.942	7.924	.009	.019		
		10233	266058	7.944	7.927	.010	.0205		
		11000	286000	7.946	7.930	.011	.022		
		11563	300638	7.947	7.933	.0115	.0235		
		11743	305318	7.947	7.935	.0115	.0245		
		12210	317460	7.948	7.936	.012	.025		
OUTDOOR (CONTAMINATES)	NO MEASURABLE WEAR, BUT INDICATIONS OF THREAD SURFACE FINISH CHANGE (SCRATCHES)	14035	364910	7.958	7.962	.017	.038	YES	YES
		14220	369720	7.960	7.968	.018	.041		
		14760	383760	7.970	8.002	.023	.058		
		14900	387400	7.974	8.010	.025	.062		
		14924	388024	7.974	8.012	.025	.063	NO	NO
		15055	391430	7.976	8.014	.026	.064		
		15166	394316	7.978	8.018	.027	.066		
		15385	400000	7.979	8.026	.0275	.070		
		15829	411554	7.980	8.052	.028	.088		
		17825	463450	7.986		.031			
		18710	486460	7.990		.033			
		19333	502658	7.991		.0335			
		19880	516880	7.992		.034			
		22673	589550	8.002		.039		YES	NO
		23595	613470	8.008		.042		NO	YES
		24245	630370	8.012		.044			

TABLE 4

SUMMARY OF NUT WEAR MEASUREMENT (1)

$Q = D_3 - (D_2 + D_1)$ $\quad Q_{ave.} = (Q + Q')/2$

$Q' = D'_3 - (D'_2 + D'_1)$

$W_B = B_d \cos^2\alpha - \frac{P}{2}\cot\alpha - \left[P_d - Q_{ave.} - B_d(1+\sin\alpha)\right]\sin\alpha$

LIFE	MATERIAL (NUT)		BALL DIA. (in.)	D_4	D_3	D_2	D_1	Q	D'_4	D'_3	D'_2	D'_1	Q'	$Q_{ave.}$	INCHES OF WEAR PER NUT USING: BALL MEASUREMENT W_B* ave.	DIAL INDICATOR MEASUREMENT W_D** APPROX.	ASSEMBLY HEIGHT MEASUREMENT W_H***
AFTER 15 YEARS OF LINEAR TRAVEL (INDOOR WITH NO RAIN AND NO SAND)	DELRIN "AF"	TOP	5/32	.725	1.505	.439	.423	.643	.726	1.505	.426	.440	.639	.6410	.016 / .0158 / .0178	.013	.012
			3/16	.725	1.505	.504	.503	.498	.726	1.505	.505	.510	.490	.4940			
		BOTTOM	5/32	.726	1.505	.422	.444	.639	.728	1.505	.443	.430	.632	.6355	.015 / .0144 / .0164	.015	
			3/16	.726	1.505	.515	.500	.490	.728	1.505	.515	.505	.485	.4875			
	TURCITE "A"	TOP	3/16	.730	1.516	.495	.488	.533	.738	1.506	.478	.487	.540	.5365	.0187	.025	.025
		BOTTOM	3/16	.728	1.502	.490	.486	.526	.736	1.510	.490	.488	.532	.5294	.0268	.030	
AFTER 30 YRS. (15 YR. INDOOR 15 YR. OUTDOOR)	DELRIN "AF"	TOP	3/16	.728	1.505	.468	.475	.562	.730	1.505	.470	.477	.558	.560	.035	.035	.044
		BOTTOM	3/16	.728	1.505	.460	.480	.565	.730	1.505	.480	.460	.565	.565	.036	.040	

* BALL MEASUREMENTS ON DELRIN NUT IS PERFORMED USING TWO DIFFERENT BALL SIZES, MEASURMENTS TAKEN USING SMALLER BALL IS BELEIVED TO BE THE MORE ACCURATE ONE.

** BACKLASH OF EACH NUT IS MEASURED ON THE SAME PORTION OF UNUSED SCREW, AND DUE TO DIFFICULTIES ASSOCIATED WITH THIS MEASUREMENTS APPROXIMATE WEAR (FINAL BACKLASH – INITIAL BACKLASH) FIGURES ARE GIVEN.

*** ASSEMBLY HEIGHT MEASUREMENT IS BELIEVED TO REPRESENT THE MOST ACCURATE WEAR FIGURES.

(1) METHOD & TERMINOLOGY FROM TOOL ENGINEERS HAND BOOK (McGRAW-HILL, 1949, 1st EDITION)

- The bottom Turcite nut failed in shear after 20 years of actual accelerated service life.
- Under clean test conditions, the actuator screw threads on the polymeric nut travel zone did not show any wear.
- A crack developed at the sharp end of each plastic nut thread and propagated.

APPENDIX D-1

THREE-WIRE METHOD FOR CHECKING THICKNESS OF ACME THREADS

(REF. TOOL ENGINEERS HANDBOOK - McGRAW HILL 1949, 1st. EDITION)

ACME thread thickness is given by the following formula:

$$T = 1.12931 * P + .25862(M - D) - W(1.29152 + .48407 S^2) \quad \text{(Ref. 4)}$$

where;

- T = Thread thickness at depth = $.25P$, (at pitch DIA.)
- P = pitch
- M = measurement over wires
- D = basic major diameter of screw
- W = diameter of wires
- S = tangent of helix angle at pitch line $\left(= \frac{\text{Lead}}{\pi(D - P/2)}\right)$

This formula transposed to give correct measurement M equivalent to a given required thread thickness is as follows:

$$M = D + \frac{W(1.29152 + .48407 S^2) + T - 1.12931 P}{.25862}$$

TEST SCREW THREAD THICKNESS:

D = 1.000
P = .250
W = .135
S = .09095
M = 1.056 measured
T = .122 calculated from measured M

SCREW THICKNESS WAS MEASURED BEFOR AND AFTER THE TEST, MEASUREMENTS SHOWED PRACTICALLY ZERO THREAD WEAR

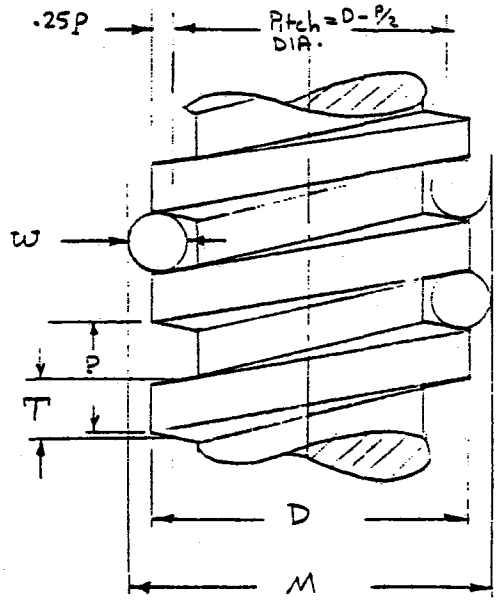

FIG. 8

APPENDIX D-2

NUT ASSEMBLY FRICTION TORQUE

1- PLASTIC

$$T_{Top} = F_S \cdot r_p \left(\frac{2\pi\mu r_p - p}{2\pi r_p + \mu p} \right)$$ Required screw torque For Top Nut

(Ref. 4)

$$T_{Bottom} = F_S \cdot r_p \left(\frac{2\pi\mu r_p + p}{2\pi r_p - \mu p} \right)$$ Required screw torque For Bottom Nut

neglecting the weight of the nut assembly

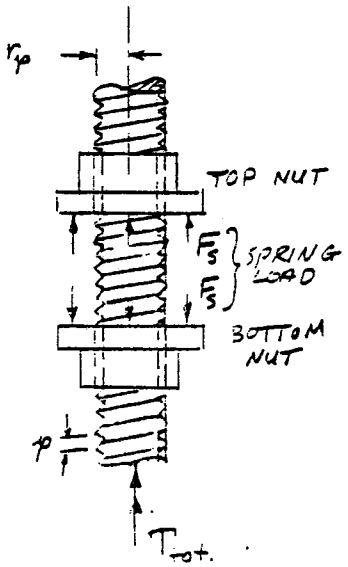

$T_{tot.} = T_{Top} + T_{Bottom}$

$F_S = 1500$ Lb spring load

$\mu = .1$ (coefficient of friction for plastic nut on steel screw)

$$T_{Top} = 1500 * \frac{.875}{2} \left(\frac{2\pi * .1 * .875/2 - .250}{2\pi * .875/2 + .1 * .250} \right) = 5.7 \text{ in-Lb}$$

$$T_{Bottom} = 1500 * \frac{.875}{2} \left(\frac{2\pi * .1 * .875/2 + .250}{2\pi * \frac{.875}{2} - .1 * .250} \right) = 126.5 \text{ in-Lb}$$

$T_{tot.} = 132.4$ in-Lb For $\mu = .1$

For $\mu = .08 \Rightarrow$ $T_{Top} = -7$, $T_{Bottom} = 113$

$T_{tot.} = 106$ in-Lb For $\mu = .08$

MEASURED ASSEMBLY TORQUE; FOR EACH PLASTIC NUT SET

TORQUE ARM = 13"
APPLIED FORCE = 9 Lb
NUT ASSEMBLY TORQUE = 13" x 9 Lb = 117 in-Lb ← Measured TORQUE (each set)

And coefficient of friction is: $\mu = .09$ ← Calculated from measured Torque

2- BRONZE NUT (K=.3)

SPRING LOAD = 1500 Lb

$$T_{top} = 1500 * .438 \left(\frac{6.28 * .3 * .438 - .250}{6.28 * .438 + .3 * .250} \right) = 134$$

$$T_{Bottom} = 1500 * .438 \left(\frac{6.28 * .3 * .438 + .250}{6.28 * .438 - .3 * .250} \right) = 264$$

$\boxed{T_{tb} = 398 \text{ in-Lb}}$ BRONZE NUT ASSEMBLY

$T_{total} = 117 * 2 + 398 = \underline{\underline{632 \text{ in-Lb}}}$ For 3 NUT SETS (2 plastic, 1 Bronze)

3- MOTOR HORSEPOWER

SCREW SPEED = 58 RPM

$$HP = \frac{RPM * TORQUE^{in-\#}}{63025}$$

$$HP = \frac{58 * 117}{63025} = 0.11 \quad \text{for each plastic nut assembly}$$

$$HP = \frac{58 * 398}{63025} = 0.37 \quad \text{for bronze nut assembly}$$

$HP = .11 * 2 + .37 = .59$ For 3 assemblies (2 plastics, 1 bronze)

IF TOTAL DRIVE EFFICIENCY is ASSUMED TO BE 50%

$\boxed{HP = 1.2}$ Motor HORSEPOWER REQUIRED TO DRIVE 3 ASSEMBLIES

$\boxed{HP = 1/2}$ Motor HORSEPOWER REQUIRED TO DRIVE 2 plastic ASSEMBLIES

APPENDIX D-3

NUT THREAD WEAR MEASUREMENT

(Using Ball & Caliper)

TEST NUT THREAD WEAR & THICKNESS CAN BE MEASURED AS FOLLOWS:
PLACE THE BALL IN THE THREAD GROOVE AND MEASURE REQUIRED DIMENSIONS IN AT LEAST 4 LOCATION (PREFERABLY 90° APART).

$$Q = D_3 - (D_2 + D_1)$$
$$Q' = D_3' - (D_2' + D_1')$$
$$K = B_d \cos\alpha - 2S\tan\alpha$$
$$W = \left(K - \frac{P}{2}\right)\cos\alpha = T\cos\alpha$$
$$S = \frac{P_d}{2} - \left(\frac{Q}{2} + \frac{B_d}{2} + \frac{B_d}{2}\sin\alpha\right)$$
$$K = B_d\cos\alpha - 2\left[\frac{P_d}{2} - \frac{Q}{2} - \frac{B_d}{2}(1+\sin\alpha)\right]\tan\alpha$$
$$\boxed{W = B_d\cos^2\alpha - \frac{P}{2}\cos\alpha - \left[\frac{P_d}{2} - \frac{Q}{2} - \frac{B_d}{2}(1+\sin\alpha)\right]\sin\alpha}$$

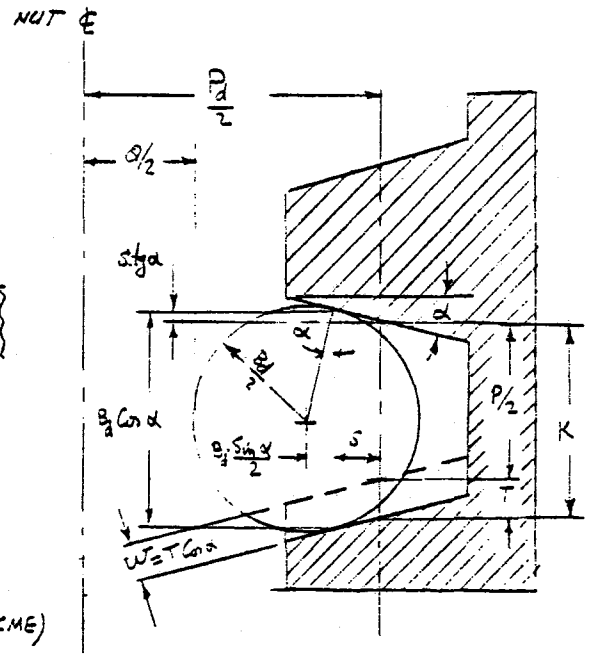

(FIG. 9)

where:
- W = wear
- B_d = Ball diameter
- P_d = Pitch diameter
- P = pitch
- Q = Ball to ball distance (180° apart)
- α = Thread taper angle (14.5° for ACME)
- T = Axil wear

TEST NUT DATA

$P_d = .875$

$P = .250$

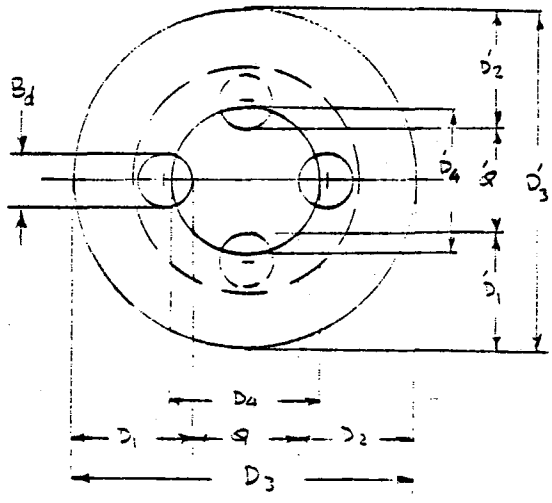

APPENDIX E

REFLECTOR MATERIALS/ASSEMBLY TESTS

APPENDIX E
REFLECTOR MATERIALS/ASSEMBLY TESTS

Engineering load tests where conducted on full size facets to verify structural and functional integrity. Coupons representing the facet construction were subjected to temperature, humidity and hailstone testing. Thirty-four facet specimens were tested to establish their modulus of rupture; and several cellular glass core samples were shear tested to establish the core shear allowable. Tests were also conducted to aid in the selection of materials, provide design data, verify design margins or substantiate analytical models. Table 1 lists the candidate facet assembly materials tested.

1.0 Optical Tests

1.1 Specular Transmittance and Reflectance

Optical properties measurements were made on coupons of 3 types of mirror glass to assist in selecting the most cost effective reflector material. Glass coupons were measured for transmittance and reflectance by Sandia Laboratories, Albuquerque, New Mexico. Unsilvered coupons were measured for specular transmittance and hemispherical transmittance. Silvered coupons were tested for specular reflectance and hemispherical reflectance. Measurements were taken on a Beckman Dk-2 spectroreflectometer (350 to 2500 nm) and a bi-directional reflectometer (500 nm; 1 mrad to 15 mrad).

Measurements of the specular transmittance agreed with the hemispherical transmittance at 500 nm, and showed good precision for apertures from 1 mrad thru 15 mrad. The same effects were observed when measuring reflectance on the 2 instruments. Thus, the solar averaged specular transmittance was the same as the solar averaged hemispherical transmittance. Similarly, the solar averaged specular reflectance was the same as the hemispherical reflectance. Results from the optical tests are shown in Table 2.

1.2 Surface Flatness

Waviness of reflector surfaces causes diffusion of the incident light, thus

Table 1 . . Facet-Assembly Materials Tested

Function	Generic Name	Trade Name
Mirror and backskin glasses	Fusion glass	0317 Corning
	Fusion glass	7809 Corning
	Float glass	Ford low iron float
Mirror adhesive	Epoxy	BMS 529
	Epoxy	DER 332/Epocast 9427
	Polyurethane	Vulkem 102L
	Polysulfide	3M EC1239–B–½
	Asphalt/urethane	PC-88
Surface densifier	Batch/silica sol	Batch/Ludox
	Gypsum cement	Hydrocal B-II
Core	12 PCF cellular glass	Pittsburg Corning Foamsil
	8.5 PCF cellular glass	Pittsburg Corning Foamglas
Core bond	Gypsum cement	Hydrocal B-II
	Asphalt/urethane	PC-88
	Polyurethane	Vulkem 102L
	Polysulfide	3M EC1239–B–½
	Batch/epoxy	Batch/BMS 529
Edge sealant	Butyl	Pittseal 444
	Cyanoacrylate	Loctite mixture
	Silicone	G.E. 1200

Table 2 Transmittance and Reflectance of Various Glasses

Glass thickness (inches)/type	Clear (C) or silvered (S) [1]	Transmittance solar averaged hemispherical (AM 1.5) Sandia [2]	Reflectance solar averaged hemispherical (AM 1.5) Sandia [2]
.060 / 0317 Corning	C	.908	
	S		.935
.070/0317 Corning	C	.909	
	S		.938
.060/7809 Corning	C	.919	
	S		.945
.118/low iron float - Ford	C	.894	
	S		.903

[1] All metalizing was done by Falconer Glass
[2] Measurements by J.M. Freese - Sandia
- Beckman spectroreflectometer, DK-2, 350-2500 nm
- Bi-directional reflectometer, 1-15 mrad aperture, 500 nm

reducing the energy reflected to the receiver. In the facet assembly, non-flatness may be caused by inadequate preparation of the core surface, variation in the thickness of the mirror glass, or a non-flat assembly table. A system was needed to measure the flatness of facet coupons and complete facets to determine whether they satisfied error budget requirements, and to aid in isolating causes of non-flatness. Two techniques were evaluated: a stationary laser ray-tracer; and a portable surface-table tester (electronic level system); they are illustrated in Figures 1 and 2.

In the laser ray trace method, a laser beam impinges on the sample mirror surface at some specified angle. The deviation of the reflected beam from the specular direction is a measurement of non-flatness. The reflected beam is incident on a linear position sensing device which produces an analog output proportional to the laser beam displacement. An angular displacement versus linear position plot may then be generated.

The second system consists of an electronic level, a desk top computer and an X-Y plotter. The level traverses the surface in a prescribed pattern, and is returned to its starting point. The data acquired is input to the computer which produces an isometric plot and a printout of statistical data.

Several facet coupons and 2 development facet assemblies were prepared to evaluate the effects of core machining, adhesive type, and fabrication process upon flatness. The coupons were first measured at Battelle Pacific Northwest Labs on their laser scanner; they were then measured at BEC with the electronic level. Direct correlation between the two measurement techniques was not possible because of fundamental differences in procedures. However, overall average flatness for each coupon did compare well for the two techniques. Flatness measurements of the 2 development panels were made using the electronic level system only. Table 3 shows the results of the measurements of coupons with 3 types of adhesive, and of the development panels fabricated on a construction table with 2 types of adhesives. Primarily because of its portability, the electronic level system was chosen for further use.

The coupon and development panel tests revealed that the core machining variations had negligible effects on flatness. The tests indicated that the

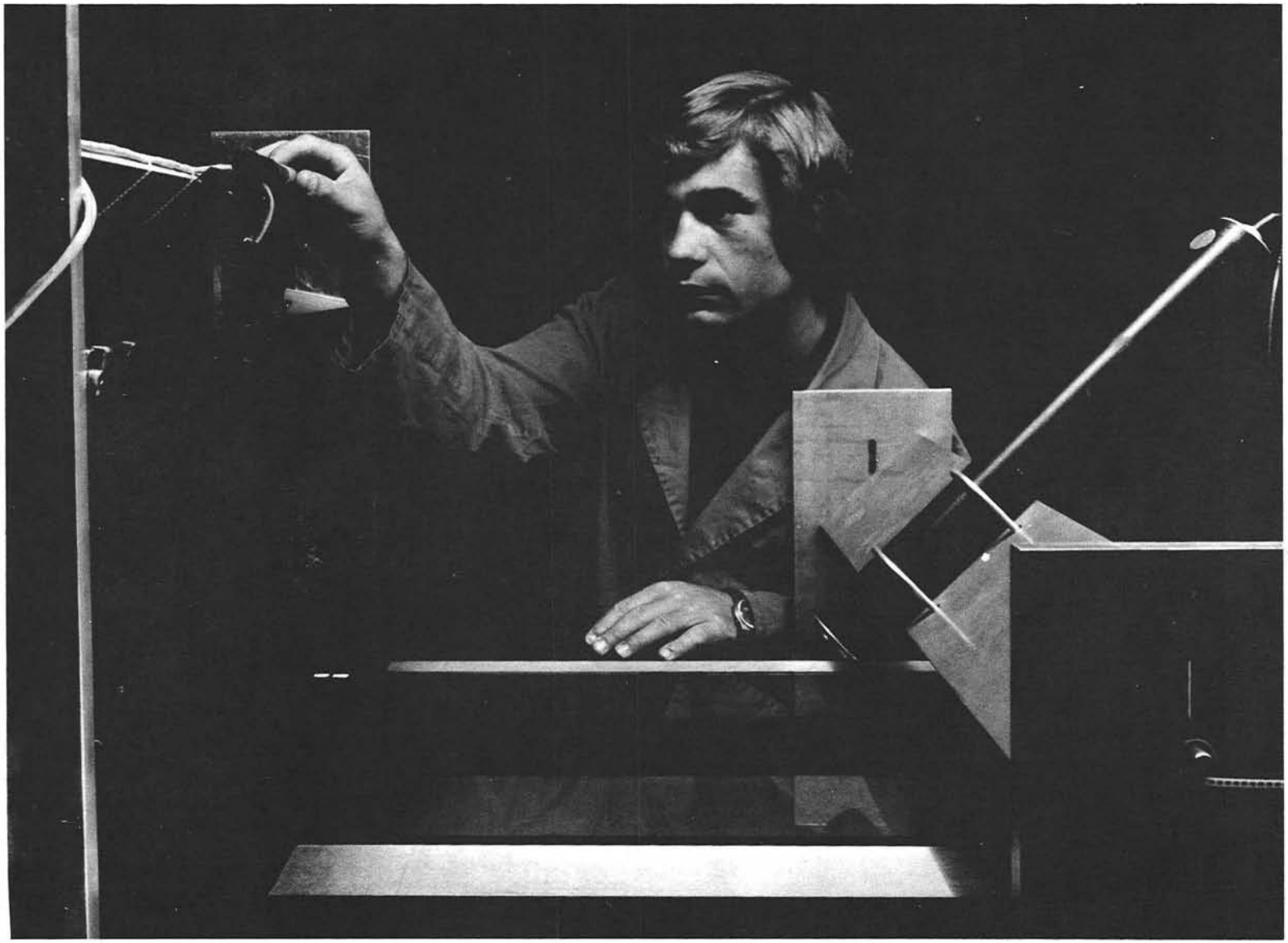

Figure 1 *Laser Scan Techniques*

Figure 2 *Electronic Level Measurement Technique*

Table 3 Results of Flatness Measurements

Configuration	Adhesive	Slope error Average ± 1σ mr
2ft x 2ft coupon	• Epoxy • Polyurethane • Polysulfide	.42 .50 — 1.83 ~3.0
4ft x 10ft panels • Fabrication table • Panel A • Panel B	 • Epoxy • Polyurethane	 .73 .81 1.28

adhesive type and application method, and the surface quality of the fabrication table do contribute to non-flatness. Epoxy and polyurethane adhesives produced coupon flatness approaching the desired 0.4 mrad (1-sigma value). Use of the polysulfide adhesive was discontinued because of the difficulties in obtaining flat coupons.

The flatness of the first 2 development facets was not satisfactory; however, analysis of the measurement data suggested that requirements could be met if an improved fabrication table was used. A new table was therefore built.

A development facet made on the new table, using epoxy adhesive, was measured to be flat within 0.35 mrad. No further full size facets were built with polyurethane adhesive because they failed to meet structural requirements. Results with the epoxy-bonded facets showed that adequate flatness could be obtained using the developed materials, procedures, and fabrication table.

1.3 Image Evaluation

Having evaluated the mirror glass specularity and the flatness of the fabricated facet, the next step was to verify that a well-shaped solar image could be produced. This will ultimately be verified by the Beam Characterization System (BCS) at the CRTF. However, a test was necessary to get a preliminary evaluation of the image prior to building the prototype facets. This was accomplished by analyzing image photographs from a single full-size facet assembly.

The development facet was mounted on a forklift truck and transported to a point 213.4 meters from the north side of a tall building, as illustrated in Figure 3. The facet orientation was adjusted until the sun's image was projected on the side of the building. The image was photographed at different exposures to obtain the best contrast between the image and building surface. Eight-by-ten-inch transparencies were produced for analysis; Figure 4 is an example of one of the photographs taken. Figure 5 shows the results of scans along the horizontal and vertical axes taken with MacBeth TR524 transmission densitometer. The data is plotted to show relative intensity

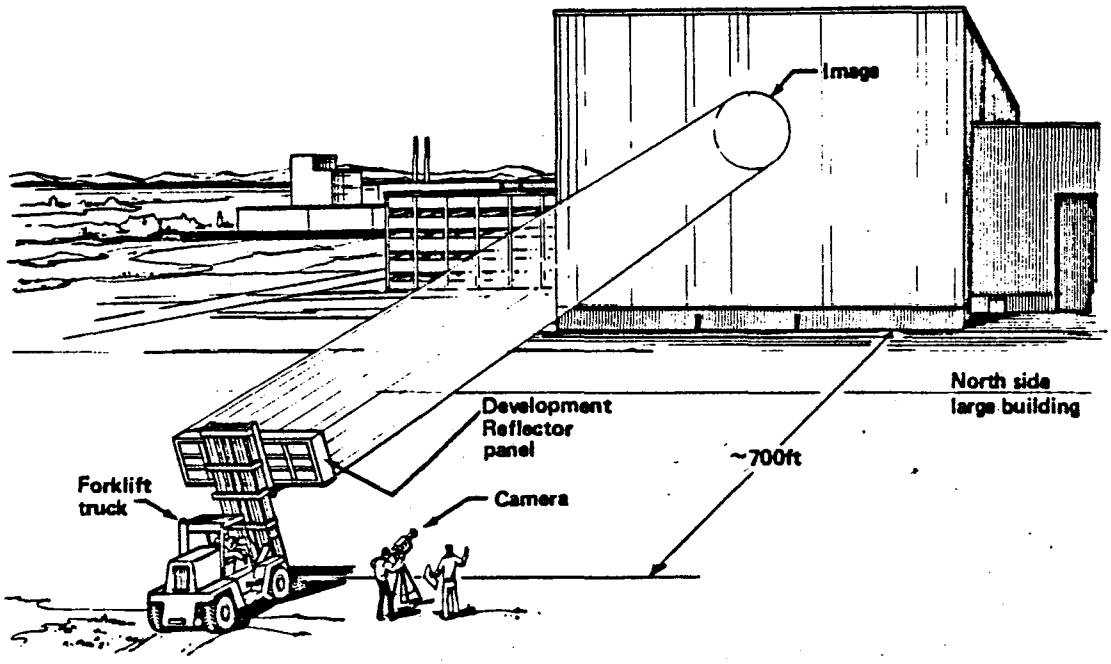

Figure 3. Facet Image Evaluation

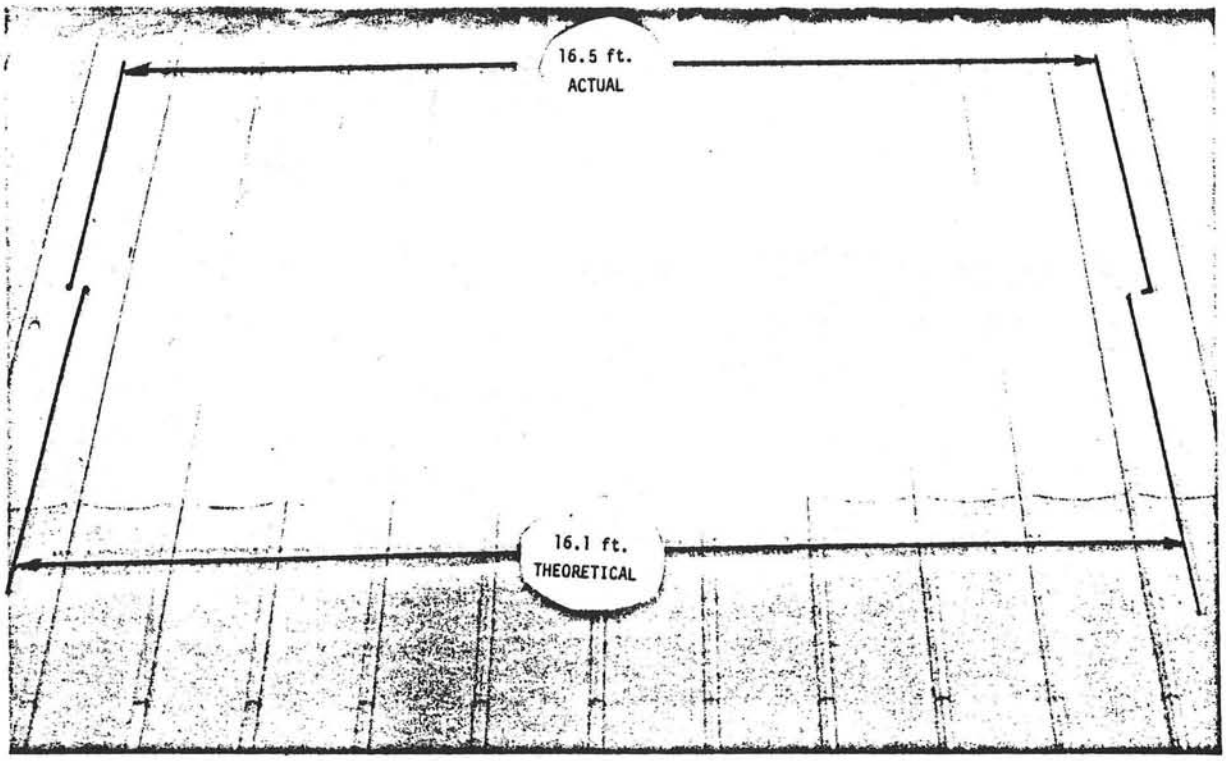

Figure 4 *Facet Image on Side of Building*

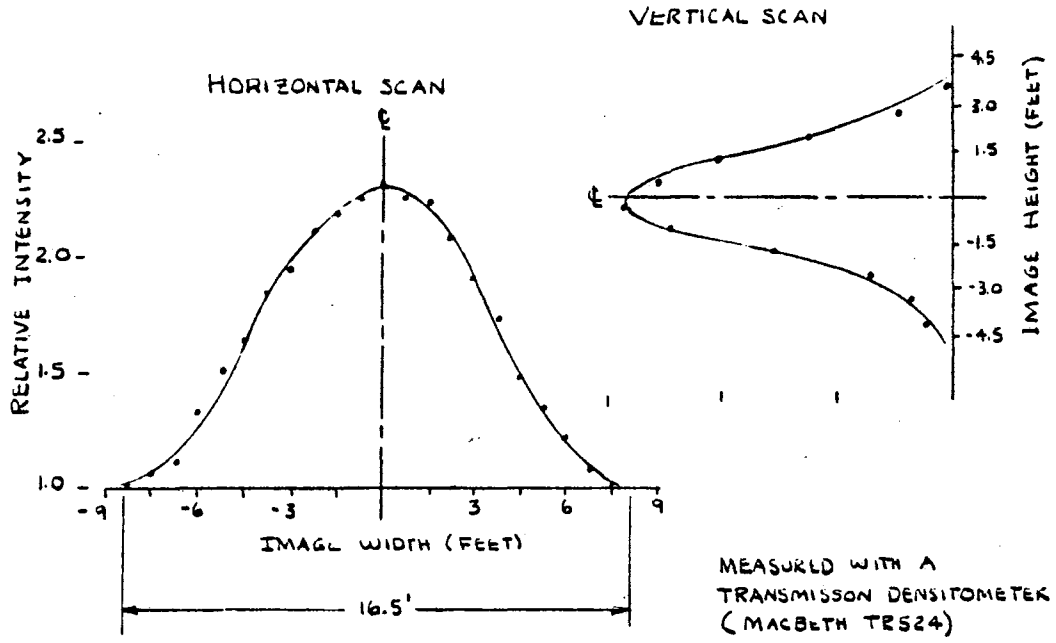

Figure 5 Intensity Plots of Facet Image

(background = 1.0) versus position in the image. These scans show that the image is symmetrical about the axes, and only slightly larger than the theoretical width for the range tested, which is given by:

$$W = L + 2(213.36 \text{ Tan } \theta/2), \text{ where}$$

W = Horizontal width of image, meters,

L = Horizontal width of facet, meters,

θ = Solar disc subtense angle, degrees,
For range = 213.36 m, we have,

$$W = 3.05 + 2(213.36 \text{ Tan } 0.25°) = 4.91 \text{ m.}$$

The observed width was 5.03 m. Subtracting the theoretical from the measured yields 0.12 m, which would be distributed on both sides of the beam. Therefore, in angular terms, we obtain 0.29 mrad. While the results are preliminary and approximate, they are of the desired order of magnitude and imply that a satisfactory reflected image can be obtained from facets which meet the design specifications.

2.0 Structural Tests

2.1 Shear Strength of Core Material

Design analyses predict the stress in the core material (Foamsil 75) will be quite small and will be primarily in shear. Under normal operating conditions of 27 mph winds the shear stress is predicted to reach a maximum of 10 psi. Previous experience with Foamsil-75 and tests run on Foamglas indicate that the material would certainly have excess margin for this load. For design purposes, it is assumed that there would be one short-term loading of 60 psi shear (90 mph wind).

To verify that an adequate margin exists between this predicted core shear stress and measured shear strength of Foamsil 75, an abbreviated shear test was performed.

Twenty samples, 15.2 cm x 5.1 cm x 1.3 cm, were cut from a single block of Foamsil 75. The samples were epoxy-bonded to knife edged mounting plates for shear loading per ASTM C273. Figure 6 shows a shear-test sample mounted in the test machine. Bending moments are minimized through the use of spherical seats and knife edges in the loading fixtures.

When shear loads are applied in this manner, the sample material failed approximately diagonally across the sample block. Figure 7 is a photograph of a sample after test. As can be seen, failure occurred diagonally down the length of the sample and was contained within the cellular glass. There was no failure at the adhesive/glass interface. All samples tested failed in a similar manner.

The 20 samples were tested to failure. The shearing stress was computed from the applied load and the dimensions of each sample. The average stress at failure was 84 psi with a standard deviation of 6 psi. Therefore, the 99% confidence interval would be 99 psi (upper confidence limit) to 69 psi (lower confidence limit). However, this result must be tempered by recognizing that all samples were taken from a single 18" x 24" block of cellular glass; block-to-block variations were not evaluated.*

2.2 Modulus of Rupture

An analytical model was prepared to size the facet to meet stiffness and strength requirements. The facet design is stiffness-limited under operating load conditions. The analytical model did not include the effects of adhesive; it assumed direct coupling of the cellular glass to the fusion glass skins. Thus it was necessary to determine the effects of various adhesives on stiffness and strength, as well as substantiate the analytical model. To accomplish this, modulus of rupture (MOR) testing was undertaken.

---

*The variation of shearing strength among different samples (blocks) from the same production run of cellular glass is not expected to be very great based on fracture testing performed by JPL. In that testing, the coefficient of variation in fracture stress of 79 samples from 16 blocks of 12 pcf Foamsil 75 was 0.147: see reference 2-2-4.

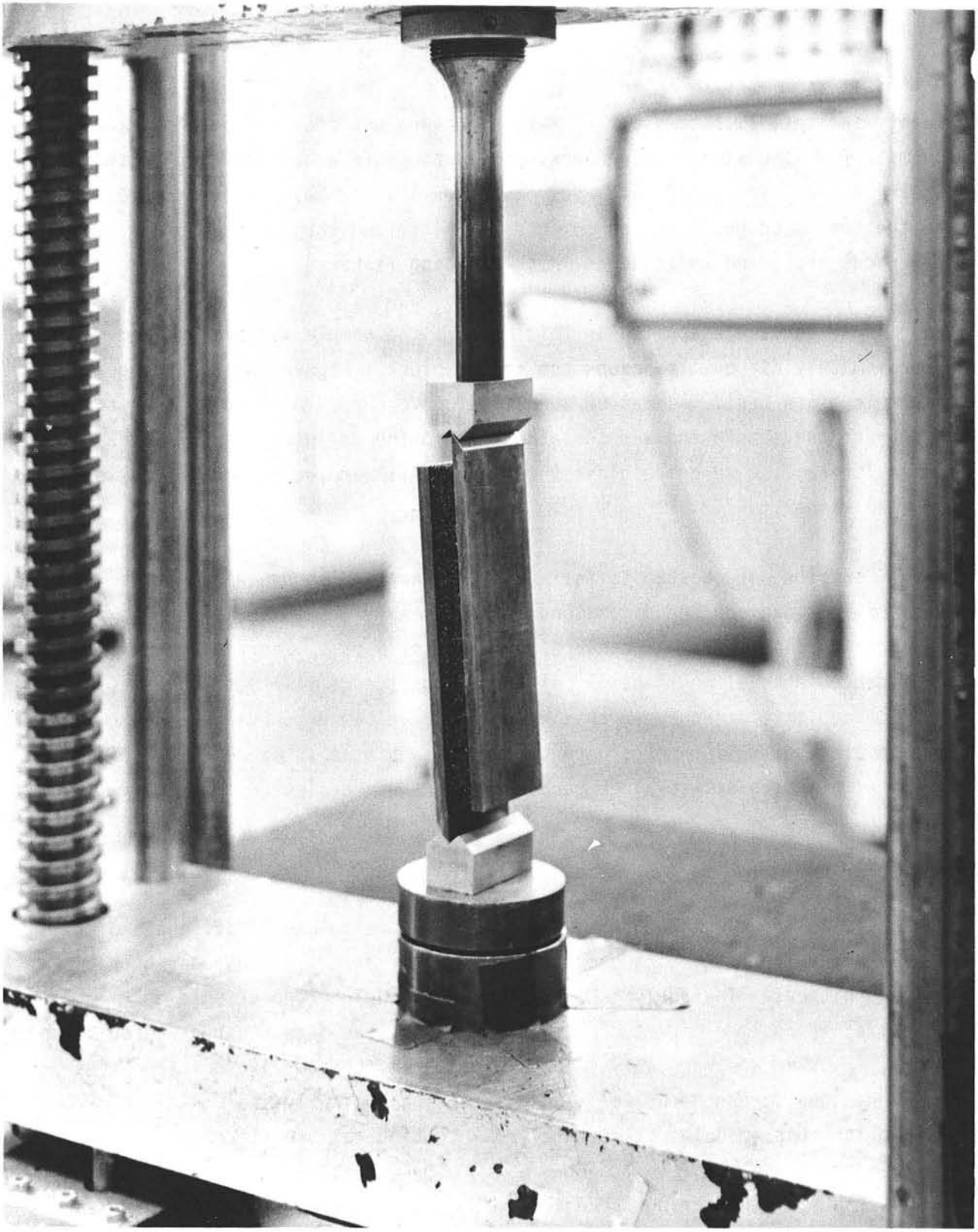

Figure 6 *Shear Testing of Facet Core Material*

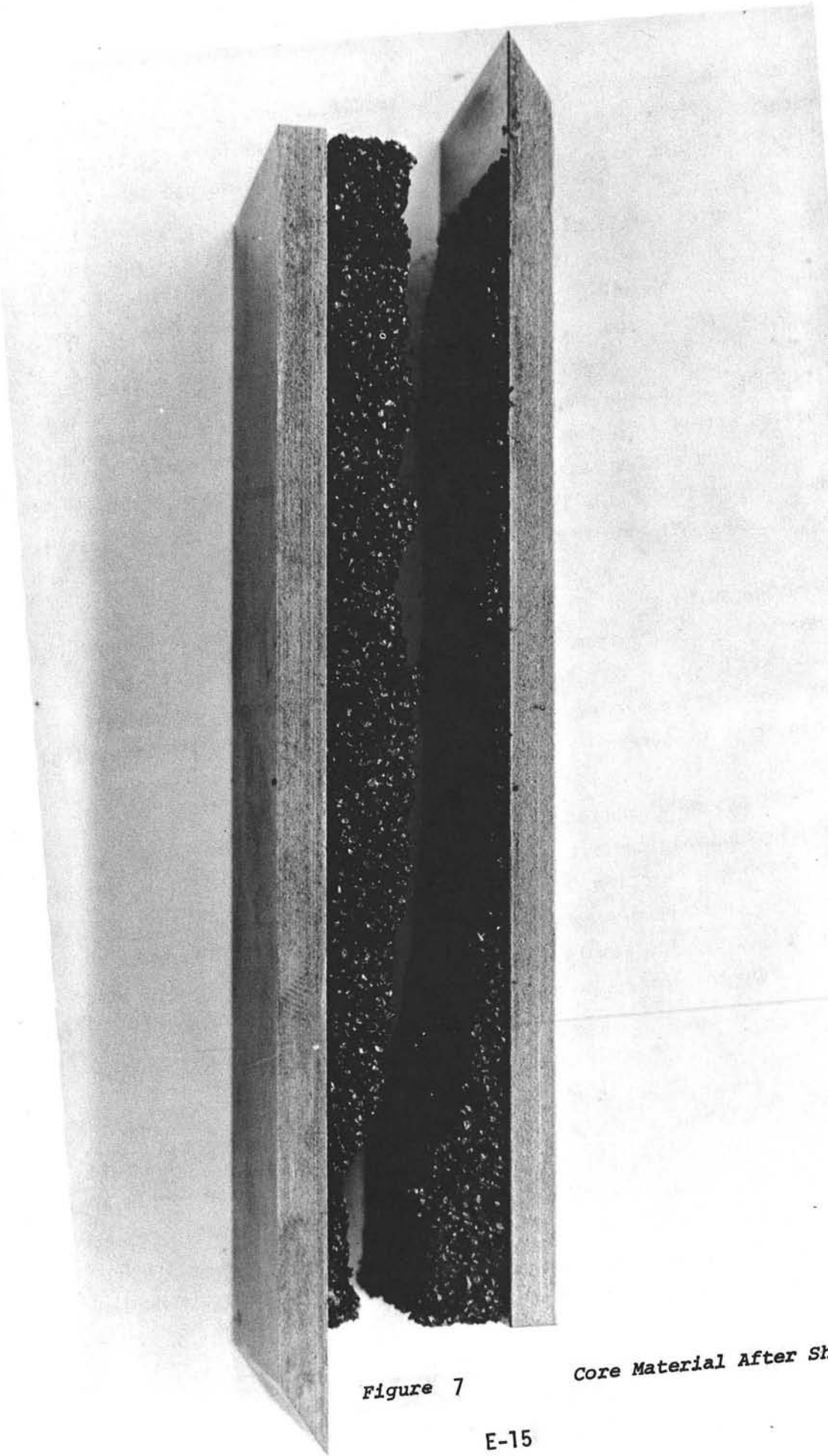

Figure 7 Core Material After Shear Test

MOR testing was performed per ASTM C203 (modified) at the Pittsburgh Corning Laboratory in Pittsburgh, Pennsylvania. Large samples were prepared to simplify deflection measurement. Figure 8 depicts the sample geometry.

Several variables were included in the MOR testing: adhesive type, glass type, geometry of core bonding, and temperature. Table 4 provides a listing of these variables and the 50 samples prepared to evaluate their effects on stiffness and strength.

In addition to the measurement of load and deflection, six samples were instrumented with strain gages on both glass skins to allow comparison of measured and predicted stresses. Prior to installing the gages, a laboratory test was performed on a small glass beam to verify the ability to use strain gages on glass.

Gages were bonded to front and back surfaces of a 5 inch cantilever beam which was incrementally loaded from 0 to 1600 psi and back to 0. Thirty-two individual measurements were taken. Repeatability, front to back gage agreement, and measured-versus-calculated stress correlation were well within normal standards for strain gage measurements.

Figure 9 shows a sample mounted in the Instron load machine equipped with quarter-point loading fixtures. Two-degree-of-freedom fixturing was used for both loading and reaction. Dial gages were provided at one end and at the sample center. Cross head speeds of 0.02 in/min were used during the application of load. The sample shown was equipped with strain gages which were monitored by the instruments on the cart in the right-hand portion of the photograph.

Figure 10 shows the test setup used for testing at elevated and reduced temperatures. The samples were enclosed in an insulating particle board box, provided with necessary penetrations for fixturing and gages. The sample and box was soaked in an oven or refrigerated until the desired temperature was reached as determined by an attached thermocouple. Next the sample and box were transported to the loading fixture and tested. The temperature during test, which was observed to remain nearly constant, was recorded.

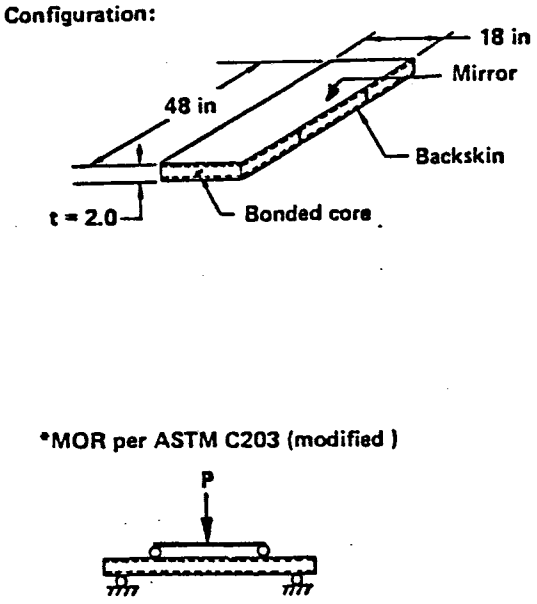

Figure 8 *Schematic of Facet MOR Test*

Table 4 *Configuration and Quantity of Facets Subjected to MOR Tests*

FACET CONFIGURATION	Mirror	Backskin	Adhesive	Core Bond Configuration	Densifier	Temperature	Quantity
Prototype	.059in(0317)		Epoxy (BMS 529)	Centered	–	Ambient	10
				Non-centered	–	Ambient	10
				" "	–	-30°C	3
				" "	–	+50°C	3
Production	.059in(7809)		Epoxy (BMS 529)	Non-centered	–	Ambient	8
Prototype with Alternate Adhesive system	.059in(0317)		Polyurethane (Vulkem 102L)	Non-centered	Silica Sol (Ludox)	Ambient	10
						-30°C	3
						+50°C	3
						Total	50

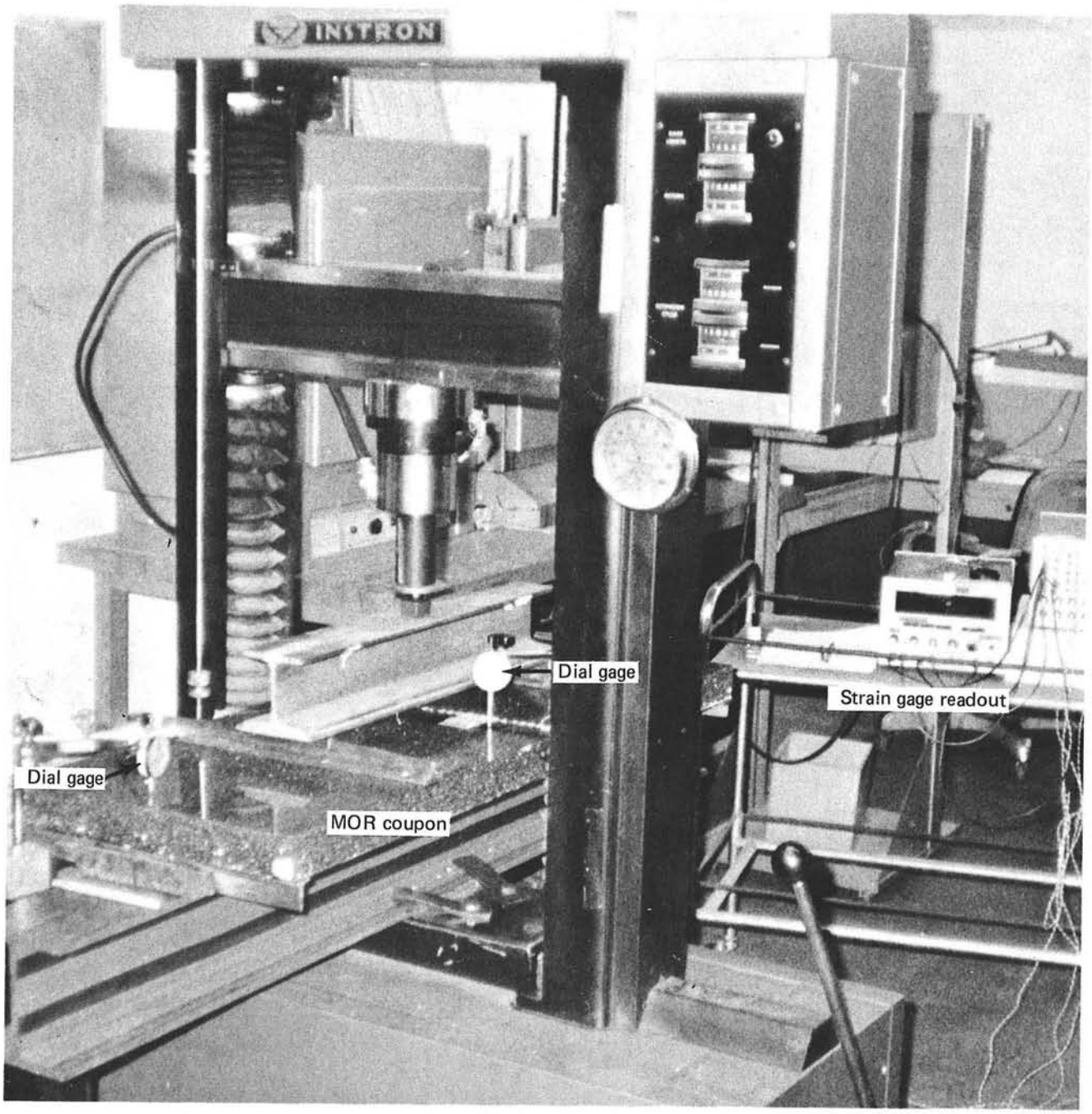

Figure 9 *MOR Test Setup*

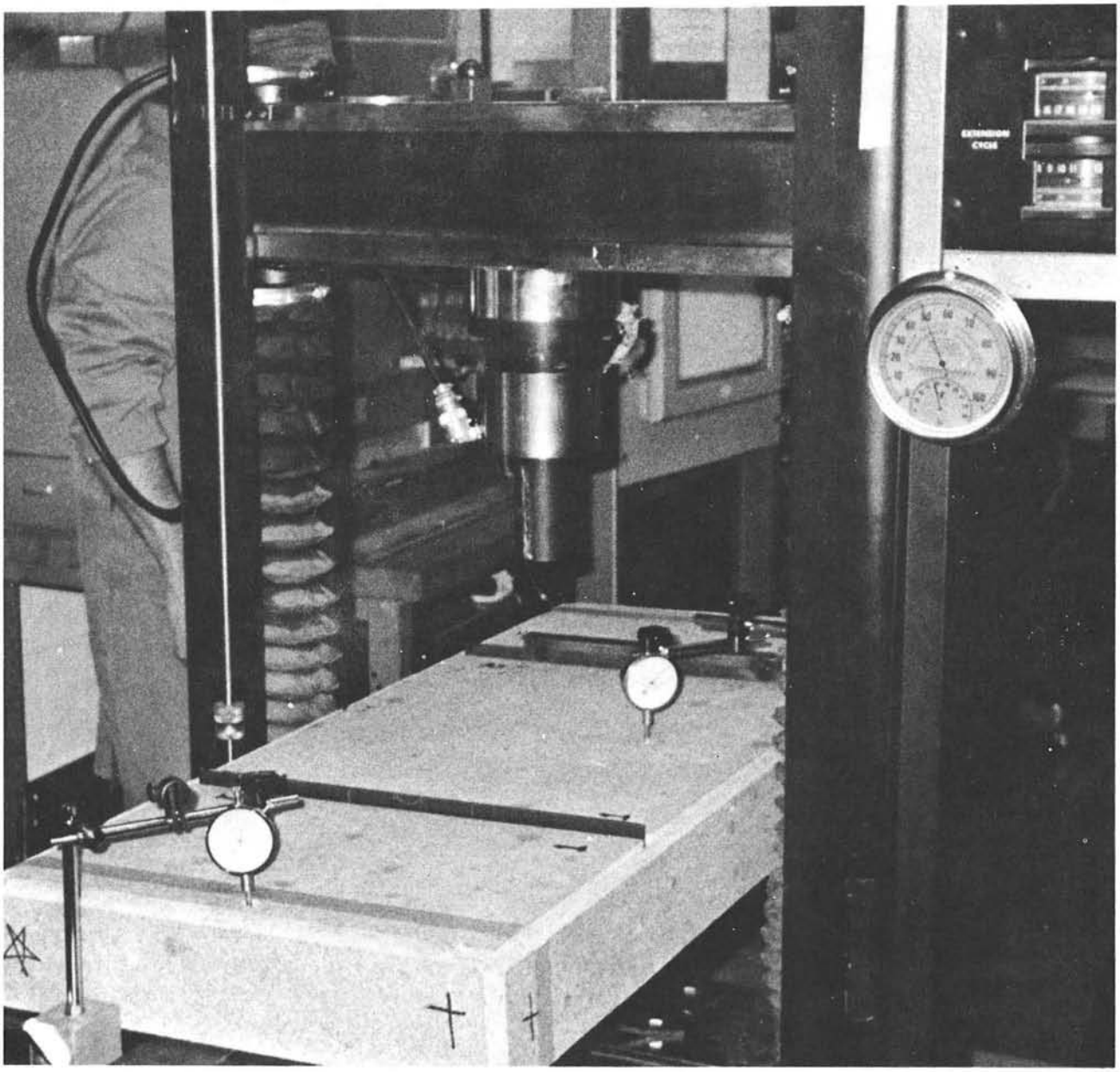

Figure 10 *Facet MOR Testing at Non-Ambient Temperatures*

Results of the MOR tests are presented in Table 5, which compares test results with analytical values. The analytical model predicted that a 1000 lb load would cause a deflection of approximately .044 inches; the skin stress would be approximately 2280 psi; and the failure load would exceed 420 lb to meet operating and survival requirements.

Samples of the prototypical facet configuration at 22°C compared well with analytical predictions. The panels were stiffer, the skin stress slightly lower and the failure load well above minimum requirements. Data for the 6 samples tested at elevated and reduced temperatures varied negligibly from the ambient temperature results indicating small or no temperature dependence throughout the range of interest (-30°C to 50°C). Samples of the production facet configuration behaved the same* as the prototype facets under ambient temperature test conditions.

Test results for the prototype facet with polyurethane adhesive revealed the effect of the adhesive on the facet's stiffness and strength. The deflection at ambient temperature was about 3 times that of the epoxy-bonded prototype, and the load at failure marginal. The temperature dependence was observed to be quite dramatic, especially at low temperatures. At -30°C, the deflection under a 1000 lb load was about half of what it was at ambient temperature, and the load at failure twice the ambient temperature value. The high temperature condition produced results more comparable with the ambient temperature tests.

Based on the results of MOR testing it was concluded that the strength and stiffness of the prototype and production facets showed good agreement with analytically-derived values, and both configurations satisfy design requirements for these characteristics.

---

*The only difference between the prototype and production samples was the glass skin (0317 versus 7809), which was not expected to introduce significant variations.

Table 5 Results of Facet MOR Testing

FACET CONFIGURATION	TEMPERATURE	Stiffness δ Max @ P=1,000		Skin Stress σ Max @ P=1,000 lb		Failure Load P_{Max}	
		Test (in.)	Analysis (in.)	Test (psi)	Analysis (psi)	Test (lb)	Analysis (lb)
Prototype 0317/BMS 529	−30°C	.036	.044	–	–	1,930	
	▷1 +22°C	.037±.003	.044	2040±86	2,280	1,870±387	>420 (1,000 psi) allow.
	+50°C	.039	.044	–	–	1,430	
Production 7809/BMS 529	+24°C	.033±.002	.044	–	–	1,907±260	
Prototype Alt. 0317/polyurethane	-30°C	.061	.044	–	–	1,240	
	▷1 +24°C	.111±.015	.044	–	–	655±127	
	+50°C	.112	.044			632	

▷1 Average ±1 std. deviation

2.3 Residual Stress Evaluation In Facet Front Skin

Samples of sheet glass, various composite coupons, and a prototype facet were evaluated for residual stress in the facet front skin. The purpose of the evaluation was to determine the front-skin stresses introduced during glass manufacture, and the stresses introduced during facet fabrication.

A portable, large-field reflecting polariscope was used to scan the samples. Due to the low stresses observed (<<1000 psi), the instrument was difficult to use in its normal mode. A small glass cantilever beam was set up and used to calibrate the polariscope in the range of interest (a few hundred psi). With this calibration, subsequent readings were believed to be accurate to approximately $\pm$100 psi; Table 6 lists the results.

The stresses measured in composite coupons and the facet assembly were not significantly different than the glass sheet stock. This suggests that the facet fabrication process does not substantially increase the front-skin residual stress. In addition, the residual stress appears to be in the range of 200 to 300 psi.

2.4 Facet Static Load

A full-size facet, fabricated according to prototype baseline design specifications, was statically loaded to simulate various anticipated environmental conditions. The facet was instrumented to measure skin stress and facet displacement under these loads. The purpose of the test was to verify the structural analysis model.

The facet was supported horizontally by its 4 mounting clips in the same fashion that it is supported on the heliostat frame. A large rigid fixture was used in place of the frame eliminating deflections from other than the facet. Ten electronic deflection indicators (EDI) were placed at points along one end, and along the transverse centerline; these were the expected points of maximum deflection. Thirteen strain gages were installed at points of anticipated maximum stress on the glass skins. Figure 11 shows the overall test setup. Figure 12 gives the locations of EDI's and strain gages on the test facet. Loading of the facet was accomplished by placing

Table 6 *Results of Residual Stress Measurements*

SAMPLE	MEASURED STRESS (PSI) ▷
GLASS SHEET STOCK, CLEAR 0317 FUSION, .060"	< 200 PSI, DISTRIBUTED
GLASS SHEET STOCK, SILVERED 0317 FUSION, .060"	< 200 PSI, DISTRIBUTED
2 FT x 2 FT x 2 IN FLATNESS COUPONS, 0317 FUSION, .060" (URETHANE ADHESIVE)	< 200 PSI, DISTRIBUTED
1 FT x 1 FT x 2 IN HAIL COUPON - 0317 FUSION, .060" (EPOXY ADHESIVE)	~ 300 PSI MAX. ALONG ONE EDGE
1 FT x 1 FT x 2 IN HAIL COUPON - FLOAT, .118" (POLYSULFIDE ADHESIVE)	~ 250 PSI MAX. ALONG EDGES
1 FT x 1 FT x 2 IN HAIL COUPON - FLOAT, .118" (EPOXY ADHESIVE)	~ 150 PSI, DISTRIBUTED
SIX, 43" x 18" x 2" MOR COUPONS - 0317 FUSION, .060"	150 PSI AVERAGE MAX. 250 PSI MAX. OBSERVED
ONE, 4' x 10' x 2" PROTOTYPE FACET	< 250 PSI DISTRIBUTED

▷ MEASUREMENTS WITH A PORTABLE, LARGE FIELD REFLECTING POLARISCOPE CALIBRATED WITH A LOADED, 0317 FUSION GLASS CANTILEVER BEAM

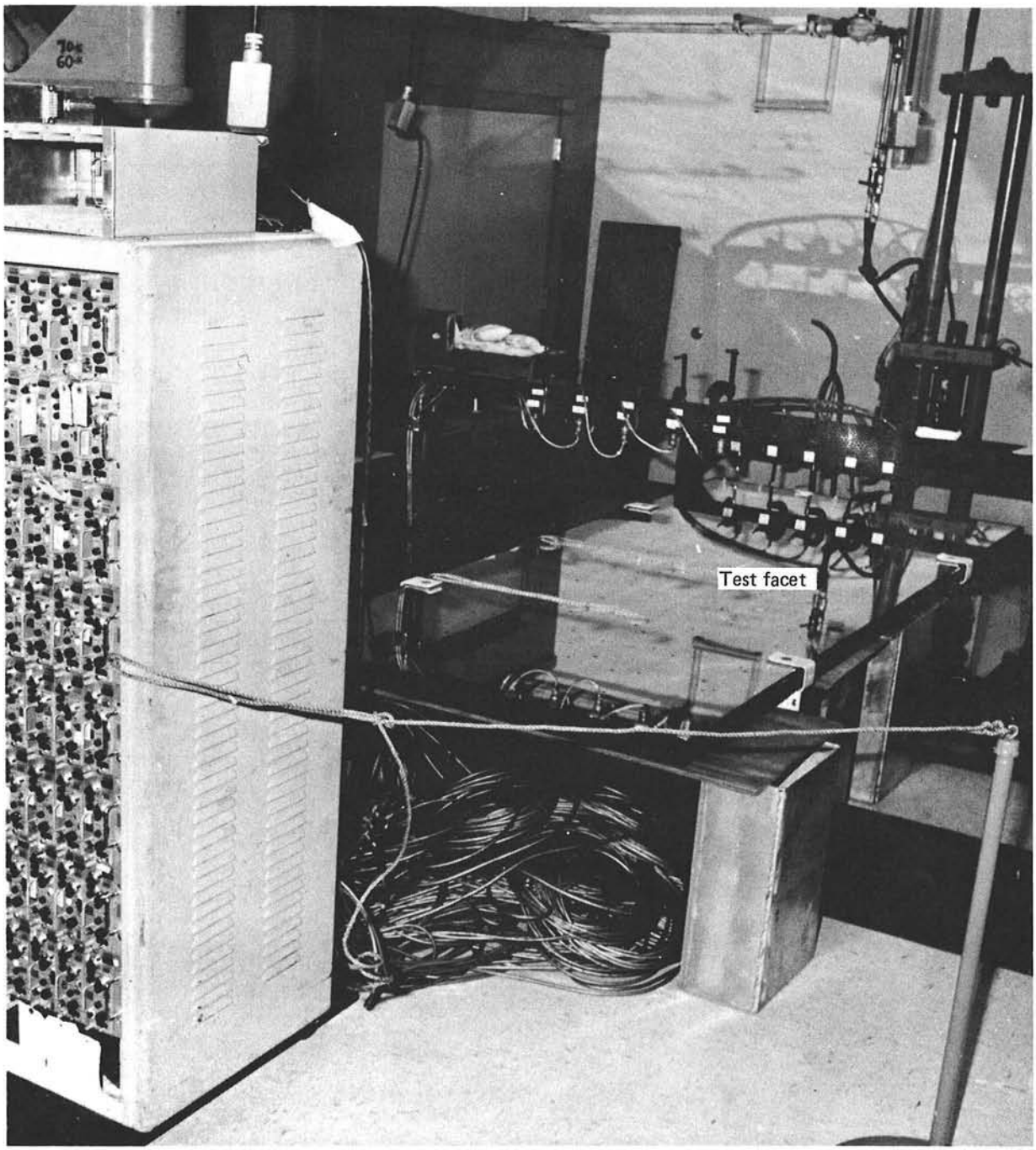

Figure 11 *Facet Static Load Test Setup*

Figure 12 *Location of EDI and Strain Gauges on Facet During Static Load Testing*

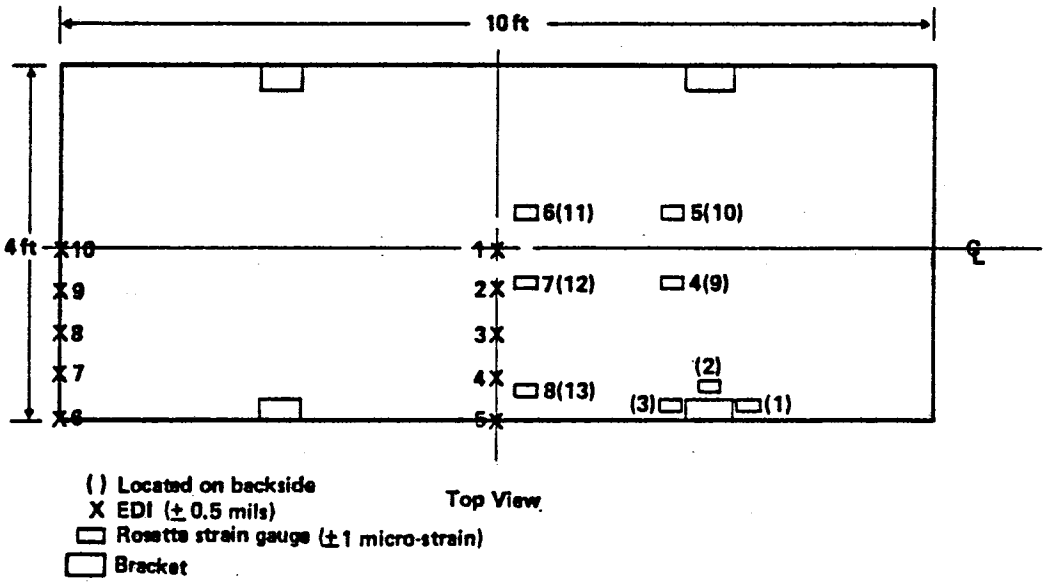

commercially packaged salt and sugar bags at predetermined intervals on the surface, as illustrated in Figure 13.

The first test simulated the load due to gravity or a 27 mph wind without gravity. The two loads are within 4% of each other. All tests made neglected gravity loads. If the effects of gravity are to be included, one need only add the results from the gravity test to those of the environmental condition measured. Table 7 lists data from the tests, comparing them with structural-analysis predicted values. In each case, the position of the analysis nodes and the test nodes on the facet coincided.

Agreement between predicted and measured values was generally good, considering the accuracies of approximately 15-20% associated with both the analytical modelling and the experimental setup measurements. The maximum principal stresses predicted and measured (near node 2) agreed within 15%.

The second test simulated the distributed load due to a 90 mph wind. Table 8 shows the test load distribution which was derived from wind load analyses. Results from the test were compared with NASTRAN model predictions. Most of the deflection data agree with the predicted values within the expected errors associated with experimentation and mathematical modelling. Greater discrepancy exists, however, with the stress data, where only about half the values are in agreement. However, the maximum predicted and measured stresses are less than the allowable stress for design, and agree within 5%.

Flatness measurements, were made with the electronic level before and after the structural load tests. The slope error for 90% of the facet area was 0.58 mrad before load test, and 0.57 mrad after.

2.5 Attachment Bracket Pad Test

The facet must react wind loads through the 4 attachment brackets. The reaction has been computed to be approximately 400 lbs for a 90 mph wind. Tests were performed to aid in the selecting of adequate pad area, and establish their preferred location relative to the facet edge.

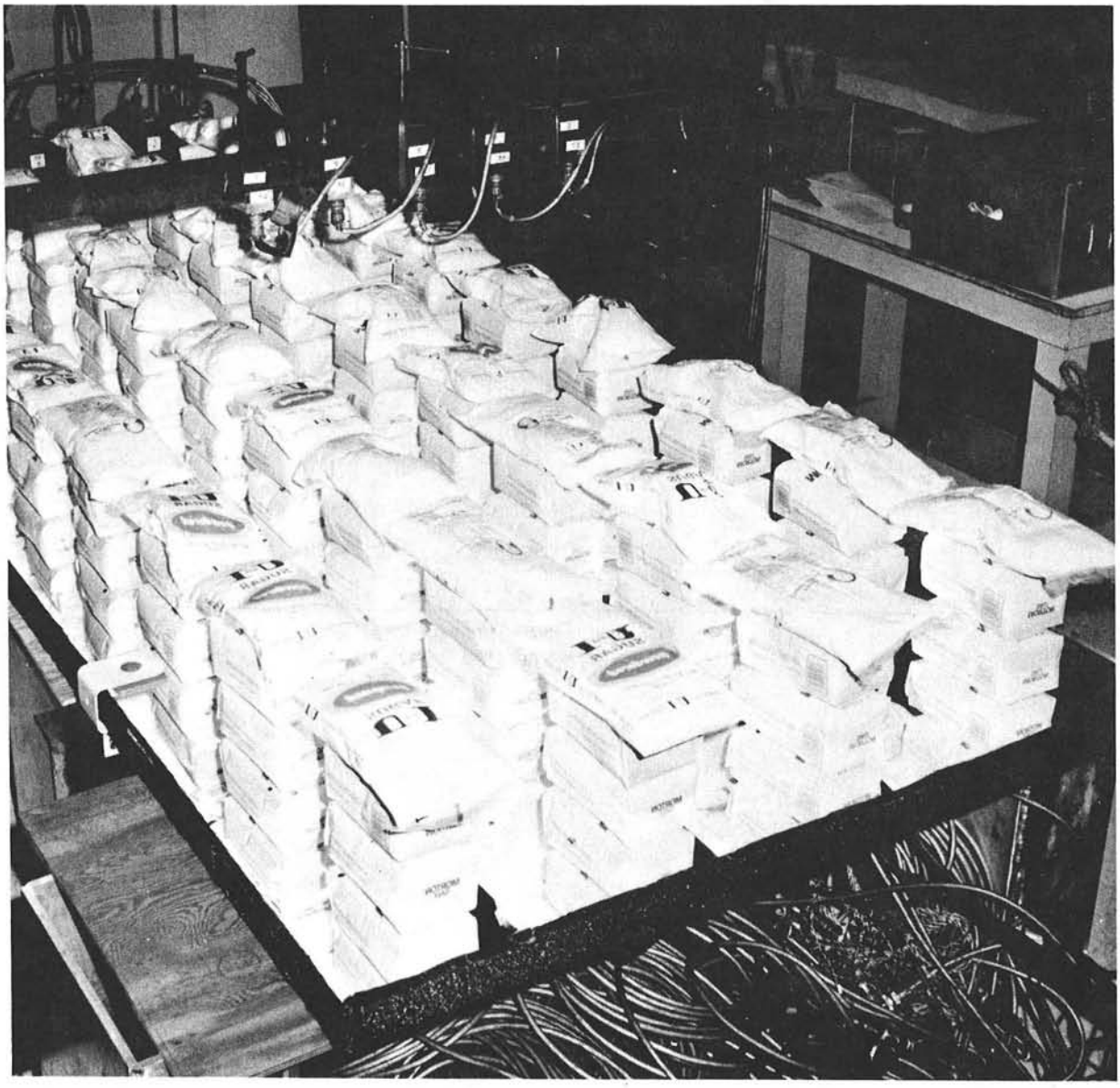

Figure 13 *Facet Assembly Under Load*

Table 7 *Results of Facet Deflection Stress Measurements Compared to Predicted Values Under Gravity (0.025 PSI) or Simulated 27 MPH (0.026) Loads*

Deflections (mils)			Stresses (psi)				
EDI No.	Test	NASTRAN	Strain Gauge No.	Test		NASTRAN	
				σ_x	σ_y	σ_x	σ_y
1	-2	-1	(1)	-110	40	-110	30
5	-1	0	(2)	-140	60		
6	-5	-6	(3)	-110	40	-110	30
10	-6	-7	5	-80	80	-50	60
			(10)	60	-80	50	-60
			6	0	40	-10	50
			(11)	20	-30	10	-50

Maximum predicted principal σ =120 psi
Maximum test principal σ = 140 psi

Table 8 *Results of Facet Deflection and Stress Measurements Under Simulated 90 mph Wind Loads*

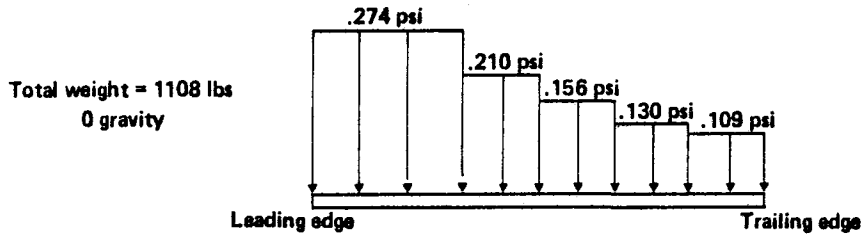

Deflections (mils)			Stresses (psi)				
EDI No.	Test	NASTRAN	Strain Gauge No.	Test		NASTRAN	
				σ_x	σ_y	σ_x	σ_y
1	-11	-7	(1)	-950	360	-840	680
5	-7	+3	(2)	-1140	530		
6	-38	-45	(3)	-940	330	-840	680
10	-44	-55	5	-570	590	-330	450
			(10)	640	-590	330	-450
			6	-170	320	-70	330
			(11)	190	-340	70	-330

Maximum predicted principal σ = 1080 psi
Maximum test principal σ = 1140 psi

Four compression load tests were conducted with a variety of pad configurations on small facet sections in a compression test machine. Figure 14 shows the test setup. Loading was gradually applied until discontinuity was observed in the load-deflection curve. This point on the curve was annotated as the failure load for each of the 4 configurations tested. The results are summarized in Table 9.

The first 3 tests were run with similar geometries, with the only variable being the pad edge-distance. There was considerable scatter among these 3 values, the lowest being only 20% greater than the predicted load; the highest, 69% greater. A larger area pad was therefore prepared and tested (12 in^2; 0.5 in from edge) to obtain a greater safety margin. The resulting failure load was 850 lbs, a 113% margin. The latter pad area was thus chosen for the design.

3.0 Environmental Tests

3.1 Hailstone Survivability

Because the BEC heliostat is non-inverting, the facet surfaces and edges may be exposed to 25 mm hailstones impacting at 23 m/s. Therefore, testing was performed to evaluate the facet's resistance to such conditions.

Several materials were selected for hailstone testing. Any combination of materials unable to pass hailstone tests were eliminated from further design consideration. Figure 15a lists the various material candidates considered for the mirror, adhesive, densifying layer, and core.

Test samples were constructed to simulate actual facets in every respect except width and length, which was 12 inches by 12 inches; they are illustrated in Figure 15b.

Hail testing was performed at the Boeing Impact Laboratory Test Range. The facility includes a pneumatic launcher, velocity measurement system, target support and impact photography system. A schematic of the test range is shown in Figure 16.

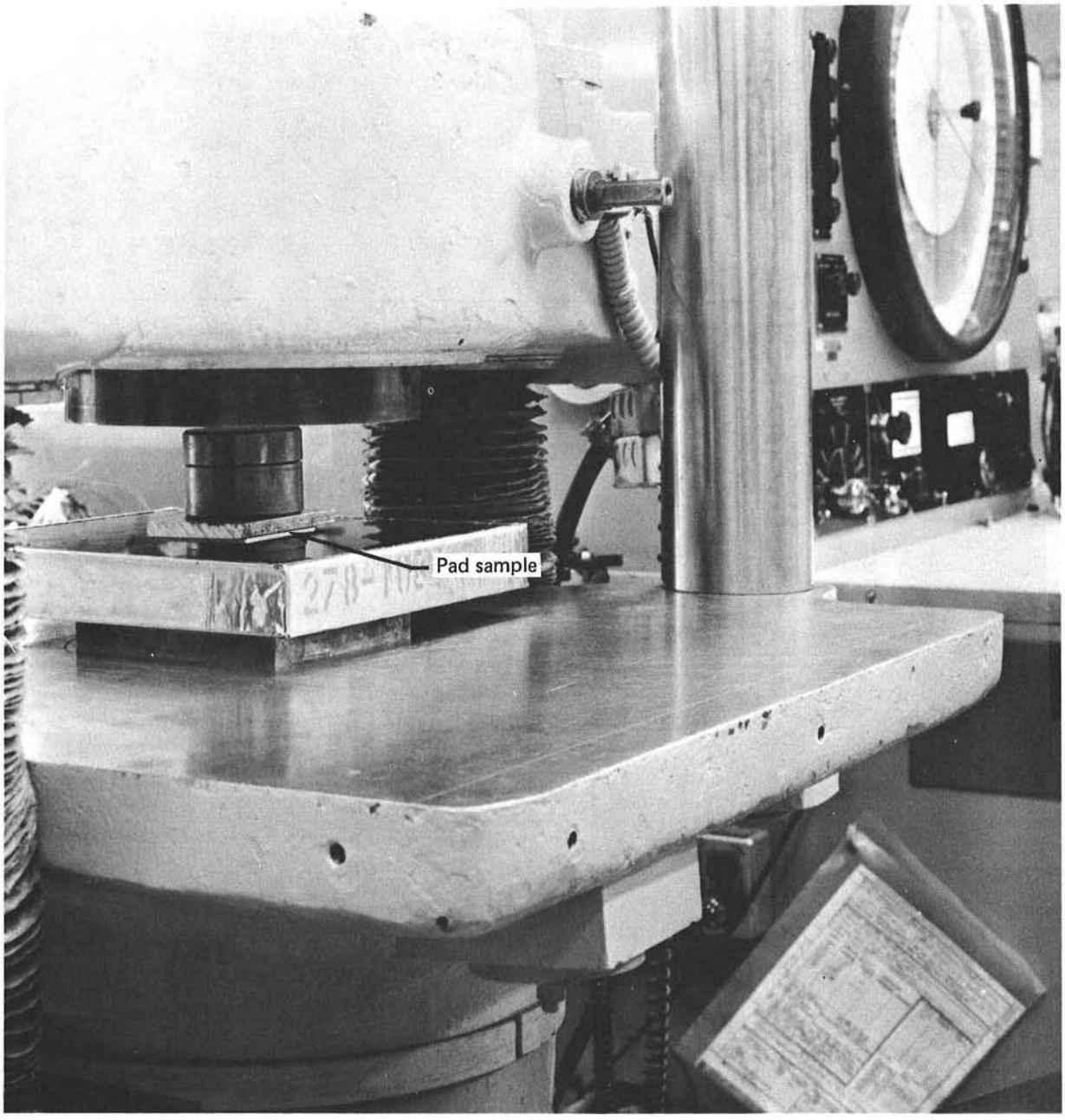

Figure 14 *Facet Mount Clip Compressive Loads Test Setup*

Table 9 *Results of Facet Mounting Clip Compressive Load Tests*

PAD AREA (IN^2)	POSITION (INCHES FROM EDGE)	MEASURED LOAD AT FAILURE (LBS)	PREDICTED 90 MPH WIND LOAD (LBS)
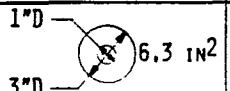 6.3 IN^2	1.75"	575	400
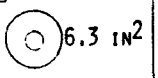 6.3 IN^2	1.75"	480	400
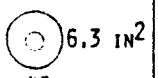 6.3 IN^2	0.5"	675	400
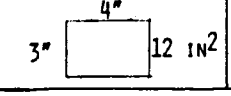 12 IN^2	0.5"	850	400

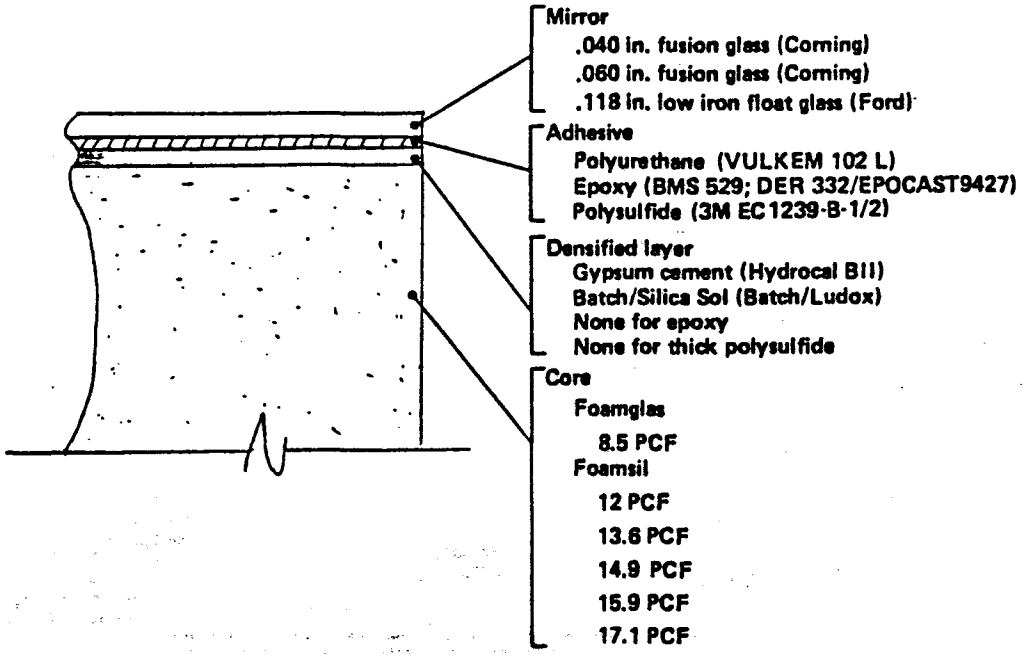

a. Specimen Core Configuration Detail

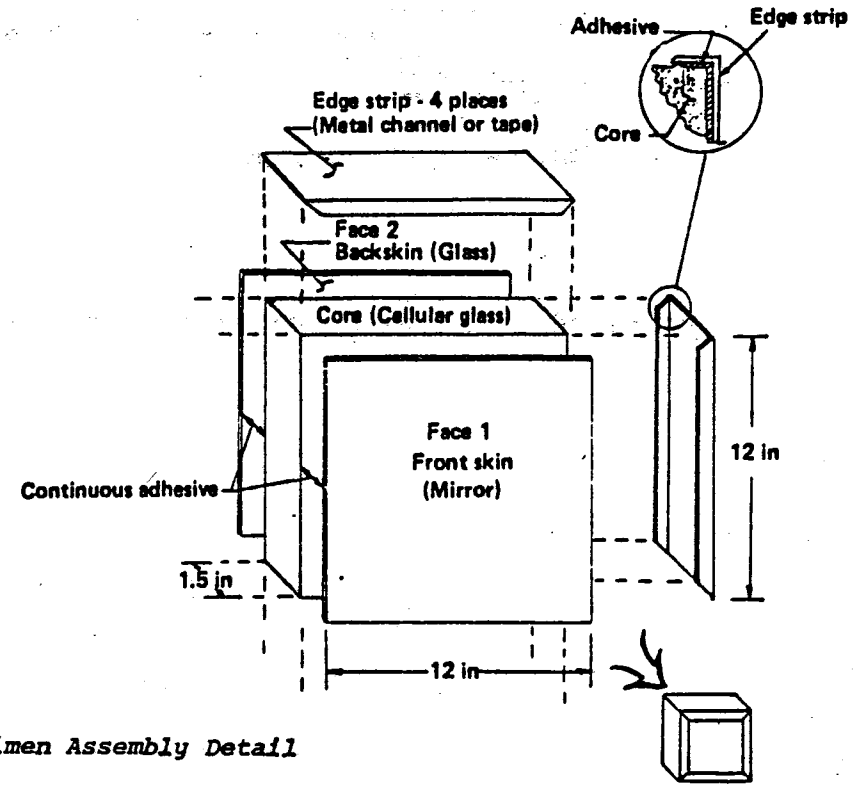

b. Specimen Assembly Detail

Figure 15 Configuration of Hail Stone Test Specimen

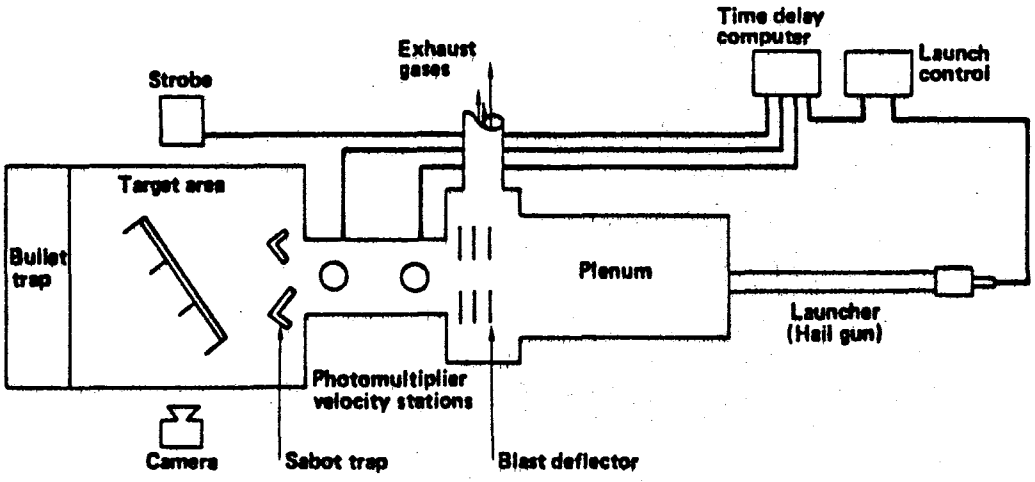

Figure 16 *Hail Stone Test-Setup Schematic*

The simulated hailstones were formed in molds called "sabots" which also serve as launching capsules that separate during flight; the sabot is illustrated in Figure 17. Water is injected into the sabots and frozen in a refrigerator which is kept at approximately 10°F. The sabot is then carefully opened, the ice ball removed and weighed. The ice ball is reinserted in the sabot which is then placed in the launcher.

The sabot and ice ball are launched by releasing air pressure into the breach with a solenoid valve. As the sabot travels down range it separates, releasing the ice ball and is caught in the sabot trap. The velocity of the ice ball is measured by 2 photo-multipliers and a computer. The computer also sends a signal to the camera strobe light which allows a photograph to be taken of the ice ball as it impacts the target.

Both 0.059 inch fusion and 0.118 inch float glasses successfully survived hail damage when used on adequate substrate combinations. The 0.040 inch fusion glass was not acceptable on any of the configurations tested.

All 3 adhesive systems were satisfactory when applied properly. The epoxy and polysulfide worked well when applied to proper thicknesses. The polyurethane worked only when a densifier (gypsum cement or batch silica-sol) was applied to the cellular glass core prior to applications of the adhesive layer. No difference in effectiveness could be detected between the 2 densifiers.

Core densities greater than 12 pcf appeared to be unnecessary for the epoxy and polysulfide adhesives and did not eliminate the need for surface densification for the polyurethane adhesive. Therefore, higher densities were eliminated from future consideration. A density of 8.5 pcf was successfully used behind .118 float glass with polyurethane and densifier.

Table 10 summarizes test parameters and results for all configurations that survived the tests.

3.2 Temperature/Moisture Cycling - Coupon Level

Specified environmental requirements for the facet include temperature extremes of -30°C to +50°C, and precipitation in the form of rain up to 75 mm

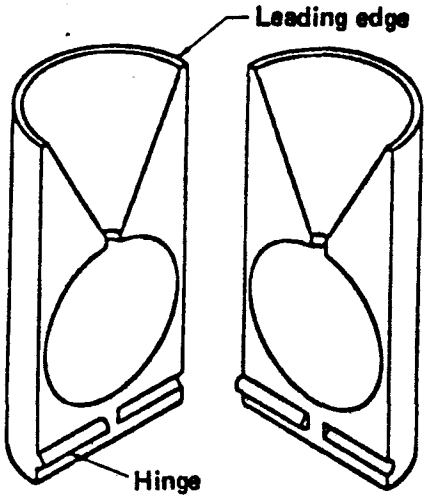

Injection molded Polycarbonate

Figure 17 *Ice-Ball Mold*

Table 10 *Summary of Test Parameters for Test Specimens Surviving Hailstone Testing*

Description Front sheet/adhesive/core	No. of impacts	Avg. velocity ±1σ FPS	Avg. weight ±1σ grams	Target Zone	
				Central	Edge
.059in fusion/epoxy type 1/12 pcf	13	74.2 ± 2.3	7.33 ±.15	X	X
.059in/epoxy type 2/12 pcf	12	74.8 ± 1.5	7.26 ±.15	X	X
.059in/polyurethane hydrocal built-up/12 pcf	17	74.1 ± 2.2	7.19 ±.19	X	X
	15	76.6 ± 1.7	7.32 ±.15	X	
.059in/polyurethane Ludox built-up/12 pcf	12	75.3 ± 2.8	7.30 ±.18	X	X
.059in/polysulfide/12pcf	14	73.0 ± 1.5	7.30 ±.24	X	X
.118in LI float/polyurethane/8.5pcf	12	75.3 ± 2.4	7.36 ±.18	X	
.118in LI float/polyurethane/12 pcf	4	74.8 ± 1.8	7.40 ±.17	X	

in a 24-hour period, and 750mm annually. In addition, it may also be subjected to freezing rain, ice deposits, and snow. Humidity was also an important design consideration. Major concerns for these conditions are the effects upon structural integrity and silver quality.

Test coupons were prepared for the variety of combinations of glasses, sealants and adhesives that were design candidates. The coupons were 6" x 6" x 1-1/2" facet miniatures, including cap strips. Each coupon was constructed with a cylindrical cavity in the core that could be viewed through one of the glass skins. The samples were carefully weighed and placed in a cycling temperature/humidity chamber. Figure 18 shows 2 coupons and the test chamber. Figure 19 is the temperature/humidity profile followed to obtain both the temperatures and moisture extremes desired.

The coupons were periodically inspected for cracks in glass sheets or cores, discoloration of silver, evidence of water inside the coupon and weight change. The inspections were visual; weight change was measured to an accuracy of $\pm$0.05 gms. A list of coupon variables and test results appears in Table 11.

Of the few samples that showed a weight gain, the gains were negligibly small. Weight losses were more common, indicating curing of adhesives and sealants. No cracks or silver discolorations were observed. Several samples were dismantled and examined. The condition of the sealants and adhesives appeared to be unchanged from the fresh materials. Pieces of silvered glass for each candidate were measured for reflectivity on the spectrophotometer and the bi-directional reflectometer. The reflectivity was unchanged from pre-test values (approximately 93% for 0317 fusion; 94.5% for 7809 fusion). All candidates were considered to have successfully passed these tests.

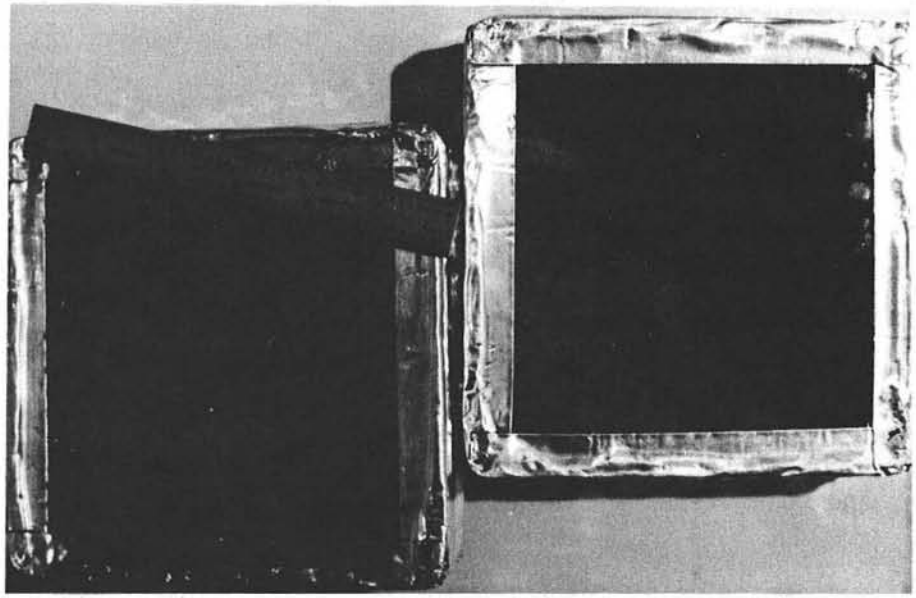

b. Test Specimens

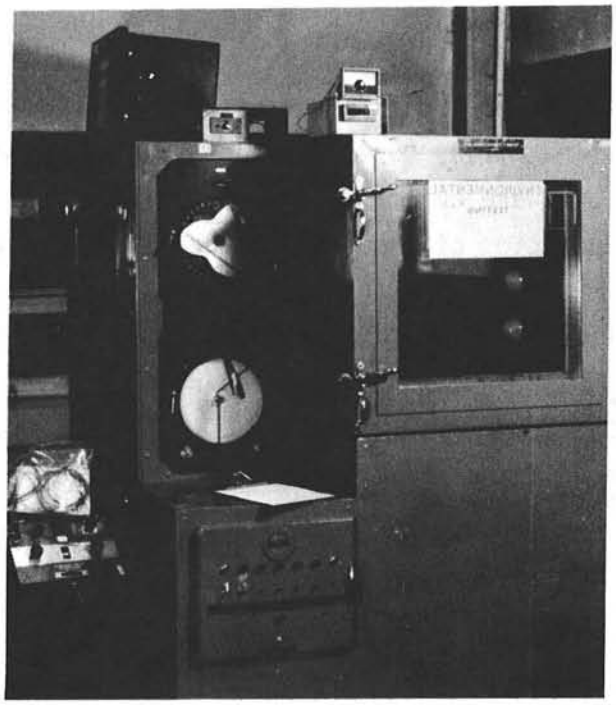

a. Test Cell

Figure 18 *Temperature-Humidity Testing of Facet Specimens*

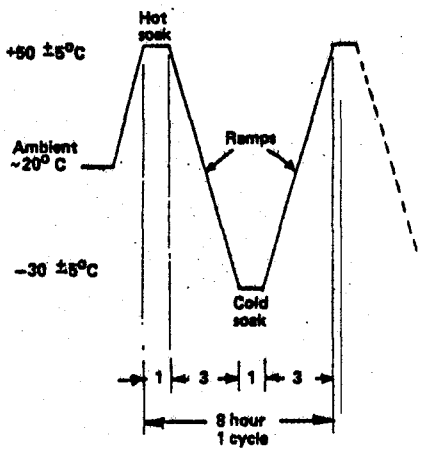

A) Continue @ 3 cycles per day for 4 days w/ relative humidity $\geq$ 90%

B) Follow with same temperature profile for 3 days w/relative humidity $\leq$ 30%

C) Repeat A) above ; then B) above alternately for 28 days for a total of 84 thermal cycles

Figure 19 . Temperature-Humidity Test Profile

Table 11 Results of Temperature-Humidity Testing

	Mirror/ Backsheet	Sample I.D.	Glass Adhesive	Refl. Sealant	Capstrip Adhesive	RESULTS: Weight Change Grams	RESULTS: Observations
Alternatives	7809/7809	1A	Polyurethane	Butyl	Butyl	[1] -.16	No moisture in cavity; no silver degradation; adhesion strong; sealant resilient
	" "	1B				-.31	
	7809/steel	1C				+.06	
	" "	4C				+.10	
	7809/7809	2A	Asphalt			+.08	Weight decreases probably due to curing of adhesive and sealants. Weight gains negligible.
	" "	2B				-.19	
	" "	2C				.00	
	" "	3A	Polyurethane			-.39	
	" "	3B				+.03	
	7809/steel	3C				+.01	
	7809/7809	4A				-.08	
	" "	4B				-.07	
	0317/0317	5	Polysulfide	Polysulfide	Polysulfide	-.52	
Baseline	7809/7809	9A	Epoxy	Butyl	Asphalt (PC 88)	[2] -.14	Sample had no capstrip
	0317/7809	9B				-.18	
	7809/7809	10				-.58	
	" "	11				-1.21	
	0317/7809	12				-1.11	
	" "	13				-1.55	
	7809/7809	14				+1.02	
	7809	15		None	None	.00	No visible change to paint or coating
			Backside coating/paint sample (Vinyl/acrylic paint)				

[1] 185 cycles

[2] 85 cycles

3.3 Temperature/Moisture Cycling - Facet Level

A full-scale structural development facet was subjected to an abbreviated temperature/moisture test similar to the one described above. The principal purpose of this test was to verify the structural integrity when exposed to temperature extremes of -30°C to +50°C. A secondary purpose was to verify that the encapsulation system prevented moisture intrusion during high humidity conditions.

Figure 20 shows the facet in the chamber before test. The chamber was operated on a 12 hour cycle basis (+50°C soak for 1 hr; 5 hr. ramp down; -30°C soak for 1 hr; 5 hr ramp up to +50°C; etc.) for 7 days, accumulating 14 cycles. The relative humidity was changed from 90% to 30% on alternate days. Posttest examination revealed no evidence of cracking, warping or delamination of the glass on core materials. The cap strip was securely fastened to the facet with no signs of moisture penetration.

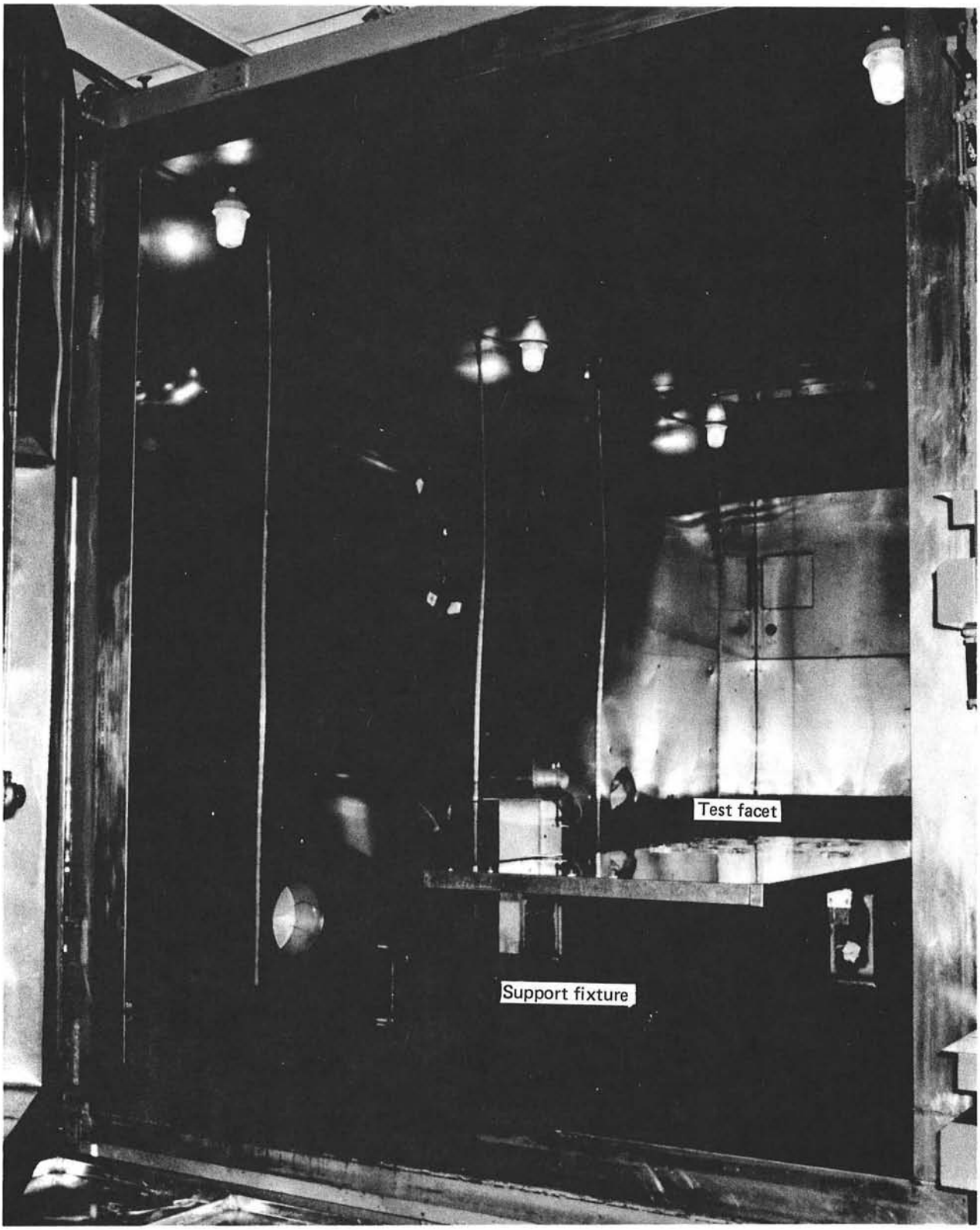

Figure 20 *Development Facet in Temperature-Humidity Test Chamber*

APPENDIX F

DRIVE MOTOR SPECIFICATION

Azimuth Drive Motor

1. Motor Description
   - 1.1 Type: 3-phase induction, winding D
   - 1.2 Ratings: 1/6 horsepower at 1750 rpm nominal, 208V, 60 Hz
   - 1.3 Frame: NEMA 48, TENV, C-FACE, FOOTLESS
   - 1.4 Protection: Automatic reset thermal overload protection
2. Environment: Exterior installation
   - 2.1 Ambient temperature: -9°C to +50°C operating;
     -30°C to +50°C storage
   - 2.2 Contaminants: Rain
     Ice
     Snow
     Blowing sand and dust
     Insects
   - 2.3 Altitude: 7000 ft MSL
3. Duty Cycle
   - 3.1 Daily Duty: Each start is full line voltage start; each stop is half-wave plug of 66 msec duration.
     Daily duty cycles of:
     - Continuous for 30 minutes.
     - Intermittent 330 msec on and 15.7 seconds off for 4-1/2 hours.
     - Intermittent 1.4 seconds on and 2.6 seconds off for 30 minutes.
     - Intermittent 330 msec on and 15.7 seconds off for 4-1/2 hours.
   - 3.2 Continuous for 15 minutes.
4. Service Life
   - 4.1 Windings and case - 30 years (no maintenance).
   - 4.2 Bearings - 30 years with maintenance.
5. Load: 4.14 in-lb peak starting torque.
   4.14 in-lb peak running torque.
   0.12 lb-in^2 inertia.

Elevation Drive Motor

1. Motor Description
   - 1.1 Type: 3-phase induction, winding D
   - 1.2 Ratings: 1/3 horsepower at 1750 RPM nominal, 208V, 60 Hz
   - 1.3 Frame: NEMA 56, TENV, C-FACE, FOOTLESS
   - 1.4 Protection: Automatic reset thermal overload protection
2. Environment: Exterior installation.
   - 2.1 Ambient temperature: -9°C to +50°C operating;
     -30°C to +50°C storage.
   - 2.2 Contaminants: Rain
     Ice
     Snow
     Blowing sand and dust
     Insects
   - 2.3 Altitude: 7000 ft MSL
3. Duty Cycle
   - 3.1 Daily Duty: Each start is full line voltage start; each stop is half-wave plug of 66 msec duration. Intermittent daily duty cycles of:
     500 msec on and 3.5 seconds off for 30 minutes.
     330 msec on and 15.7 seconds off for 9 hours.
     500 msec on and 3.5 seconds off for 30 minutes
   - 3.2 Continuous duty for 30 minutes can be imposed once a day at any time.
4. Service Life
   - 4.1 Windings and case - 30 years (no maintenance).
   - 4.2 Bearings - 30 years with maintenance.
5. Load: 6.74 in-lb peak starting torque.
   12.32 in-lb peak running torque.
   0.12 lb-in^2 inertia.

APPENDIX G

MODE OPERATIONS AND SOFTWARE ORGANIZATION

APPENDIX G

MODE OPERATIONS AND SOFTWARE ORGANIZATION

1.0 MODE OPERATIONS

1.1 Mode 0 - Halt (HLT)

The halt mode indicates the motors are not being commanded to achieve any defined track or position. The halt mode will be a default mode the system will automatically select when no other mode is commanded, e.g., at power up the system will come up in the halt mode or when any mode which transitions to a fixed mirror position is complete, the transition will end with the system in the halt mode.

1.2 Mode 1 - Track (TRK)

This mode tracks to keep the beam on the receiver. The normal entry is from standby. Entry from HLT is allowed so one can manually steer the image onto the target and then go to track mode via HLT. Exit from the track mode is to either STB or HLT.

A track entry from HLT will move mirror over a shortest time path to the TRK position. The real time service for the track and standby modes are similar except for the difference in aim point coordinates.

1.3 Mode 2 - Standby (STB)

The standby mode tracks to keep the beam in a position offset to the side of the receiver. It is implemented by replacing the target coordinates by the standby coordinates and then calling the same pointing routine called by the track mode.

1.4 Mode 3 - Vertical Stow (VSW) Mode

The VSW mode will cause the heliostat to move to the designated vertical stow position. When it reaches there, the mode will change to HLT. The path followed to the stow position depends upon the starting position. If the initial azimuth of the beam is within 10° of standby, the beam will go to the standby azimuth, move vertically down until below horizontal, and then move directly to stow. If the initial beam azimuth is more than 10° away from standby, the mirror moves directly to standby. The vertical stow position can be changed by changing the data base values stored in the F34 and F35 for heliostat #1 or F84 and F85 for heliostat #2.

1.5 Mode 4 - Stow-to-Standby (STS)

Mode entry is from halt mode only; there is no entry test. If the initial beam elevation exceeds 10°, the beam is commanded to move directly to the standby position. When it reaches there, the mode changes to STB. If the initial beam elevation is less than 10°, the beam is commanded to move to the bottom of the wire-walk, and then up the wire-walk to standby position, after which the mode changes to STB. From the HSW position, this mode will move the beam directly to standby.

1.6 Mode 5 - Horizontal Stow (HSW)

The HSW mode moves the mirror from the Standby position to the horizontal stow position. When stow position is reached, transition to the HLT mode is automatic. Entry is via the HSW command when in the standby mode. Also while transitioning, the HLT mode can be requested followed by a request for any other mode. The beam path for HSW is to move the elevation axis up to about 87° from the standby position. Then the azimuth axis is moved to the desired stow position. The stow position can be changed by changing the data base values F36 and F37 for heliostat #1 or F86 and F87 for heliostat #2.

1.7 Mode 6 - Manual Mirror Control (MMC)

The MMC mode is used to move directly to the azimuth and elevation specified by the operator (F1 and F2 or F51 and F52 in data base). If it should pass a reference mark, the mode will change to HLT - to continue, the operator must again command MMC. Tilt corrections are done in the MMC mode so the azimuth may not behave correctly for elevation angles above 87°. The MMC request will cause the MMC command positions to be displayed. Then to activate the MMC mode, type P and carriage return.

1.8 Mode 7 - Locate Azimuth Reference (LAR)

The LAR mode moves the mirror in azimuth from its present position toward a "target" azimuth. When it passes the reference mark, moving to the left, the current count is saved, then replaced by the values stored in K28 and K29 or K58 and K59, and the mode is changed to HLT. To assure success, the initial azimuth must be to the right of the reference mark. It can be so positioned, using the MMC mode. If the motor count has erroneously become a negative number, it may be necessary to load an approximate MTR count into K12 and K13 or K42 and K44 for the LAR to operate properly.

1.9 Mode 8 - Locate Elevations Reference (LER)

The LER mode behaves similar to the LAR. The initial elevation angle must be above the reference mark. The reference mark is near the lower limit. If the mirror is not above 5° elevation, it should be prepositioned using the MMC mode. The update values for elevation position are stored in K30 or K60. If the motor count (K14 or K44) has become a large negative number, then K14 or K44 should be loaded with a positive value (e.g., 27,000) to assure LER will operate properly.

1.10 Mode 9 - Manual Beam Control (MBC)

The MBC mode moves the mirror so the reflected beam points in the commanded direction as specified by the azimuth and elevations target positions, loaded in the data base locations F3 and F4 for heliostat #1, or F53 and F54 for heliostat #2. This mode was added for possible assistance in sorting out tracking errors.

In addition to the above mode commands, the system recognizes the following task commands. Each task request must contain 3 characters and be followed by a carriage return.

SHD - Shtudown This command halts the motors, waits until they come to rest, and stores the current values of the data base, including the motor counts, on the disk, and ceases execution of the helio control program. SHD can be commanded from any program state or mode.

LON -Log On This causes the automatic logging to turn on as it is set up by K74 through K94. The LA-120 DEC writer must be turned on and set online (as opposed to local) for the logging to print out. A buffer fills in computer memory before the print out begins so there may be a delay of several minutes before printing begins. LON should not be requested twice without an LOF as the second request will cause an abort of the program.

LOF - Log Off This closes out the data logging file sending the last of the data to the printer, and stops the logging operation. The log print gives the following information in addition to the requested K and A array values.

1) A floating point number giving time in seconds past midnight.
2) Two fixed point numbers composing a double precision integer number constituting time in seconds past midnight. The least significant part of this double precision number will print out as a negative number anytime it's most significant bit is set. To interpret a negative value, substrate it from 65,535.
3) A print of the heliostat modes each time a mode change occurs and the time at which it occurred.

RDP - Renew Display Before executing this task code, the screen should be cleared by using the shift and clear keys on the CRT. The RDP command will then put the main display titles back on the screen.

2.0 Software Organization

The software was organized into the following files and routines.

2.1 File HCP5 - This file contains all the background program which constitutes the FORTRAN MAIN program.

2.2 File LIBR5 This is a library file containing the following subroutines most of which are called to support the background processing (HCP5)

MMCD (C, A1, A2)

MMCD = Manual Mirror Command Display

This routine is called to display the command values when the MMC mode is requested.

C = Column to begin typing the values.
A1 = Azimuth position command (F1 or F51)
A2 = Elevation position command (F2 or F52)

LOCCUR (Row, Col)
LOCCUR = Locate Cursor

This routine locates the cursor to begin a message in a specific space on the CRT screen.

CLRDSP (Row, Col, Num)
CLRDSP = Clear Display

This routine is called to clear a NUM spaces on the CRT screen, starting at location (Row, Col)

DSPLYM () = Display Modes

This routine is called to display the modes for both heliostat #1 and heliostat #2 on the CRT screen.

DSPLYP = Display Positions

This routine is called to display the gimbal axis positions for both heliostat #1 and heliostat #2.
GPIO (N)
GPIO = General Purpose Input/Output

This routine is called to display and change values in the data base.

RNDSP - Renew Display

This routine is called by the task RDP. It rewrites all the headings on the CRT display.

TYPMD (MDNUM)
TYPMD = Type Mode
MDNUM = Mode Number

This routine is used to type a mode name for the mode number when a mode change occurs during the automatic data logging.

2.3 File - CLOK This file contains the clock interrupt service routine written in assembly language. It calls the MODE routine and the MCR routine to do the heliostat control computations. It also contains the handler for the serial data from the instrumentation encoders.

This file contains two routines, MCR and MODE. They are

2.4 File - MODE written in FORTRAN.

a. The MODE (A,K) subroutine is called in frames 1 and 3 by the CLOK routine to do the mode setup and mode jump. The arguments A, K specify the data base values for servicing heliostat #1 or heliostat #2. The mode subroutine calls the track subroutine (TRK) for pointing calculations.

b. The MCR (A,K) subroutine is the motor control routine called by CLOK in frames 2 and 4. It compares the ideal point values to the gimbal axis positions and turns the motors on if the error exceeds 1/2 step size.

2.5 File - TRK Contains subroutines TRK, MVP and NMR.

The TRK (A,K,KL) subroutine does the pointing calculations. The arguments designate the data base locations for heliostat #1 or heliostat #2.

The MVP (A,B,C.) subroutine does the multiplications to produce

Vector C = (Matrix A) times (Vector B)

The NMR (A) subroutine normalizes the Vector A.

2.6 File - MIR Contains all the interrupt service routines for interrupts being generated at the heliostats. These routines are written in assembly language and structured to share as much common code as possible.

APPENDIX H

CONTROL SYSTEM DATA BASE

Table 1. K Array (Integers)

Helio No.1		Helio No.2		Descriptions
K	Value	K	Value	
1		31		Active mode, 1 = HLT, 2 = TRK, 3 = STB, 4 = VSW, 5 = STS, 6 =HSW, 7 = MMC, 8 = MBC, 9 = LAR, 10 = LER
2		32		MSB is FLG used in TRK LSB prevents setting MTR run CMDS IF = 0.
3		33		MTR CMDS at previous running MS byte for elev, LS byte for azim.
4		34		Mode CMD (K1, or K31) at prev. setting
5	−6076	35	−6074	Address of output reg. $164104_8 = -6076_{10}$, $164106_8 = -6074_{10}$
6		36		Target designator, 0 = BCS target, 1 = STB PT, 2 = MBC, 3 = Wirewalk, 4 = Beam angle, 5 = MMC
7 8		37 38		Az MTR CMD, (cw, stop, ccw) = (1, 0, -1) El MTR CMD, (up, stop, dn) = (1, 0, -1)
9 10 11		39 40 41		LSP, MSP } Az. MTR rev. count at last CCW passing of ref. mark El MTR rev. count at last downward passing of ref. mark
12 13 14		42 43 44		LSP, MSP } Current AZ MTR count Current El MTR count
15 16 17		45 46 47		LSP, MSP } Current desired Az MTR counts Current desired El MTR count
18 19 20		48 49 50		LSP, MSP } Az MTR count CMD, corrected for coast and step size El MTR, CNT, CMD, corrected for coast and step size
21 22		51 52		Az MTR coast count – last running El MTR coast count – last running
23 24	 16	53 54		Az, El } Allowed CNTS err before motor is run

Table 1. K Array (Integers)—(Continued)

Helio No.1		Helio No.2		Description
K	Value	K	Value	
25		55		LSP } Az ref. mark search command position — motor counts
26		56		MSP }
27		57		El ref mark search CMD position — counts
28		58		LSP } Az MTR count to load at ref mark (LAR mode)
29		59		MSP }
30		60		El count to load at ref. mark (LER)

Parameters below are common to both heliostats		
K	Value	Description
61		LSP } Time - seconds after midnight
62		MSP }
63		Day of month (1 to 31)
64		Month (1 to 12)
65	−17275	Time to return to VSW for life cycle test
		(Spare for HCP5)
66		Month for current ephemeris
67		Frame index
68		Print flag for auto logging
69		CRT display update flag
70		Month } Used to set calendar clock
71		Date }
72		Hour }
73		Minute }
74	N_i	Number of integers to be logged (max = 10)
75	N_f	Number of floating point numbers to be logged (max = 8)
76	I	Log print interval - seconds

Table 1. K Array (Integers)—(Continued)

K	Value	Description
77	K_i	K number for 1st integer to be logged
78		2nd
79		3rd
80		4th
81		5th
82		⋮
83		
84		
85		
86		10th
87	F_i	F num for 1st floating PT to be logged
88		2nd
89		3rd
90		⋮
91		
92		
93		
94		8th
95	8	Azimuth step size at 0 elev. (MTR counts)
96	4	Azimuth allowed overshoot error without reversing motor to correct (MTR counts)
97		El — Values read from position encoders for instrumentation
98		Az — Values read from position encoders for instrumentation
99		Date for which ephemeris constants have been computed
100	4	Elev. allowed overshoot (MTR counts) without reversing motor to correct
101	—	Flag to enable life cycle test, set to 0 (zero) to disable.
102		Cycle counts for life cycle test.
103	−29535	Time loaded into KG1 at beginning of each cycle of life cycle test.

Table 2. F Array for HCP5

Helio No.1		Helio No.2		Descriptions
F	Value	F	Value	
1		51		Az } MMC mode gimbal position
2		52		El } CMDS–(degrees)
3		53		Az } MBC mode beam position
4		54		El } CMDS–(degrees)
5	HLT VSW	55		Az } Beam position CMD during
6	3.0778 0.102	56		El } wire walk (radians)
7	176.35	57	170.78	As of wire walk (degrees)
8	–5.0	58	–1.5	El at bottom of wire walk (degrees)
9	5.88	59	7.9	El at standby PT (degrees)
10		60		Spares
11	0	61	0	Mirror orthogonality error (rad) to right is +
12	.00056	62	0	Elev. axis of orthogonality error (rad) left end up is +
13	–.310515	63	–.2340605	X } BCS target vector in tilted axis (kilometers)
14	.038325	64	.0188626	Y } (for KG=0)
15	.0311948	65	.0346039	Z }
16	–.99272	66	–.978590	X } Normalized standby PT vector
17	–.06333	67	–.158850	Y } (for KG=1)
18	.10245	68	.130870	Z }
19		69		X } MBC mode target vector
20		70		Y } (for KG=2)
21		71		Z }
22		72		X } Target for beam pointing during wire walk
23		73		Y } (KG=3)
24		74		Z }
25	.8173000	75	.82399	f_1e_1 } fe matrix
26	–.003363	76	–.005226	f_1e_2
27	–.562100	77	–.56658	f_1e_3
28	0	78	0	f_2e_1
29	.99997597	79	.99996	f_2e_2
30	–.583630	80	–.0092234	f_2e_3
31	.57622	81	.56661	f_3e_1
32	.00477	82	.0076	f_3e_2
33	.817280	83	.82395	f_3e_3
34	180.	84	180.	Az } Vert. stow position (degrees)
35	0	85	0 5 = HLCT }	El }
36	180.	86	180.	Az } Horizontal stow position (degrees)
37	89.	87	89.	El }

Table 2. F Array for HCP5 (Continued)

Helio No.1		Helio No.2		
F	Value	F	Value	Descriptions
38	32102.887	88	32102.887	Units — Jack screw parameters
39	1.086740	89	1.086740	—
40	2.1134193	90	2.1116216	Rad. $\left(\frac{\text{MTR}}{\text{CNTS}}\right) = 40{,}000 - (38)\sqrt{(39)\cdot\cos\left((40) - \text{El}\right)}$
41	90.	91	90.	Az origin (degrees) Az CMD's lie between origin & origin + 360°
42	145.62674	92	145.62674	Az (MTR counts)/degree
43		93		
44		94		Az — Gimbal angle CMDS calc. in TRK (degrees)
45		95		El — Gimbal angle CMDS calc. in TRK (degrees)
46		96		Az — Beam position based on current MTR counts (degrees)
47		97		El — Beam position based on current MTR counts (degrees)
48		98		
49		99		Az — MMC CMD's last frame used to initiate MMC display update in HCP6
50		100		El — MMC CMD's last frame used to initiate MMC display update in HCP6

F	Value	Descriptions — Parameters common to both heliostats
101		Time—seconds past midnight
102		Degrees per Az MTR count = 1/F (42)
103		Spares
117		
118	.02	Gimbal lock parameter ~ radians
119		
120	178.491	Δ Hr. angle = 180° + ($\text{Long}_{\text{ref}} - \text{long}_{\text{helio}}$) w
121		Declination—degree, for day 1 (LCT = 0 hrs)
122		day 2
⋮		⋮
160		day 40
161		$(\text{GHA—GMT} \times 15)_{\text{degree}}$ + 180 for day = 1 (LCT = 0 hr)

Table 2. F Array for HCP5 (Continued)

F	Value	Descriptions – Parameters Common to Both Heliostats
162 ⋮ 200		2 ⋮ 40
201 ⋮ 216		Azimuth values for mode 21–sequencial points CMD program*
217 ⋮ 232		Elev. values for mode 21–sequencial points CMD program*
233 ⋮ 240		Spares

*There is no planned use for mode 21

UNLIMITED RELEASE

INITIAL DISTRIBUTION

UC-62d (350)

U.S. Department of Energy
600 E Street NW
Washington, D. C. 20585
Attn: W. W. Auer
G. W. Braun
K. Cherian
M. U. Gutstein
L. Melamed
J. E. Rannels

U.S. Department of Energy
San Francisco Operations Office
1333 Broadway
Oakland, CA 94612
Attn: S. D. Elliott
S. Fisk
R. W. Hughey
W. Nettleton

U.S. Department of Energy
Solar Ten Megawatt Project Office
P. O. Box 1449
Canoga Park, CA 91304
Attn: M. Slaminski

U.S. Department of Energy
Solar Ten Megawatt Project Office
5301 Bolsa Ave. MS14-1
Huntington Beach, CA 92649
Attn: R. N. Schweinberg

USAF Logistics Command
P. O. Box 33140
Wright-Patterson AFB
Ohio 45433
Attn: G. Kastanos

UCLA
900 Veteran Avenue
Los Angeles, CA 90024
Attn: F. Turner

Georgia Institute of Technology
Engineering Experiment St.
Atlanta, GA 30332
Attn: S. H. Bomar, Jr.

University of Houston
Houston
Solar Energy Laboratory
4800 Calhoun
Houston, TX 77004
Attn: A. F. Hildebrandt
L. L. Vant-Hull

U.S. Department of Interior
Water & Power Res. Service
P.O. Box 427
Boulder City, NV 89005
Attn: J. Sundberg

Acurex
485 Clyde Avenue
Mountain View, CA 94042
Attn: J. Hull

Aerospace Corporation
Solar Thermal Projects
Energy Systems Group, D-5
Room 1110
P.O. Box 92957
El Segundo, CA 90009
Attn: P. deRienzo
P. Mathur

Airesearch Manufacturing Co.
2525 West 190th Street
Torrance, CA 90509
Attn: M. G. Coombs
For: P. F. Connelly

AMFAC
700 Bishop Street
Honolulu, HI 96801
Attn: G. St. John

ARCO
911 Wilshire Blvd
Los Angeles, CA 90017
Attn: J. H. Caldwell, Jr.

Arizona Public Service
P. O. Box 21666
Phoenix, AZ 85036
Attn: D. L. Barnes
For: E. Weber

Arizona Solar Energy Commission
1700 W. Washington - 502
Phoenix, AZ 85007
Attn: R. Sears

Babcock & Wilcox
91 Stirling Avenue
Barberton, OH 44203
Attn: G. Grant
For: J. Pletcher
M. Seale

Babcock & Wilcox
P. O. Box 1260
Lynchburg, VA 24505
Attn: W. Smith

Babcock & Wilcox
20 S. VanBuren Avenue
Barberton, OH 44203
Attn: M. Wiener

Badger Energy, Inc.
One Broadway
Cambridge, MA 02142
Attn: F. D. Gardner

Battelle Pacific Northwest Labs
P. O. Box 999
Richland, WA 99352
Attn: M. A. Lind

Bechtel National, Inc.
P. O. Box 3965
San Francisco, CA 94119
Attn: E. Lam
For: J. B. Darnell
R. L. Lessley

Black & Veatch
P. O. Box 8405
Kansas City, MO 64114
Attn: C. Grosskreutz
For: J. E. Harder
S. Levy

Boeing Engineering & Construction
P. O. Box 3707
Seattle, WA 98124
Attn: R. L. Campbell
R. Gillette
J. R. Gintz

Booz, Allen & Hamilton, Inc.
8801 E. Pleasant Valley Road
Cleveland, OH 44131
Attn: W. Hahn

Brookhaven National Laboratory
Upton, NY 11973
Attn: G. Cottingham

Burns and Roe, Inc.
550 Kinderkamack Rd.
Oradell, NJ 07649
Attn: J. Willson

Burns and Roe, Inc.
185 Crossways Park Drive
Woodbury, NY 11797
Attn: R. Vondrasek

Busche Energy Systems
7288 Murdy Circle
Huntington Beach, CA 92647
Attn: K. Busche

California Public Utilities Commission
350 McAllister St., Room 5024
San Francisco, CA 94102
Attn: B. Barkovich
For: C. Waddell

Chevron Research
P. O. Box 1627
Richmond, CA 94804
Attn: L. Fraas

Chevron Oil Research
P. O. Box 446
La Habra, CA 90631
Attn: W. Peake
For: J. Ploeg
W. Stiles

Colt Industries
Trent Tube Division
East Troy, WI 53170
Attn: J. Thackray

Corning Glass Works
Advanced Products Dept.
M/S 25
Corning, NY 14830
Attn: W. M. Baldwin
A. Shoemaker

Custom Metals Enterprises, Inc.
3288 Main Street
Chula Vista, CA 92011
Attn: T. J. Bauer

Data Science Corp.
1189 Oddstad Drive
Redwood City, CA 94063
Attn: M. Liang

Electric Power Research Institute
P. O. Box 10412
Palo Alto, CA 93403
Attn: J. Bigger

El Paso Electric Company
P. O. Box 982
El Paso, TX 79946
Attn: J. E. Brown

Energy, Inc.
P. O. Box 736
Idaho Falls, ID 83401
Attn: G. Meredith

Exxon Enterprises-Solar Thermal Systems
P. O. Box 592
Florham Park, NJ 07932
Attn: P. Joy
For: D. Nelson
G. Yenetchi

Ford Aerospace
3939 Fabian Way, T33
Palo Alto, CA 94303
Attn: I. E. Lewis
For: H. Sund

Foster-Miller Associates
135 Second Avenue
Waltham, MA 02154
Attn: E. Poulin

Foster Wheeler Dev. Corp.
12 Peach Tree Hill Road
Livingston, NJ 07039
Attn: A. C. Gangadharan
For: R. Zoschak

GAI Consultants, Inc.
570 Beatty Rd.
Monroeville, PA 15146
Attn: H. Davidson

General Atomic Company
P. O. Box 81608
San Diego, CA 92138
Attn: H. A. Chiger

General Electric Company
Advanced Energy Programs
P. O. Box 8661
Philadelphia, PA 19101
Attn: A. A. Koenig

General Electric Company
1 River Road
Schenectady, NY 12345
tric Company
1 River Road
Schenectady, NY 12345
Attn: J. A. Elsner
For: R. N. Griffin
R. Horton

GM Transportation System Center
GM Technical Center
Warren, MI 48090
Attn: J. Britt

GM Corp. Harrison Rad. Division
A and E Building
Lockport, NY 14094
Attn: A. Stocker

Houston Lighting and Power
P. O. Box 1700
Houston, TX 77001
Attn: J. Ridgway

Institute of Gas Technology
Suite 218
1825 K Street, NW
Washington, D. C. 25006
Attn: D. R. Glenn

Jet Propulsion Laboratory
Building 520-201
4800 Oak Grove Drive
Pasadena, CA 91103
Attn: M. Adams
H. Bank
W. Carley
E. Cuddihy
J. Sheldon
J. Swan
V. Truscello

Kaiser Engineers, Inc.
300 Lakeside Drive
Oakland, CA 94612
Attn: I. Kornyey

Lawrence Berkeley National Laboratory
University of California
Berkeley, CA 94720
Attn: A. J. Hunt

Los Alamos National Laboratory
P. O. Box 1663
Los Alamos, NM 87545
Attn: S. W. Moore

Los Angeles Water and Power
111 North Hope Street
Los Angeles, CA 90051
Attn: B. M. Tuller
R. Radmacher

Martin Marietta Corporation
P. O. Box 179
Denver, CO 80201
Attn: P. R. Brown
A. E. Hawkins
T. Heaton
L. Oldham
H. C. Wroton

McDonnell Douglas Astronautics Co.
5301 Bolsa Avenue
Huntington Beach, CA 92647
Attn: P. Drummond
R. L. Gervais
D. A. Steinmeyer
L. Weinstein

Meridian Corporation
5515 Cherokee Avenue
Alexandria, VA 22312
Attn: B. S. Macazeer

Nielsen Engineering. & Research
510 Clyde Avenue
Mt. View, CA 94043
Attn: R. Schwind

Northrup, Inc.
302 Nichols Drive
Hutchins, TX 75141
Attn: J. A. Pietsch

ARCO Power Systems
Suite 301
7061 S. University Boulevard
Littleton, CO 80122
Attn: J. Anderson
F. Blake

Olin Corporation
275 Winchester Avenue
New Haven, CT 06511
Attn: S. L. Goldstein

OSC Department of Commerce
341 West 2d Street
San Bernardino, CA 92401
Attn: M. G. Heaviside

Pacific Gas and Electric Co.
77 Beale Street
San Francisco, CA 94105
Attn: P. D. Hindley
For: J. F. Doyle
A. Lam

Pacific Gas and Electric Co.
3400 Crow Canyon Road
San Ramon, CA 9426
Attn: H. Seielstad
For: J. Raggio

Phillips Chemical Co.
13-D2 Phillips Building
Bartlesville, OK 74004
Attn: M. Bowman

Pittsburgh Corning
800 Presque Isle Drive
Pittsburgh, PA 15239
Attn: W. F. Lynsavage

Pittsburgh Corning
723 N. Main Street
Port Allegany, PA 16743
Attn: W. J. Binder
For: R. Greene

PPG Industries, Inc.
One Gateway Center
Pittsburgh, PA 15222
Attn: C. R. Frownfelter

Public Service Co. of New Mexico
P. O. Box 2267
Albuquerque, NM 87103
Attn: A. Akhil

Research and Development
Public Service Co. of Oklahoma
P. O. Box 201
Tulsa, OK 74102
Attn: F. Meyer

Rockwell International
Energy Systems Group
8900 De Soto Avenue
Canoga Park, CA 91304
Attn: T. Springer

S. C. Plotkin & Associates
6451 West 83rd Street
Los Angeles, CA 90045
Attn: W. Raser

Safeguard Power Transmission Co.
Hub City Division
P. O. Box 1089
Aberdeen, SD 57401
Attn: R. E. Feldges

Sargent and Lundy
55 East Monroe
Chicago, IL 60603
Attn: N. Weber

Schumacher & Associates
2550 Fair Oaks Blvd., Suite 120
Sacramento, CA 95825
Attn: J. C. Schumacher

Sierra Pacific Power Co.
P. O. Box 10100
Reno, NV 89510
Attn: W. K. Branch

Solar Energy Research Institute
1617 Cole Boulevard
Golden, CO 80401
Attn: L. Duhham, TID
G. Gross
B. Gupta
D. W. Kearney
L. M. Murphy
R. Ortiz, SEIDB
J. Thornton

Solar Thermal Test Facility
User Association
Suite 1205
First National Bank East
Albuquerque, NM 87112
Attn: F. Smith

Solar Turbines International
P. O. Box 80966
San Diego, CA 92138
Attn: P. Roberts

Southern California Edison
2244 Walnut Grove Road
Rosemead, CA 91770
Attn: J. Reeves
For: C. Winarski

Southwestern Public Service Co.
P. O. Box 1261
Amarillo, TX 78170
Attn: A. Higgins

Standard Oil of California
555 Market Street
San Francisco, CA 94105
Attn: S. Kleespies

Stanford Research Institute
333 Ravenswood Avenue
Menlo Park, CA 94025
Attn: A. Slemmons

Stearns-Roger
P. O. Box 5888
Denver, CO 80217
Attn: W. Lang
For: J. Hopson

Stone & Webster Engineering Corp.
245 Summer Street
P. O. Box 2325
Boston, MA 02107
Attn: R. Kuhr

Townsend and Bottum
9550 Flair Drive
El Monte, CA 91731
Attn: R. Schwing

US Gypsum
101 S. Wacker Drive
Chicago, IL 60606
Attn: Ray McCleary

US Water & Power Resources Service
Bureau of Reclamation
Code 1500 E
Denver Federal Center
P. O. Box 25007
Denver, CO 80225
Attn: S. J. Hightower

Van Leer Plastics
15581 Computer Lane
Huntington Beach, CA 92649
Attn: Larry Nelson

Veda, Inc.
400 N. Mobile, Building D
Camarillo, CA 90310
Attn: L. E. Ehrhardt
For: W. Moore

Westinghouse Corporation
Box 10864
Pittsburgh, PA 15236
Attn: J. J. Buggy
For: R. W. Devlin
W. Parker

Winsmith
Division of UMC Industries
Springville, NY 14141
Attn: W. H. Heller

K. R. Miller, 3153
G. E. Brandvold, 4710; Attn: J. F. Banas, 4716
J. A. Leonard, 4717
B. W. Marshall, 4713; Attn: D. L. King
A. B. Maish, 4724
R. G. Kepler, 5810; Attn: L. A. Harrah, 5811
J. G. Curro, 5813
F. P. Gerstle, 5814
J. N. Sweet, 5824; Attn: R. B. Pettit and E. P. Roth
T. B. Cook, 8000; Attn: A. N. Blackwell, 8200
B. F. Murphey, 8300
C. S. Hoyle, 8122; Attn: V. D. Dunder
R. J. Gallagher, 8124; Attn: B. A. Meyer
D. M. Schuster, 8310; Attn: R. E. Stoltz, 8312, for M. D. Skibo
A. J. West, 8314
W. R. Even, 8315
R. L. Rinne, 8320
C. T. Yokomizo, 8326; Attn: L. D. Brandt
P. L. Mattern, 8342
L. Gutierrez, 8400; Attn: R. A. Baroody, 8410
D. E. Gregson, 8440
C. M. Tapp, 8460
C. S. Selvage, 8420
V. Burolla, 8424; Attn: C. B. Frost
R. C. Wayne, 8450
T. D. Brumleve, 8451
W. R. Delameter, 8451
P. J. Eicker, 8451 (5)
R. M. Houser, 8451
C. L. Mavis, 8451
W. L. Morehouse, 8451
H. F. Norris, Jr., 8451
W. S. Rorke, Jr., 8451
D. N. Tanner, 8451
S. S. White, 8451
A. C. Skinrood, 8452
W. G. Wilson, 8453
Publications Division, 8265/Technical Library Processes Division, 3141
Technical Library Processes Division, 3141 (2)
M. A. Pound, 8214, for Central Technical Files (3)

☆ U.S. GOVERNMENT PRINTING OFFICE: 1981 - 791-810/330 9-II